An Improved Understanding of Fluorescent Zn(II) Sensors and Their Uses in Biological Settings

by

Brian Alexander Wong
B. S. Chemistry
University of California, Berkeley, 2004

SUBMITTED TO THE DEPARTMENT OF CHEMISTRY IN PARTIAL FULFILLMENT OF THE REQUIREMENTS FOR THE DEGREE OF

DOCTOR OF PHILOSOPHY IN INORGANIC CHEMISTRY
AT THE
MASSACHUSETTS INSTITUTE OF TECHNOLOGY

July 2009

Signature of Author:_____
Department of Chemistry
July 1, 2009

Certified By:_____
Stephen J. Lippard
Arthur Amos Noyes Professor of Chemistry
Thesis Supervisor

Accepted By:_____
Robert W. Field
Chairman, Department Committee on Graduate Studies

This doctoral thesis has been examined by a committee of the Department of Chemistry as follows:

Alice Y. Ting
Committee Chairperson
Pfizer-Laubach Career Development Associate Professor of Chemistry

Stephen J. Lippard
Arthur Amos Noyes Professor of Chemistry
Thesis Supervisor

Christopher C. Cummins
Professor of Chemistry

An Improved Understanding of Fluorescent Zn(II) Sensors and Their Uses in Biological Settings

By
Brian Alexander Wong

Submitted to the Department of Chemistry on July 21, 2009 in partial fulfillment of the requirements for the Degree of Doctor of Philosophy in Inorganic Chemistry

Abstract

Chapter 1. An Introduction to Fluorescent Zn(II) Sensors and Their Applications in Biological Systems

This chapter opens with an overview of the numerous roles of zinc in biology, with an emphasis on labile Zn(II), that is, loosely bound or kinetically available stores of the ion. The synthesis, characterization, and application of fluorescent sensors for Zn(II) detection constitute an active field of research. A survey of the history and development of these sensors is presented, along with a sample of the knowledge acquired through their use in biological systems. An examination of methods for the subcellular localization of fluorescent probes is included.

Chapter 2. Solution and Fluorescence Properties of Symmetric Dipicolylamine-Containing Dichlorofluorescein-Based Zn^{2+} Sensors

The syntheses of five new analogues of the 2′,7′-dichlorofluorescein-based Zn^{2+} sensor Zinpyr-1 (ZP1) are reported. Analysis of these fluorophores by absorption and emission spectroscopy, in combination with potentiometric titrations, produced a detailed molecular picture of the Zn^{2+} and H^{+} binding properties of the ZP1 family of sensors. The

two separate N_3O donor atom sets on ZP1 converge to form binding pockets in which all four heteroatoms participate in coordination to either Zn^{2+} or protons. The position of the pyridyl group nitrogen atom, 2-pyridyl or 4-pyridyl, has a large impact on the fluorescence response of the dyes to protons in spite of relatively small changes in pK_a values. Despite the structural complexity of ZP1, we provide evidence that the pyridyl arms of the DPA appendages participate in the quenching process, in addition to the contribution from the tertiary nitrogen amine atom. Potentiometric titrations reveal ZP1 dissociation constants (K_d) for Zn^{2+} of 0.04 pM and 1.2 nM for binding to the first and second binding pockets of the ligand, respectively, the second of which correlates with the value observed by fluorescence titration.

Chapter 3. Subtle Modification of 2,2-Dipicolylamine Lowers the Affinity and Improves the Turn-On of Zn(II)-Selective Fluorescent Sensors

The spectroscopic and proton- and Zn(II)-binding properties of two new members of the Zinpyr family of fluorescent sensors are reported. In ZP1B and ZP3B, a (2-picolyl)(4-picolyl)amine (2,4-DPA) moiety is installed in place of the di(2-picolyl)amine (2,2-DPA) ligand used in the parent sensors ZP1 and ZP3. This modification has the benefit of both lowering the proton-induced turn-on at physiological pH levels and altering the Zn(II) affinity so as to detect only the most concentrated stores of this ion in biological samples. Comparison of the proton affinities of all four sensors, as determined by potentiometric titrations, contributes to our understanding of the solution properties of this family of sensors.

Chapter 4. Labeling of the Cell Membrane with Fluorescent Sensors to Track Extracellular Zn(II)

With the goal of labeling the plasma membrane of living cells to track fluctuations in extracellular Zn(II), the sulfosuccinimidyl ester of Zinpyr-1, ZP1ss, was synthesized. Incubation of HeLa cells with this probe does result in fluorescent labeling of the cell surface but no response to exogenous Zn(II) was observed. Partial syntheses of potentially more sensitive versions of ZP1ss are also reported.

Appendix 1. Synthesis of Components for the Construction of Tethered Zn(II)-Responsive Fluorophores

This appendix describes efforts to synthesize membrane-targeted fluorescent Zn(II) sensors based on two different coupling partners for azide-bearing cellular components. Zinpyr derivatives with a water-soluble amine tethering group were synthesized as precursors to the final phosphine and strained cyclooctyne constructs. The reported compounds should serve as useful synthons for future studies in probe localization.

Appendix 2. Miscellaneous NMR Spectra

Thesis Supervisor: Professor Stephen J. Lippard

Title: Arthur Amos Noyes Professor of Chemistry

For all who have come before

Acknowledgments

Although it is tempting to isolate these last five years as a distinct experience, concentrating on those individuals who have only recently come into my life, I find that I am compelled to reflect upon the full course of events that have led me to this moment. Many people have contributed to the tapestry of my life, influencing its pattern in ways both fundamental and subtle. I cannot name them all here but there are those who cannot be overlooked.

My educational and personal influences cannot be easily separated, as I am told that my brother, David, taught me both the alphabet and basic arithmetic before I entered kindergarten. He also expanded the horizons of his introverted sibling, as I grafted onto many of his interests, from Monty Python to RPGs to awesome rock music, although I will never get used to the Grateful Dead. My stepfather, Bill, taught me a lot about the simple pleasures of country life during our years living in the foothills of Northern California. Although we did not have the opportunity to bond much when I was younger, my father, Michael, has steadfastly supported my delayed efforts to complete my schooling.

I was truly fortunate to encounter a number of teachers during my early education who decided to take an interest in and support a rather lackluster student such as myself. Mr. Barhight, Ms. Lehman, and Mr. Gilbert, to name a few, not only helped me through those troublesome teenage years but also acted as fine role models for teaching. It would eventually be another of my teachers, Dennis Fujita, who would awaken my interest in chemistry and start me on the path that I travel to this day. It is due to Dr. Fujita, Gary DeCicco, Fred Martin, Douglas Kuula, Vicki Reed, and the remaining faculty and staff at Santa Rosa Junior College that I came to appreciate the devotion required to construct a truly superior teaching environment. During my short time attending the University of California, Berkeley, I had the privilege of working in the laboratories of Ahamindra Jain and T. Don Tilley, both of whom generously let a student with little research experience work on projects that expanded my skills significantly.

When I think of my first year at MIT, my mind turns to the others that joined me on this crazy ride. Dustin, Meiliana, and Christine were among my earliest friends here, back when I had time for friends. Classmates Simone, Katie, and Erik infiltrated the

Lippard lab with me, carving out our own spaces in each subgroup. Liz shared her lab space with me that first year and made sure I could perform basic fluorescein synthesis. Mi Hee, Lindsey, and Elisa were also members of team fluorescein, taming the great beast to make it light up our cells. Mi Hee and Simone were especially good friends, sharing high times and low. I must also acknowledge my deskmates Christy, Ryan, Mike, and Yongwon for putting up with me all these years.

I would like to thank the members of my thesis committee, starting with Professor Cummins. Although demanding, I found his course in main group chemistry stimulating and it opened my eyes to a variety of work to which I had never been exposed. If my efforts at cell labeling were less than successful, I can only blame myself for not taking greater advantage of Professor Ting's knowledge and experience. Of course, I must thank Professor Lippard for taking a chance on a late bloomer like myself and for tolerating my often unyielding personality. Steve's stated goal of tackling questions in bioinorganic chemistry does not allow you to hide behind one or two techniques but, instead, pushes you to expose yourself to a number of analytical methods and learn many laboratory skills and he provides an environment in which that is possible.

I conclude with my most personal acknowledgments. I was raised under the influence of some very strong-willed women, including my grandmother Elizabeth and her sister Gloria, who pampered me unreasonably as a child. As for my mother, Kathleen, I am not sure if she ever knew what to make of her precocious yet dreamy boy. She was unwavering in her encouragement and sometimes threw me into new situations in the hopes of stimulating fresh interests in me but was also ferociously protective, like a mother bear. She was the most important person in my life and although she left us far too early, she must have felt that I could make it the rest of the way on my own. My final years at MIT proved to be personally challenging and I take this opportunity to encourage anyone facing difficult times to take advantage of the free Mental Health Services provided on campus. My counselor Audra Bartz has made all the difference in coping during these troubling times. A final thanks goes to my dear friends Giovanni and Jennifer who have given so much love and support from afar. I'm finally on my way home.

Table of Contents

List of Figures

Chapter 1

Chapter 2

Chapter 4

Appendix 1

Appendix 2

List of Schemes

Chapter 2

Chapter 4

Appendix 1

List of Tables

Chapter 2

Chapter 3

Chapter 1. An Introduction to Fluorescent Zn(II) Sensors and Their Applications in Biological Systems

An introduction to the roles of biological zinc

Zinc is a vital nutrient in all living systems, from microorganisms to humans,[1] and a variety of pathologies are associated with zinc dietary deficiencies.[2] Despite being only the 27th most abundant element in the earth's crust, zinc is the second most abundant d-block metal in humans after iron.[3] Unlike iron, the majority of which is bound to heme units in a few major proteins, zinc is widely distributed throughout all tissues, interacting with hundreds of different proteins in a multitude of catalytic and structural roles.[4,5]

This versatility of function can be attributed to the particular chemical characteristics of the Zn(II) ion. The filled d^{10} valence shell provides no crystal field stabilization energy, permitting greater flexibility in coordination geometry than other first row metals, and its intermediate polarizability allows a diversity of ligand types, depending on functional requirements.[6] In addition, its lack of redox activity enables Zn(II) to function in a variety of enzyme actives sites without promoting radical reactions that could damage crucial substrates such as DNA.[7] Examples of enzymes that utilize zinc are found in each of the six recognized classes of enzymes and include carbonic anhydrase, alcohol dehydrogenase, carboxypeptidase, and RNA polymerase.[3] Besides its capacity to act as a catalytic center, zinc also plays a structural role in numerous proteins containing solvent-isolated, tetrahedral coordination centers. Thousands of distinct "zinc finger" domains have been identified in hundreds of proteins that function as DNA-binding transcription factors.[7]

The requirement for zinc in these systems demands the tight regulation of metal concentrations and availability. There are currently 14 known members of the ZIP family of cation transport proteins that are responsible for translocating Zn(II) into the cytosol of various cell types, either from the extracellular environment or from intracellular stores.[8] Ten ZnT

proteins transport Zn(II) ions in the reverse direction, lowering cytosolic concentrations. Apart from the high-affinity zinc metalloproteins discussed above, many intracellular buffers of zinc can be imagined, so that the levels of "free" intracellular zinc are much lower than the total zinc required by the cell.[9] Perhaps the most important buffer of cellular zinc levels is metallothionein (MT), known as thionein in its apoprotein form.[10,11] Although estimates of free cytosolic zinc generally fall in the fM to pM range due to the large number of available cellular ligands, alterations in the oxidative state of the cell can cause a release of zinc bound by MT. These small Zn(II) transients only raise the concentration to the low nM range, but this level is sufficient for regulatory or apoptotic signaling.[12]

Much higher free or "labile" zinc concentrations were observed in certain tissues over 60 years ago using the organic dye dithizone.[13,14] Later, sample handling and spatial resolution were improved with silver staining techniques.[15] Although these early staining methods revealed only weakly bound populations of the ion, labile zinc also includes more tightly bound but kinetically available stores that can be released through some signaling pathway. It has since been revealed that there are labile zinc populations in several tissues including, but not limited to, pancreas, intestine, prostate, and perhaps most interestingly, brain.

Prominent regions of interest

Brain

Zinc is abundant in brain tissues but histochemically available (labile) zinc makes up only ca. 10% of the total content, the rest belonging to the population tightly associated with proteins.[16] Still, labile zinc is estimated to reach 0.3 mM in the synapse-containing mossy fiber region between the dentate granule cell bodies and the CA3 pyramidal cell bodies in the hippocampus.

Zn(II) is colocalized with the neurotransmitter glutamate in the presynaptic secretory vesicles of these mossy fiber neurons, but not all glutamatergic vesicles contain zinc.[17] This presence of labile zinc in vesicles that excrete a neurotransmitter has led to a great deal of speculation and a number of studies aimed at identifying roles for Zn(II) as a signaling agent.[16-18]

Three general categories of Zn(II)-based signaling in neuronal cells have been outlined.[14] First, zinc can act as a traditional neurotransmitter upon release into the synapse, modulating the response of various postsynaptic membrane receptors.[19-22] Second, extracellular Zn(II) has been observed to translocate into the dendrites or soma of postsynaptic neurons through a variety of ion channels.[23,24] Lastly, free zinc fluctuations within the cell have been connected to neuronal injury and apoptosis, although small transients may serve other signaling functions.[25-27]

Zinc has also been associated with neurodegenerative diseases, most notably Alzheimer's disease (AD) and amyotrophic lateral sclerosis (ALS). Dyshomeostasis of extracellular zinc is partially responsible for formation of the amyloid-β plaques indicative of AD[28] and moderate-affinity Zn(II) chelators have been tested as therapeutic agents for this condition.[29] Mutations in Cu/Zn-superoxide dismutase which result in the loss of Zn(II) from the enzyme and diminishment of superoxide scavenging are known factors in ALS pathology.[30]

Pancreas

Like the mossy fiber axons of the hippocampus, pancreatic β-cells contain zinc-rich secretory vesicles, which contain concentrations of Zn(II) as high as 20 mM.[31,32] Zn(II) is intimately related to both the biosynthesis and storage of insulin in the secretory pathway, playing a structural role in the mature insulin hexamer.[33] Beyond this structural role, zinc coreleased with insulin has been implicated in the normal suppression of glucagon secretion from neighboring α-cells.[34] Pathologically, zinc deficiencies have been connected to both Type 1 and 2 diabetes.[35]

Zinc supplementation is effective in mitigating the symptoms of diabetes in rodent models but there are several proposed routes of action involved.[36] Additionally, upregulation of the zinc transporter ZIP4 has been associated with pancreatic cancer pathogenesis and progression.[37]

Prostate

There is a direct correlation between high cellular zinc levels and healthy prostate. Under normal conditions, Zn(II) is accumulated in the mitochondria where it acts as an inhibitor of aconitase activity.[38] This blockade of the Krebs cycle creates a surplus of citrate, which is excreted in prostatic fluids; moreover, it also reduces the efficiency of ATP production in this gland, suppressing net energy production. Zinc also participates in an apoptotic signaling pathway in malignant cells, inhibiting cell proliferation.[39] Through an as-yet-unknown mechanism, ZIP1 zinc transporter expression is down-regulated in cancerous prostate cells.[40] The resulting decreased Zn(II) uptake leads to increased metabolic consumption of citrate and attenuation of apoptotic signals, conditions supporting malignant cell proliferation. Monitoring altered levels of both citrate and zinc in prostatic fluids has been proposed as a diagnostic test for early detection of prostate cancer.[41,42]

The preceding topics only offer a flavor of the current research areas that involve biological functions of labile zinc. Other areas of active interest include examining the regulation and secretion of zinc in retinal cells[43,44] and the gastrointestinal tract.[45,46] Besides ongoing investigations into these topics, whole new avenues of exploration are being uncovered, such as the interplay between Ca(II) and Zn(II) transients in cardiomyocytes.[47]

Small molecule fluorescent probes for Zn(II)

Analytical techniques for the examination of metalloproteins are manifold and capable of providing a wealth of information such as metal-binding stoichiometry, ligand environment,

redox potentials, reactivity, and kinetics. The fact that Zn(II) is a redox-inactive, spectroscopically silent d^{10} metal is sometimes cited as a barrier to the elucidation of its roles in biology because of the analytical limitations imposed by these properties.[48,49] These limitations are most relevant to species or samples isolated from their cellular environment, however. Like Ca(II), the stability of the Zn(II) ion and its labile nature in a variety of tissues makes its roles as a signaling agent ideally suited for examination in living cells by fluorescence microscopy.

Design parameters for fluorescent probes that are to be used in biological settings are much more restrictive than those for simple cuvette measurements. In practical terms, the sensors must be water-soluble, non-toxic, and, if they are meant to function intracellularly, must display membrane permeability. Ideally, insensitivity to environmental factors such as changes in pH or redox potential should also be features of biological probes. Spectroscopic features should include excitation and emission profiles in the visible or longer wavelengths in order to avoid tissue damage and autofluorescence from cellular components. Intense absorption bands and large dynamic ranges, defined alternatively as increases in either quantum yield or integrated emission, upon analyte binding are also desirable. Finally, selective detection of the desired analyte with an appropriate binding affinity is ideal in order to mitigate contaminating signals and to avoid either saturation of the probe or lack of response due to low concentrations. Selection of an appropriate analyte receptor unit and probe affinity also aids in rapid and reversible binding, improving spatial and temporal detection resolution.

Fluorescent sensors can be divided into a variety of categories built from a wide range of criteria. Here, the small-molecule probes are divided into two major categories: those that exhibit an intensity-based "turn-on" response and those that display a ratiometric shift in their spectral bands. Further subdivisions are based on the known physical mechanisms of fluorescence

response, each of which is briefly described as they arise. Additonally, probes designed from biomolecular platforms are given their own brief section, as they have a direct connection to recent efforts to selectively localize sensor constructs to various subcellular regions.

The following survey of fluorescent sensors for Zn(II) is admittedly limited. Compounds that are least compatible with biological settings are not mentioned. These include those with limited water solubility and high-energy excitation profiles. Also omitted is an entire category of probes with macrocyclic receptor units, as these tend to suffer from a combination of slow metal-binding kinetics and signal interference due to protonation. Finally, repetition was avoided wherever close structural relatives to the presented compounds exhibit similar properties. For more extensive surveys, many excellent reviews of fluorescent sensors selective for both Zn(II) and a variety of other analytes are available.[18,49-52]

Intensity-based, turn-on probes

Quinoline-based sensors

Many categories of Zn(II)-responsive fluorescent sensors were developed from probes initially recognized for their ability to detect Mg(II) or Ca(II). 8-Hydroxyquinoline (8-HQ, **1**, Figure 1.1), also known as oxine, and its derivatives have been recognized as second only to EDTA in terms of importance in their applications in analytical chemistry.[53,54] With the discovery that 8-HQ forms a fluorescent complex with Mg(II), other metal ions were screened and it was noted that Zn(II) binding also induced a fluorescent response from this ligand.[55] Later studies observed that the selectivity of 8-HQ for Zn(II) could be optimized under specific conditions[56,57] and these methods were used to demonstrate the localization of Zn(II) in the granules of human leukocytes as long as 40 years ago.[58] The mechanism of fluorescence increase

upon Zn(II) binding is based on an excited state intramolecular proton transfer (ESIPT), which provides a non-radiative decay path in the absence of a bound metal ion.[59,60] Chelation of Zn(II) is accompanied by deprotonation that prevents this excited-state reaction, activating the fluorescence pathway (Figure 1.1).

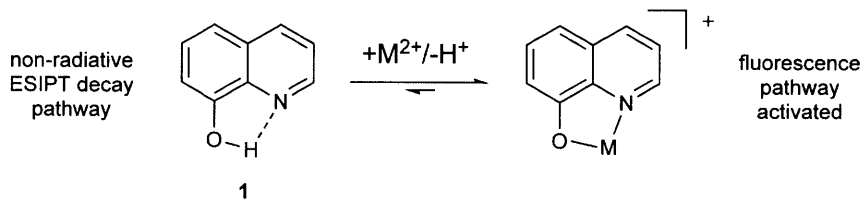

Figure 1.1 Mechanism of 8-HQ fluorescence turn-on

An 8-aminoquinoline derivative, specifically the quinoline sulfonamide **2** (Figure 1.2), found application in detecting Zn(II) distribution in biological tissue around the same time as 8-HQ,[61] but it was several years before this family of compounds started to make a large impact. The commercially available compound TSQ, **3**, was screened against a few 8-HQ derivatives and found to exhibit a large (ca. 100-fold) fluorescence response and excellent selectivity for Zn(II) over both Ca(II) and Mg(II).[62] This sensor is also selective over Cd(II), which commonly interferes with Zn(II) sensors.[52] Zinquin, in its acid and ester forms (**4a,b**), was later developed to improve cell staining and retention properties.[63,64] The related compound, 2-Me-TSQ (**5**), was also synthesized to improve the understanding of the solution properties of this family of sensors.[65] These bidentate ligands form both 1:1 and 2:1 complexes with Zn(II), and the proton- and metal-binding equilibria are challenging to analyze. However, the affinity of these probes for Zn(II) is very high, with detection limits in the pM range.[66] Although the quenching mechanism is not as well characterized as for 8-HQ, a similar ESIPT deactivation pathway is believed to contribute to the low fluorescence of the metal-free aminoquinoline derivatives.[51,65,67]

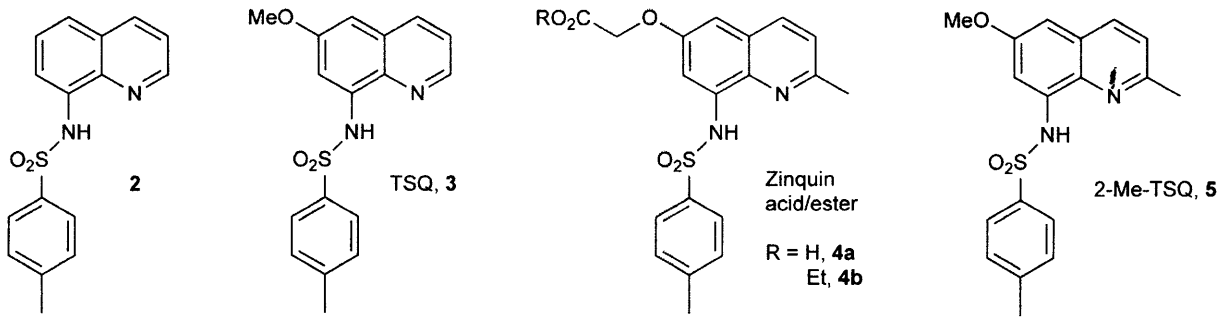

Figure 1.2 Major quinoline sulfonamide Zn(II) sensors

PET-based sensors

Despite the early success of the quinoline-based probes, the rigid platform does not allow for facile modification of either the optical properties or the metal affinity. The most flexible, and therefore the most widely used, design scheme for fluorescent sensors is based on the modular fluorophore-spacer-receptor pattern (Figure 1.3a).[52] Receptor units for cations contain electron-rich donor moieties and, in the absence of the analyte, the excited fluorophore is quenched through a process known as photoinduced electron transfer (PET).[68] With the proviso that the electron donor and acceptor must be properly matched energetically for this quenching mechanism to operate efficiently (Figure 1.3b),[69,70] both the fluorophore and the receptor units can be chosen to fit the specific needs of the system under consideration. The main criterion for the choice of fluorophore is obviously its optical properties, but other design elements, such as those mentioned above, may be considered. The receptor will ideally be selective for the desired analyte and have the desired affinity. Knowledge of coordination chemistry provides a basis for choosing this latter component.

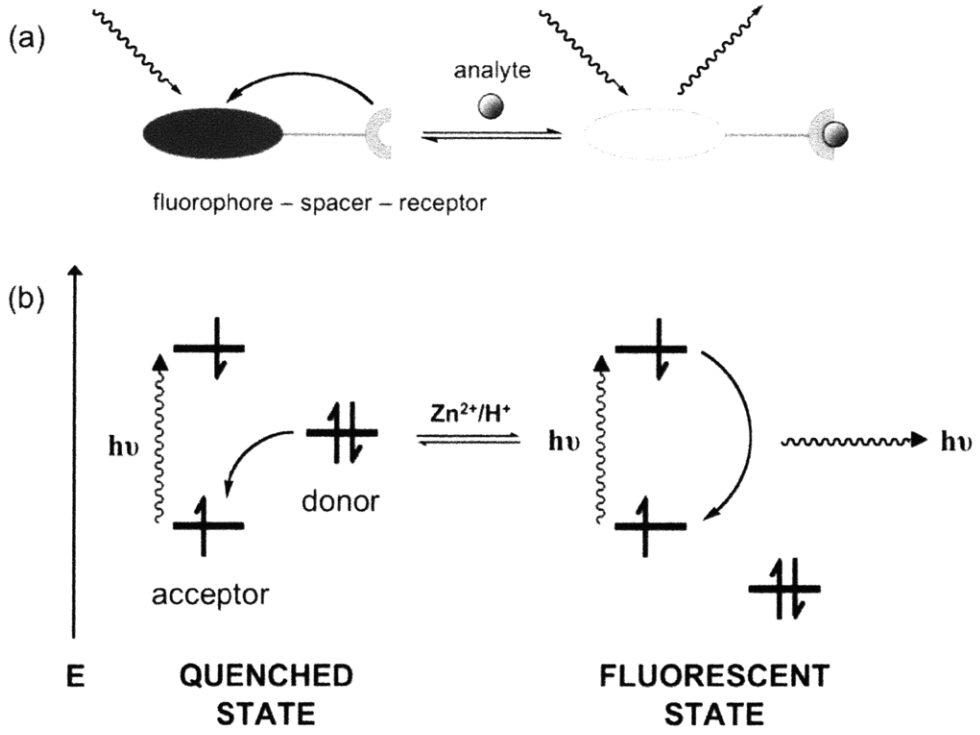

Figure 1.3 PET-based fluorophore-spacer-receptor design (a) and PET mechanism (b)

Like 8-HQ, some PET-based Ca(II) sensors respond to Zn(II)[71,72] and a number of these probes were modified to achieve better selectivity (Figure 1.4). The Fluo family of Ca(II) sensors[73,74] are composed of a fluorescein platform appended with a BAPTA (1,2-bis(o-aminophenoxy)ethane-*N*,*N*,*N*',*N*'-tetraacetic acid) receptor unit. Fluorescein has many benefits as a reporter unit including water solubility, strong absorption and emission in the visible light range, and compatibility with available filter sets for fluorescence microscopy. Removal of one *N*-acetic acid moiety from Fluo-4, **6**, yielded FluoZin-3, **7**, which retains nM affinity for Zn(II) while greatly reducing the affinity for Ca(II). High concentrations of the latter cation will cause significant fluorescence response, however.[75] More extensive truncation of the receptor unit resulted in the probe FluoZin-1, **8**, which has μM Zn(II) affinity but exhibits no response to Ca(II) concentrations up to 100 μM.[71,76] The modularity of PET sensor design was demonstrated by replacing the fluorescein reporter group with rhodamine. The resulting RhodZin probe, **9**,

retains the Zn(II) affinity of FluoZin-1 but redshifts the emission wavelength by ca. 70 nm.[76] Another strategy to drastically modulate the selectivity of the receptor units toward Zn(II) is to remove the 'hard' oxygen atom donors entirely in favor of 'softer' pyridyl donors. Replacement of the BAPTA unit on Calcium Green-1, **10**, with di(2-picolyl)amine (DPA)[77] produced Newport Green DCF, **11**, which has a low affinity for Zn(II) (K_d = 1 μM) but is insensitive to even mM concentrations of Ca(II) and Mg(II), as expected from this ligand.[71,78] However, the extent of fluorescent turn-on of **11** is small compared to that of other sensors.[79]

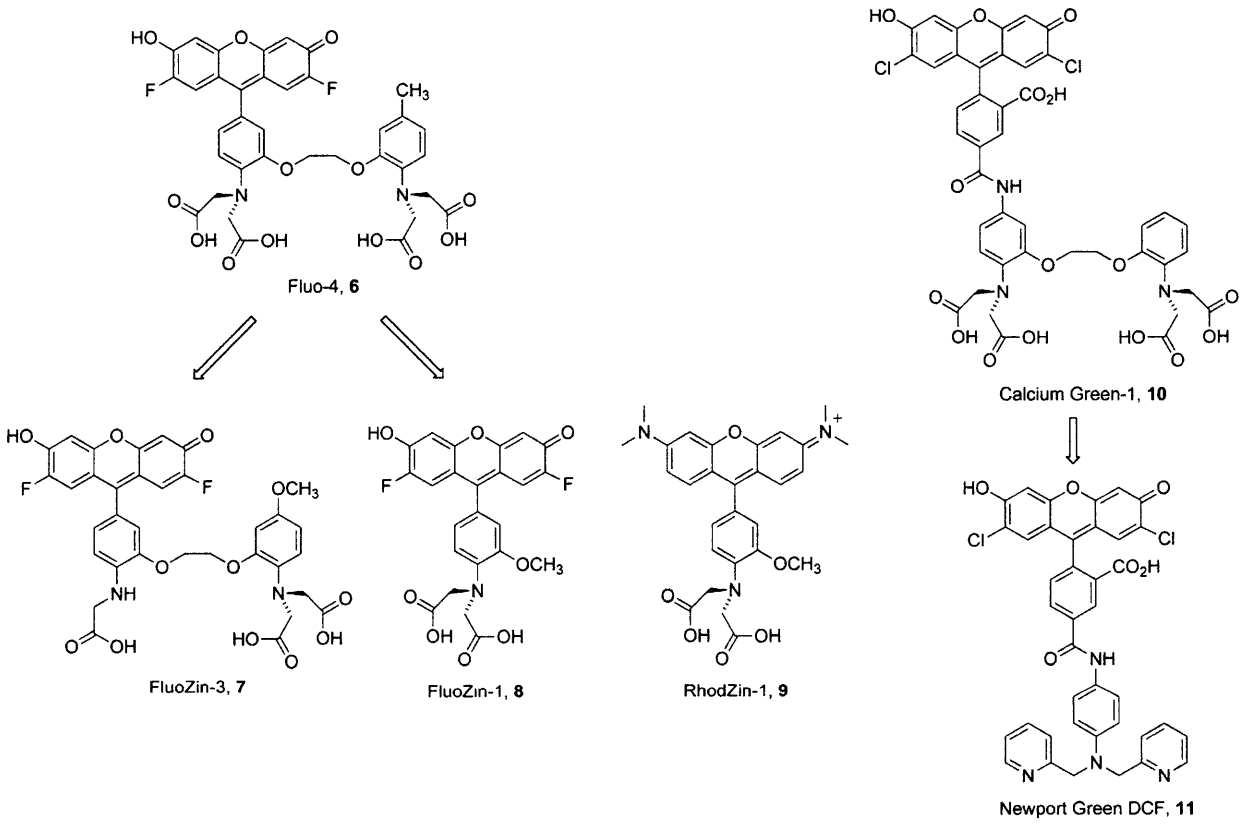

Figure 1.4 Zn(II) sensors developed from "bottom-ring" derivatized Ca(II) sensors

This "bottom-ring" substitution of fluorescein was further developed by the Nagano group, with the synthesis of the ZnAF family of sensors (Figure 1.5). The receptor group of **12a-d** combines DPA with an additional aniline nitrogen atom, resulting in low nM K_d values and good selectivity for Zn(II).[80,81] Further modifications to the binding unit, including addition of steric

bulk on one or both pyridyl rings (**13a,b**), extra methylene units between donor atoms (**14** and **16**), or removal of a picolyl group (**15**) afforded a series of probes with K_d values ranging from 2.7 nM to 0.6 mM.[82] All of these sensors exhibit at least a 10-fold increase in emission quantum yield (Φ) upon saturation with Zn(II), but these values maximize at no higher than 0.38, far from the full quantum yield of the fluorescein platform ($\Phi = 0.95$).[83]

Receptor units have also been attached to the "top" xanthenone moiety of fluorescein, as with the Ca(II) colorimetric probe Calcein, **17** (Figure 1.6).[84] Substitution of the iminodiacetic acid units with DPA yielded the first members of the Zinpyr (ZP) family of Zn(II) sensors, ZP1-3, **18a-c**, which all display similar sub-nM K_d values.[85-87] Unfortunately, sufficiently basic donor atoms within the receptor unit of a PET sensor will bind protons at physiological pH levels, inhibiting the quenching pathway. Although the Zn(II)-saturated Φ values approach that of fluorescein, partial protonation of the DPA units at pH 7 causes the background fluorescence levels to be relatively high, yielding lower dynamic ranges compared to the ZnAFs. Fortunately, the ZP platform is synthetically more amenable to modification and ZP1 has provided a good starting point for improving the properties of these sensors.

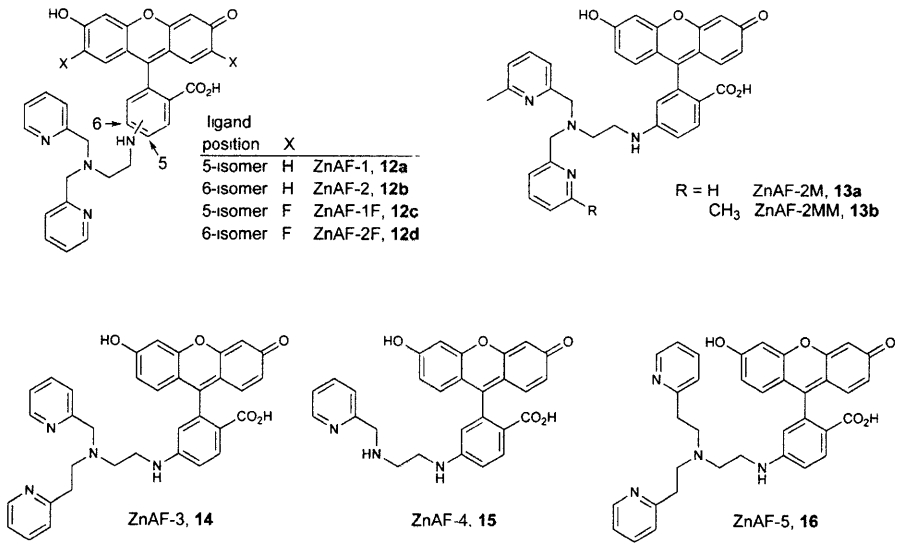

Figure 1.5 ZnAF family of Zn(II) sensors

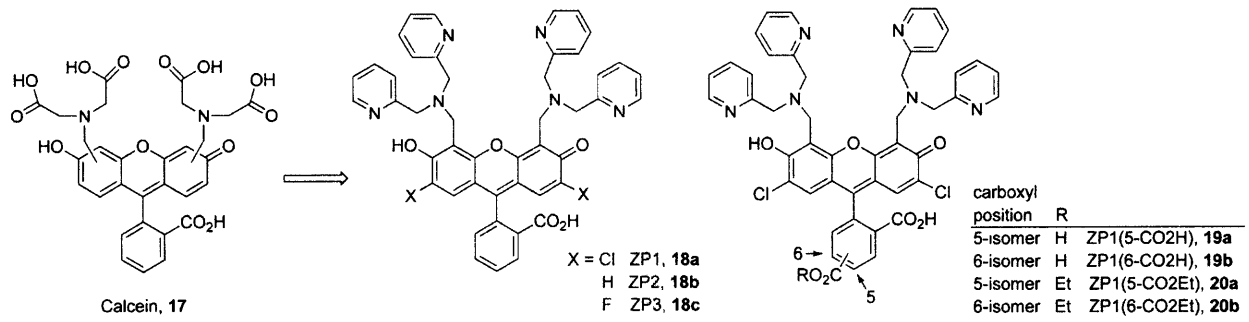

Figure 1.6 First generation of Zinpyr Zn(II) probes based on Ca(II) indicator Calcein

ZP1 is readily cell permeable but addition of carboxylate groups to the bottom ring blocks passage across the cell membrane.[88] Like the Ca(II) probes and their Zn(II)-sensing derivatives mentioned above, esterification of these carboxylate moieties increases permeability and makes the dyes "trappable."[89] After entering the cytosol, the ester groups are hydrolyzed by intracellular esterases, preventing diffusion out of the cell. The carboxylate derivatives of ZP1 and their ethyl esters (**19a,b** and **20a,b**) retain the Zn(II) and proton affinities of the parent sensor, but their use in hippocampal tissue provided better resolution of cells injured by pilocarpine-induced seizures.

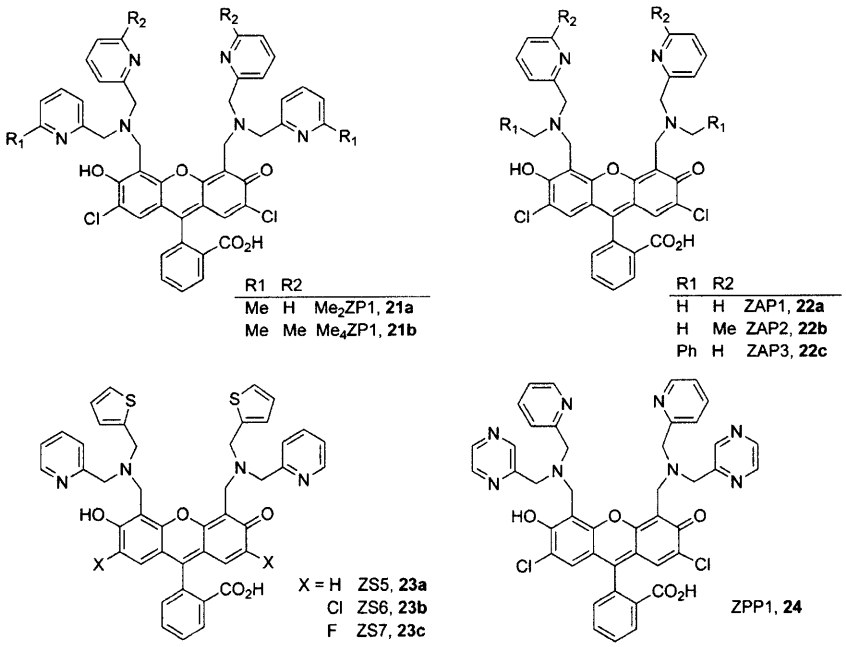

Figure 1.7 Zinpyr-derived Zn(II) sensors with modified receptor units

Efforts to modify the Zn(II) response and binding affinities of the DPA-bearing ZP sensors have followed multiple paths. Like **13a,b**, addition of sterically-hindering methyl groups to the pyridyl rings lowers the Zn(II) affinities compared to the parent compound; K_d = 3.3 nM for **21a** and 630 nM for **21b** (Figure 1.7).[90] Lower affinities are also achieved by substitution of one picolyl group in DPA for a non-coordinating moiety. The ZAP dyes, **22a-c**, have K_d values in the μM range but, due to high receptor group basicities, they are almost entirely turned-on by protons at physiological pH and only respond to Zn(II) at pH ≥ 9.[91] Replacement of a pyridyl unit with a thiophenyl group also lowers the denticity of each binding arm but yields lower proton affinities compared to the ZAP dyes. ZS5-7, **23a-c**, have μM affinities and sufficient turn-on response to visualize cytosolic Zn(II) release from hippocampal cells under nitrosative stress.[92] Lastly, substitution of a pyridyl unit with the more weakly coordinating and less basic pyrazyl ring yields ZPP1, **24**, which maintains nM affinity for Zn(II) but exhibits ca. 3-fold greater turn-on than ZP1.[93] This compound further exhibits the ability to quantify Zn(II) concentrations in biological fluids through a novel protocol.

The Lippard group has also synthesized a series of compounds based on aromatic amine PET receptor units. The first of these asymmetric probes, ZP4 (**25**, Figure 1.8), combines DPA with an aniline group, which acts as the PET switch.[94] Fluorine substitution on the xanthenone unit yields ZP8 (**26**), lowering the proton interference at pH 7 and increasing the Zn(II)-induced turn-on.[95] Replacement of one pyridyl group with a pyrrolyl (**27a**) or N-methylpyrrolyl (**27b**) moiety significantly reduces the Zn(II) affinity without altering the spectroscopic properties.[96] Like the ZnAF probes, which also bear an aniline PET switch and a distal DPA unit, the quantum yields of the apo sensors are quite low and full fluorescein-like emission is not recovered in the Zn(II) complex. The reason for this behavior and the extent of quenching contribution from the pendant

DPA unit remain unresolved. In contrast, the 8-aminoquinoline-appended sensors QZ1 (**28**) and QZ2 (**29**) exhibit very low Φ values in their apo forms and ZP1-like Φ values when saturated with Zn(II), yielding the largest turn-on values (42- and 150-fold, respectively) of sensors from our laboratory.[97] The mid-range μM affinities also allow for a non-saturative response to physiologically relevant levels of labile Zn(II) compared to a tightly binding probe in fluorescence microscopy experiments.

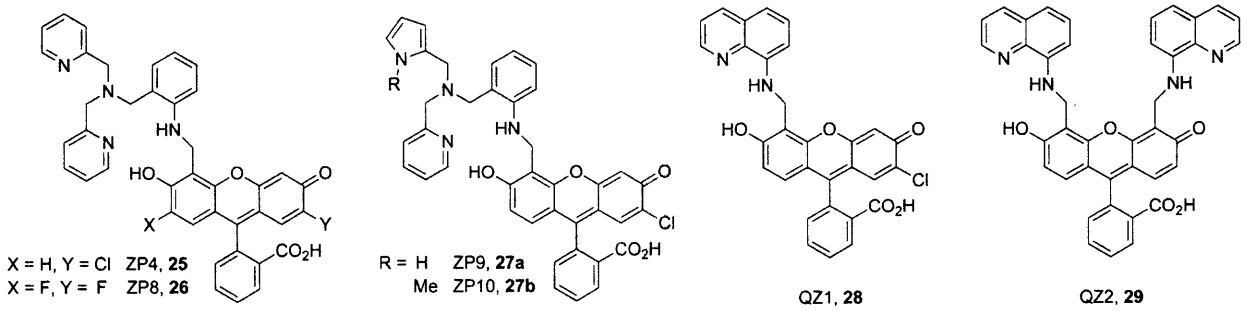

Figure 1.8 Fluorescein-based Zn(II) sensors with aniline- or aminoquinoline-derived receptor units

Just as fluorescein has been appended with a variety of receptor units, the modularity of the PET sensor design has enabled the use of the popular DPA ligand on a number of fluorophore platforms. For example, DPA has been linked to 8-HQ derivatives that lack the hydroxyl proton and therefore behave purely as PET sensors (**30a-d**, Figure 1.9).[98,99] By varying the substituent on the oxygen atom, a range of high Zn(II) affinities (K_d = 0.45 fM to 1.38 nM) was attained; however, the absorption bands fall in the UV range, limiting utility in biological applications. Simple BODIPY derivatives have photophysical characteristics similar to those of fluorescein but are more photostable and relatively insensitive to solvent polarity and pH.[100] Two simple DPA-bearing BODIPY sensors (**31** and **32**) have high affinities and decent selectivities for Zn(II), with 11-fold and 20-fold increases, respectively, in Φ.[101,102] The potential to extend the emission of BODIPY dyes to longer wavelengths increases the value of these initial designs.

Cyanine dyes are common long-wavelength fluorophores, and probe **33** exhibits both near-infrared (NIR) absorption and emission profiles. Despite having a small plateau in proton interference in the physiological pH range, **33** displays a 20-fold turn-on when complexed to Zn(II) at pH 7.4, with K_d = 63 nM.[103] Like NIR dyes, sensors that respond to two-photon excitation are also sought for biological applications. Just one example is **34**, based on the 2-acetyl-6-(dimethylamino)naphthalene fluorophore, coupled to the aniline-DPA receptor unit used previously in the ZnAFs.[104] This sensor yields a 52-fold turn-on response to Zn(II), based on two-photon excitation at 780 nm, and has been used to image endogenous Zn(II) in acute hippocampal tissues slices at a depth of 120 μm.

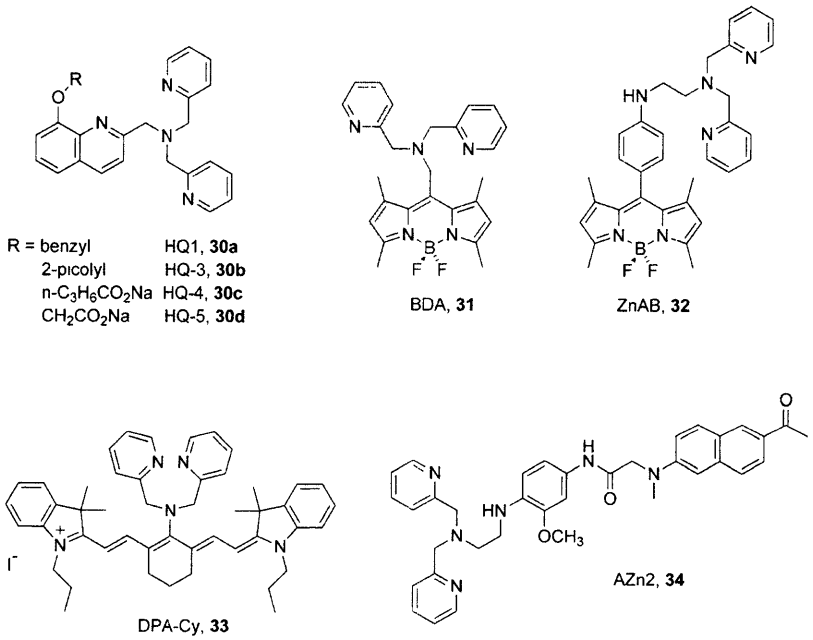

Figure 1.9 Miscellaneous fluorophore platforms utilizing DPA receptor units

Ratiometric probes

Internal charge transfer sensors

All of the top-ring Zinpyr-derived sensors include one or both of the phenolic oxygen atoms of the xanthenone fluorophore in the coordination sphere of the Zn(II) complex. This interaction

results in a slight hypsochromic shift in both absorption and emission upon Zn(II) binding, but the spectroscopic change is insufficiently large to be useful analytically. Larger spectral shifts are possible in sensors that display a pronounced internal charge transfer (ICT) effect. Heteroatom-bearing π-conjugated systems experience a change in polarity, or charge distribution, upon electronic excitation. When a component of the receptor unit is a part of either the donor or acceptor group in this charge transfer process, wavelength shifts in the absorption and/or emission profiles occur upon analyte binding.[52] These spectral changes may result in a useful ratiometric response, which has certain advantages over turn-on fluorescence, such as independence from sensor concentration and minimized effects from sample heterogeneity and instrumental parameters.[49]

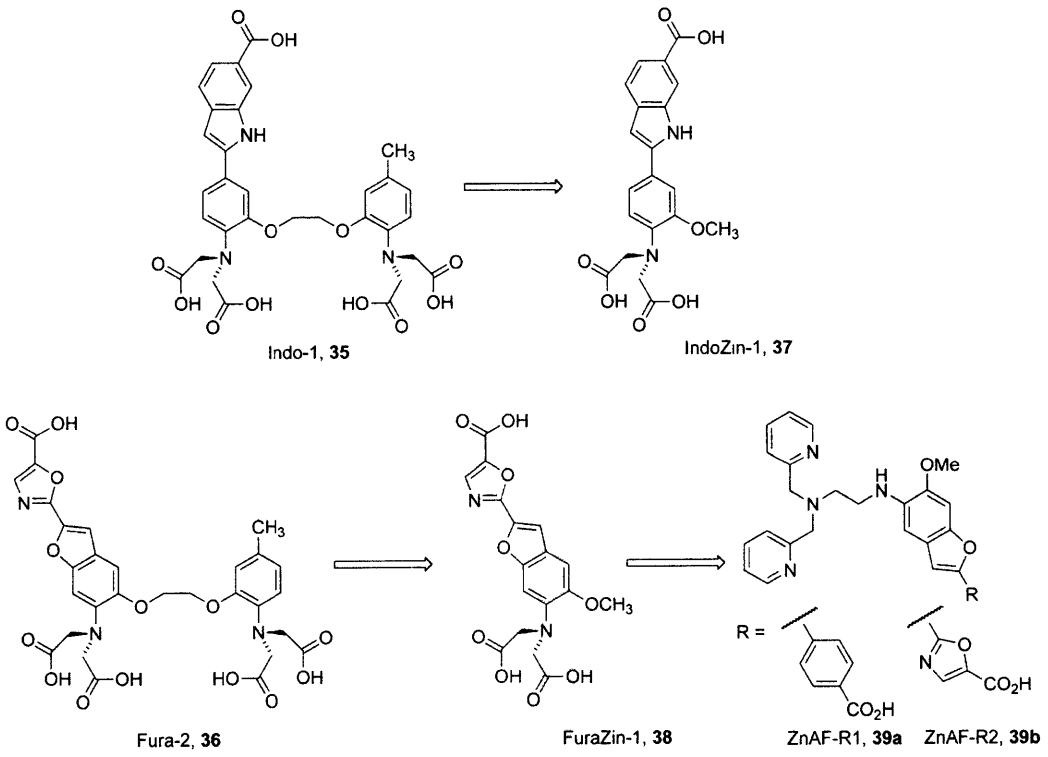

Figure 1.10 ICT Zn(II) sensors developed from Ca(II) sensors

As with the PET-based fluorophores, modification of established Ca(II) and Mg(II) probes yielded some early ICT ratiometric Zn(II) sensors (Figure 1.10). Truncation of the BAPTA

receptor units on Indo-1 (**35**) and Fura-2 (**36**)[105] produced IndoZin-1 (**37**) and FuraZin-1 (**38**), respectively.[76] Both Zn(II) sensors have identical mM affinities, but **37** displays a blueshift in emission, whereas **38** exhibits a blueshift in absorption upon Zn(II)-binding. Nagano added a DPA-based ligand moiety to this platform to produce ZnAF-R1/2 (**39a,b**), which have low nM affinity.[106]

Because the preceding compounds require UV excitation, more recent efforts have focused on producing ICT probes with biologically compatible, longer wavelength absorption. Again, DPA-bearing fluorophores are popular targets. ZnIC (**40**, Figure 1.11) is a very high-affinity sensor (K_d = 1.3 pM) with a fairly small Zn(II)-induced emission shift, but the ratiometric response is sufficient for imaging of endogenous hippocampal zinc.[107] Incorporation of a receptor group donor atom into the ring system of the fluorophore, as with FQ1 (**41**), can yield a dramatic effect on emission wavelength upon Zn(II) binding (ca. 75 nm). However, the reported spectral shift is from a mixed ethanolic:aqueous solution and the effect may not be as pronounced in pure aqueous buffers.[108] Two-photon ICT probes can also be rationally designed based on quantum chemical calculations.[109] Sensor **42** has excellent two-photon excitation properties when coordinated with Zn(II) and a large ratiometric response. As with **41**, these qualities may not be as significant in purely aqueous solvent, the spectral characterization having been performed in ethanol, but both compounds provide promising starting points for future studies.

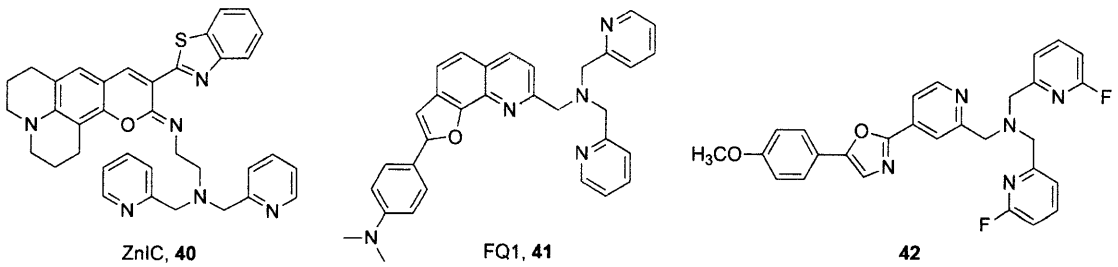

Figure 1.11 Miscellaneous ICT Zn(II) sensors with DPA receptor units

Excited-state intramolecular proton transfer-based sensors

The ESIPT mechanism can also be employed for ratiometric measurements in systems with more extended conjugated systems than the quinoline fluorophores described above. In these cases, the excited state tautomer fluoresces, but emits at longer wavelengths than the Zn(II) complex, in which the proton that participates in ESIPT has been displaced (Figure 1.12). Fahrni's group laid some important groundwork[110] for the application of this mechanism towards Zn(II) sensing and they were able to produce a series of ratiometric probes (**43a-d**, Figure 1.13) with affinities ranging from 0.8 mM to 0.8 pM.[111] Zinbo-5 (**44**) is structurally similar to these compounds but, in contrast, displays a redshift in emission upon Zn(II) binding, a behavior that has not been adequately explored.[112] Each of these ESIPT-based compounds require UV excitation, which limits their use in biological systems, but it may be possible to correct this limitation by extending the π-system of the fluorophores or utilizing two-photon excitation.

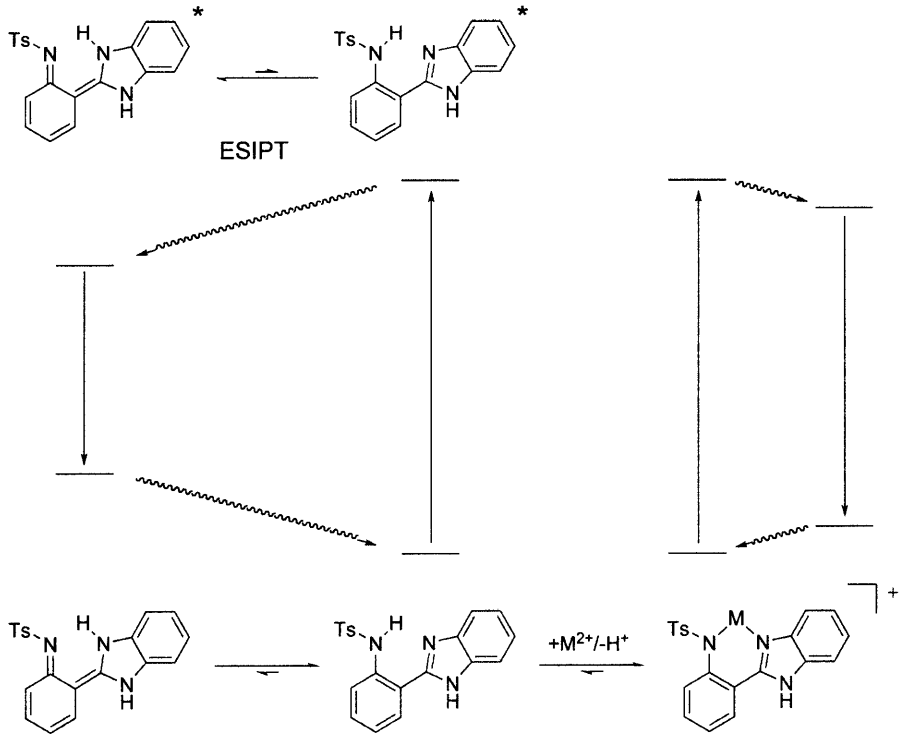

Figure 1.12 ESIPT mechanism

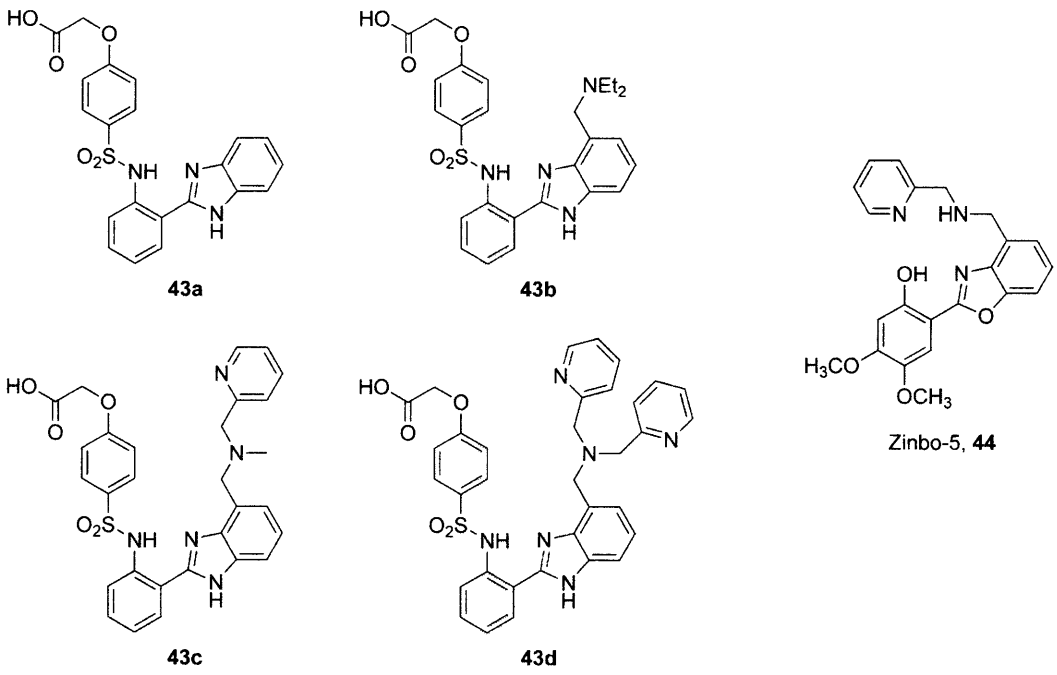

Figure 1.13 ESIPT-based Zn(II) sensors

Additional ratiometric sensors

Two additional ratiometric approaches of note were explored in the Lippard group. The seminaphthofluorescein fluorophore exhibits a blending of optical properties based on its two tautomeric forms. Upon Zn(II) coordination, both the absorption and emission spectra of ZP4 analogue ZNP1 (**45**, Figure 1.14) are dominated by the naphthofluorescein-like features of the phenoxynaphthoquinone tautomer, yielding a large ratiometric response.[113] The CZ1,2 (**46a,b**) systems are composed of a Zn(II)-insensitive coumarin unit tethered to the ZP1 probe.[114,115] The full constructs are very weakly emitting but, upon hydrolysis, fluorescence from both dyes is activated. Low wavelength coumarin emission acts as an internal calibrant of ZP1 concentration, while changes in longer wavelength emission correspond to Zn(II)-induced turn-on. A small ratiometric change was observed in HeLa cells incubated with CZ2, following treatment with zinc-pyrithione.

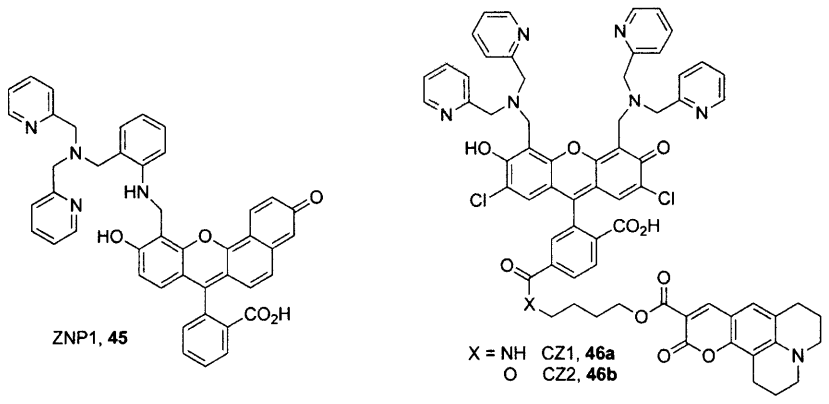

Figure 1.14 Ratiometric Zn(II) sensors based on distinct mechanisms

Fluorescent Probes Based on Biomolecules

Rather than rely on synthetic molecular receptor units for zinc recognition and binding, some research groups were inspired by examples of biomolecules that selectively ligate Zn(II). Extensive work has been performed using variations of the protein carbonic anhydrase (CA) as the Zn(II) receptor platform.[116] Aryl sulfonamides are inhibitors of CA, displacing the exchangeable zinc aqua ligand, and binding of a fluorescent sulfonamide such as dansylamide in the hydrophobic pocket of the holoenzyme causes an increase in emission compared to the unbound fluorophore.[117] Site-directed mutagenesis of human CA II resulted in modulated selectivity and binding rates of the apoenzyme towards Zn(II), as well as tuned affinities to cover a range K_d values from fM to μM.[116] A variety of sulfonamides have been tested as the reporter unit, resulting in different types of fluorescence response, including increases in emission, lifetime, and anisotropy.[51]

The Imperiali group has produced a series of probes consisting of short peptide sequences that incorporate an unnatural fluorescent amino acid based on 8-HQ.[118,119] As with the CA full protein system, the modular nature of peptides allowed for the synthesis of a set of related probes with K_d values ranging from nM to near-μM. Solid-state synthesis of these peptides is more

facile than expression of the CA-based platforms; however, no biological applications were reported.

Peptides have also been used as receptor units for FRET-based Zn(II) sensors, using either synthetic or green fluorescent protein (GFP)-based fluorophores. A zinc finger peptide was appended with fluorescein and lissamine as the donor and acceptor fluorophores, respectively. Although FRET was observed even in the apo probe, the emission bands responded to different extents upon Zn(II) addition, making the system ratiometric with a nM affinity.[120] A system using two AlexaFluor dyes coupled to metallothionein has been reported, but most of the characterization was performed on the Cd(II)-loaded complex.[121] In connection to their work on related "cameleon" Ca(II) indicators,[122] the Tsien group constructed a FRET-based Zn(II) probe consisting of a zinc finger motif bracketed by the modified GFP proteins ECFP and EYFP.1.[123] There was considerable FRET even in the Zn(II)-free construct, but a significant emission ratio change was observed with the addition of 100 μM Zn(II). More recent studies have produced similar protein-based probes with a range of affinities and increased ratiometric response.[124,125]

Applications of fluorescent Zn(II) sensors in biological studies

It is worthwhile to highlight both the effectiveness of Zn(II) probes in biological applications and a selection of the more significant findings concerning the roles of biological zinc that have been uncovered through the use of fluorescent sensing. Early studies with the quinoline probe TSQ helped to improve the protocols used for dithizone and silver staining techniques and to clarify the distributions of labile zinc populations.[16] Fluorescent staining experiments over the intervening 20 years have brought both insight and controversy to this field and much remains to

be learned. The most common areas of study are the brain and pancreas, with several examples following.

Due to the low levels of free zinc in the cytosol of healthy cells of all types, even high-affinity probes tend to illuminate only the labile pools of Zn(II) found in the organelles of certain tissues. Many sensors are tested on cells with no significant labile zinc, instead relying on signals induced by addition of exogenous zinc to prove their biological compatibility. Since the use of TSQ to visualize vesicular zinc in well-defined regions of the hippocampus,[62] this application has been used to test the biological potential of many dyes for imaging endogenous zinc. Significantly, ZnIC has been used for ratiometric imaging in the hippocampus[107] and both ZP3[95] and AZn2[104] have provided two-photon microscopy images of the same region. Staining with ZP4 shows that the duration of incubation can have an effect on the perceived cell permeability of sensors, as short incubation times result in specific staining of neurons damaged by seizure induction[94] but longer incubation times in healthy tissue yield normal staining patterns.[95] Membrane-impermeable probes FluoZin-3 and Newport Green also stain damaged neuronal cells.[126]

Extracellular release and subsequent uptake of hippocampal zinc has also been imaged using a number of sensors. Due to issues relating to sensor concentration, rates of binding, and cation interference, the observed concentration of synaptically released Zn(II) is under debate, but reasonable estimates are in the range of 1-10 μM.[82,127] There are also questions of whether the conditions used to stimulate exocytosis, and therefore the amount of zinc released, are physiologically relevant[128] or whether the addition of a chelating sensor might cause an artificially high amount of zinc to be released from the synaptic vesicles.[129,130] Evidence for zinc translocation into the postsynaptic neuron has been obtained with Newport Green[24] and ZP1,[131]

whereas zinc recycling into the presynaptic neuron cytosol after release was observed using ZnAF-2.[132] Additionally, cytosolic release of Zn(II) from intracellular stores in neuronal cells was detected under conditions of nitrosative stress by both ZS5[92] and FluoZin-3.[133]

Zinc release from isolated pancreatic β-cells has been monitored with impressive spatial and temporal resolution using FluoZin-3.[75] The concentration of Zn(II) released by glucose stimulation of β-cells was also quantified using ZPP1.[93] Mechanisms for zinc uptake into β-cells have been explored using FluoZin-3[134] and a combination of Newport Green and the Ca(II) sensor Fura-2.[135] These studies show that the L-type voltage-gated Ca(II) channel is the main uptake transporter for Zn(II) but that other channels are at work under conditions of low glucose.

Directing fluorescent sensors to biological targets

Labeling of biomolecules with fluorophores

In order to provide more detail about the roles of labile zinc, methods for the subcellular localization of fluorescent probes are desired. Limitations of optical resolution inherent to fluorescent microscopy create barriers to the interpretation of data from many experiments. Freely diffusing sensors can provide ambiguous results, especially with regard to the spatial distribution of mobile zinc populations. Therefore, targeting fluorescent sensors to specific biological targets is an active area of research.

Methods for the fluorescent labeling of proteins, glycans, and nucleic acids are too numerous to properly survey here.[136,137] Instead, a few techniques that have either direct or potential relevance to the targeting of analyte-responsive probes to cellular components are presented. A number of more detailed reviews are also available.[138-141]

Proteins can be modified with short peptide sequences that are either directly reactive with small fluorescent tags or act as substrates for enzymatic modification. Examples of the first type include tetracysteine labels that are reactive with biarsenical dyes such as FlAsH[142] or its multihued descendents.[143,144] Also, polyhistidine sequences form binding sites for Ni(II)-nitrilotriacetic acid (NTA) complexes. The NTA moiety has been linked to dichlorofluorescein[145] and rhodamine-based[146] dyes to label plasma membrane proteins. Acceptor peptide (AP) sequences provide labeling sites on proteins for enzymatic ligation to small chemical tags. Examples of this type from the Ting group include a biotin ligase AP, which becomes modified by either biotin or a biotin-derived ketone for coupling to streptavidin conjugates[147,148] or hydrazide derivatives,[149] respectively. Alternatively, an AP for lipoic acid ligase can be modified with an azide unit for coupling to alkyne conjugates.[150]

Azide moieties can also be directed to the plasma membrane by supplying cells with artificial azido-bearing sugars. The sugars are processed through the normal metabolic machinery of the cell and expressed as covalently bound sialic acid residues on surface glycans. These azides can act as bioorthogonal coupling partners to either specially designed phosphines[151] or strained cyclooctynes.[152,153]

Another type of protein-labeling protocol involves fusing a protein of interest with an enzyme that forms a covalent bond with its substrate. The substrate is labeled with a fluorescent tag, which becomes attached to the protein construct. An example of this type of system is the O^6-alkylguanine-DNA alkyltransferase (AGT) enzyme, which reacts with a benzylguanine-bound probe.[154] This system has been used for multicolor imaging of different regions of a single cell.[155]

Potential lessons from targeted Ca(II) sensors

As with the small-molecule systems above, advances in Ca(II) sensing technology are relevant to developing improved methods for biological Zn(II) detection. The previously mentioned cameleon indicators for Ca(II) are based on variants of GFP which are linked by calmodulin and calmodulin-binding peptide domains.[122] Upon Ca(II) binding, conformational changes in the linker domains bring the fluorescent protein domains within range for FRET. The first generation of cameleons were successfully directed to the cytosol, nucleus, and lumen of the endoplasmic reticulum by genetic expression in HeLa cells. A wide range of related probes are now available with varied binding affinities, spectral responses, and targetability.[123,156]

Tsien's group has also used their FlAsH system to construct a Ca(II)-sensitive probe that can be directed to specific tetracysteine-labeled proteins.[157] The biarsenical dye is based on Calcium Green-1 (**10**) which, being a small-molecule sensor, exhibits faster responses than the large, protein-based systems. Labeling of cell-connecting gap junction proteins and L-type calcium channels resulted in imaging of stimulus-induced cytosolic Ca(II) transients. The temporal resolution was sufficient to acquire video imaging of these transients.

Targeted Zn(II) sensors

Our laboratory has had success using a protocol for targeting Zn(II) sensors to cellular components based on the AGT system mentioned above. HeLa cells were transfected with organelle-directed AGT fusion proteins and application of a ZP1-benzylguanine construct resulted in programmed labeling of either the mitochondria or Golgi apparatus.[158] Images of Zn(II)-induced fluorescence turn-on were qualitative in nature, but the modular character of the probe allows for multiple paths to improve the system. Other cellular compartments are also being targeted.

Another method that promises to have general utility in the detection of extracellular zinc release is not based on targeting to a cellular structure. Instead, ZnAF-2 was covalently attached to specially prepared glass slides, on which pancreatic β-cells, grown on a polycarbonate membrane, were placed. A clear increase in fluorescence was observed upon glucose-induced stimulation of the cells.[159] Improvements in spatial resolution and turn-on are necessary, but there is room to optimize this system.

Most recently, fluorescent protein-based FRET sensors, related to Tsien's cameleon indicators have been designed as cell-expressible constructs. Similar to the earlier example,[123] a zinc finger domain is bracketed by two fluorescent proteins, CFP and YFP, resulting in FRET and a measureable ratiometric response upon Zn(II) binding.[160] These probes were directed to the cytosol and mitochondrial matrix, as well as being anchored to the extracellular membrane of HeLa cells. In addition, expression of sensor in the mitochondria of hippocampal neurons revealed glutamate-induced fluctuations in zinc levels.

Concluding remarks and prospectus

The localization and function of labile zinc in biological systems are topics of great interest. Despite the extensive work devoted to understanding the roles of zinc as a cellular signaling agent, there remains much to be discovered. One of the most powerful tools used in these studies is fluorescence microscopy. Although many Zn(II)-responsive fluorescent sensors have been developed, no one probe is appropriate for all systems. Detailed analyses of the properties and limitations of these sensors inform the rational design of new compounds and new protocols for their use in biochemical studies.

The research reported in this thesis continues the previous efforts in our laboratory to understand the basic chemical properties of fluorescent Zn(II) sensors. Chapter 2 focuses on the detailed solution properties of the Zinpyr family of sensors and Chapter 3 describes the function of two new sensors having decreased sensitivity to protons at physiological pH levels and improved dynamic ranges. Chapter 4 reports progress toward labeling cell membranes with Zn(II)-responsive fluorophores and Appendix 1 describes the synthesis of a number of compounds that should be helpful as synthons for future cell labeling work.

References

(1) Vallee, B. L. In *Zinc Enzymes*; Bertini, I., Luchinat, C., Maret, W., Zeppezauer, M., Eds.; Birkhäuser: Boston, 1986.

(2) Hambridge, M. *J. Nutr.* **2000**, *130*, 1344S-1349S.

(3) Vallee, B. L.; Falchuk, K. H. *Physiol. Rev.* **1993**, *73*, 79-118.

(4) Coleman, J. E. *Annu. Rev. Biochem.* **1992**, *61*, 897-946.

(5) McCall, K. A.; Huang, C.; Fierke, C. A. *J. Nutr.* **2000**, *130*, 1437S-1446S.

(6) Lipscomb, W. N.; Sträter, N. *Chem. Rev.* **1996**, *96*, 2375-2433.

(7) Berg, J. M.; Shi, Y. *Science* **1996**, *271*, 1081-1085.

(8) Lichten, L. A.; Cousins, R. J. *Annu. Rev. Nutr.* **2009**, *29*, 1-24.

(9) Finney, L. A.; O'Halloran, T. V. *Science* **2003**, *300*, 931-936.

(10) Maret, W.; Krezel, A. *Mol. Med.* **2007**, *13*, 371-375.

(11) Rana, U.; Kothinti, R.; Meeusen, J.; Tabatabai, N. M.; Krezoski, S.; Petering, D. H. *J. Inorg. Biochem.* **2008**, *102*, 489-499.

(12) Krezel, A.; Maret, W. *J. Biol. Inorg. Chem.* **2006**, *11*, 1049-1062.

(13) McNary, W. F., Jr. *J. Histochem. Cytochem.* **1954**, *2*, 185-194.

(14) Frederickson, C. J.; Bush, A. I. *BioMetals* **2001**, *14*, 353-366.

(15) Danscher, G.; Stoltenberg, M.; Bruhn, M.; Sondergaard, C.; Jensen, D. *J. Histochem. Cytochem.* **2004**, *52*, 1619-1625.

(16) Frederickson, C. J. *Int. Rev. Neurobiol.* **1989**, *31*, 145-238.

(17) Frederickson, C. J.; Koh, J.-Y.; Bush, A. I. *Nat. Rev. Neurosci.* **2005**, *6*, 449-462.

(18) Chang, C. J.; Lippard, S. J. In *Neurodegenerative diseases and metal ions*; Siegl, A., Siegl, H., Sigel, R. K. O., Eds.; Wiley: Hoboken, NJ, 2006.

(19) Smart, T. G.; Hosie, A. M.; Miller, P. S. *Neuroscientist* **2004**, *10*, 432-442.

(20) Vogt, K.; Mellor, J.; Tong, G.; Nicoll, R. *Neuron* **2000**, *26*, 187-196.

(21) Hirzel, K.; Müller, U.; Latal, A. T.; Hülsmann, S.; Grudzinska, J.; Seeliger, M. W.; Betz, H.; Laube, B. *Neuron* **2006**, *52*, 679-690.

(22) Huang, Y. Z.; Pan, E.; Xiong, Z.-Q.; McNamara, J. O. *Neuron* **2008**, *57*, 546-558.

(23) Sheline, C. T.; Ying, H. S.; Ling, C. S.; Canzoniero, L. M. T.; Choi, D. W. *Neurobiol. Dis.* **2002**, *10*, 41-53.

(24) Li, Y.; Hough, C. J.; Suh, S. W.; Sarvey, J. M.; Frederickson, C. J. *J. Neurophysiol.* **2001**, *86*, 2597-2604.

(25) Frederickson, C. J.; Maret, W.; Cuajungco, M. P. *Neuroscientist* **2004**, *10*, 18-25.

(26) Côté, A.; Chiasson, M.; Peralta, M. R., III; Lafortune, K.; Pellegrini, L.; Tóth, K. *J. Physiol.* **2005**, *566*, 821-837.

(27) Galasso, S. L.; Dyck, R. H. *Mol. Med.* **2007**, *13*, 380-387.

(28) Huang, X.; Atwood, C. S.; Moir, R. D.; Hartshorn, M. A.; Vonsattel, J.-P.; Tanzi, R. E.; Bush, A. I. *J. Biol. Chem.* **1997**, *272*, 26464-26470.

(29) Adlard, P. A.; Cherny, R. A.; Finkelstein, D. I.; Gautier, E.; Robb, E.; Cortes, M.; Volitakis, I.; Liu, X.; Smith, J. P.; Perez, K.; Laughton, K.; Li, Q.-X.; Charman, S. A.; Nicolazzo, J. A.; Wilkins, S.; Deleva, K.; Lynch, T.; Kok, G.; Ritchie, C. W.; Tanzi, R. E.; Cappai, R.; Masters, C. L.; Barnham, K. J.; Bush, A. I. *Neuron* **2008**, *59*, 43-55.

(30) Estévez, A. G.; Crow, J. P.; Sampson, J. B.; Reiter, C.; Zhuang, Y.; Richardson, G. J.; Tarpey, M. M.; Barbeito, L.; Beckman, J. S. *Science* **1999**, *286*, 2498-2500.

(31) Hutton, J. C.; Penn, E. J.; Peshavaria, M. *Biochem. J.* **1983**, *210*, 297-305.

(32) Foster, M. C.; Leapman, R. D.; Li, M. X.; Atwater, I. *Biophys. J.* **1993**, *64*, 525-532.

(33) Dodson, G.; Steiner, D. *Curr. Opin. Struct. Biol.* **1998**, *8*, 189-194.

(34) Ishihara, H.; Maechler, P.; Gjinovci, A.; Herrera, P.-L.; Wollheim, C. B. *Nat. Cell Biol.* **2003**, *5*, 330-335.

(35) Chausmer, A. B. *J. Am. Coll. Nutr.* **1998**, *17*, 109-115.

(36) Taylor, C. G. *BioMetals* **2005**, *18*, 305-312.

(37) Li, M.; Zhang, Y.; Liu, Z.; Bharadwaj, U.; Wang, H.; Wang, X.; Zhang, S.; Liuzzi, J. P.; Chang, S.-M.; Cousins, R. J.; Fisher, W. E.; Brunicardi, F. C.; Logsdon, C. D.; Chen, C.; Yao, Q. *Proc. Natl. Acad. Sci. USA* **2007**, *104*, 18636-18641.

(38) Costello, L. C.; Liu, Y.; Franklin, R. B.; Kennedy, M. C. *J. Biol. Chem.* **1997**, *272*, 28875-28881.

(39) Franklin, R. B.; Costello, L. C. *Arch. Biochem. Biophys.* **2007**, *463*, 211-217.

(40) Franklin, R. B.; Feng, P.; Milon, B.; Desouki, M. M.; Singh, K. K.; Kajdacsy-Balla, A.; Bagasra, O.; Costello, L. C. *Mol. Cancer* **2005**, *4*, 32.

(41) Costello, L. C.; Franklin, R. B. *Prostate Cancer Prostatic Dis.* **2009**, *12*, 17-24.

(42) Cortesi, M.; Chechik, R.; Breskin, A.; Vartsky, D.; Ramon, J.; Raviv, G.; Volkov, A.; Fridman, E. *Phys. Med. Biol.* **2009**, *54*, 781-796.

(43) Redenti, S.; Chappell, R. L. *Mol. Med.* **2007**, *13*, 376-379.

(44) Redenti, S.; Ripps, H.; Chappell, R. L. *Exp. Eye Res.* **2007**, *85*, 580-584.

(45) Giblin, L. J.; Chang, C. J.; Bentley, A. F.; Frederickson, C.; Lippard, S. J.; Frederickson, C. J. *J. Histochem. Cytochem.* **2006**, *54*, 311-316.

(46) Faa, G.; Nurchi, V. M.; Ravarino, A.; Fanni, D.; Nemolato, S.; Gerosa, C.; Van Eyken, P.; Geboes, K. *Coord. Chem. Rev.* **2008**, *252*, 1257-1269.

(47) Palmer, B. M.; Vogt, S.; Chen, Z.; Lachapelle, R. R.; LeWinter, M. M. *J. Struct. Biol.* **2006**, *155*, 12-21.

(48) Lim, N. C.; Freake, H. C.; Brückner, C. *Chem. Eur. J.* **2005**, *11*, 38-49.

(49) Que, E. L.; Domaille, D. W.; Chang, C. J. *Chem. Rev.* **2008**, *108*, 1517-1549.

(50) Kikuchi, K.; Komatsu, K.; Nagano, T. *Curr. Opin. Chem. Biol.* **2004**, *8*, 182-191.

(51) Jiang, P.; Guo, Z. *Coord. Chem. Rev.* **2004**, *248*, 205-229.

(52) Callan, J. F.; de Silva, A. P.; Magri, D. C. *Tetrahedron* **2005**, *61*, 8551-8588.

(53) Hollingshead, R. G. W. *Oxine and Its Derivatives*; Butterworths Scientific Publications: London, 1954; Vol. 1.

(54) Soroka, K.; Vithanage, R. S.; Phillips, D. A.; Walker, B.; Dasgupta, P. K. *Anal. Chem.* **1987**, *59*, 629-636.

(55) Schachter, D. *J. Lab. Clin. Med.* **1959**, *54*, 763-768.

(56) Watanabe, S.; Frantz, W.; Trottier, D. *Anal. Biochem.* **1963**, *5*, 345-359.

(57) Mahanand, D.; Houck, J. C. *Clin. Chem.* **1968**, *14*, 6-11.

(58) Smith, G. L.; Jenkins, R. A.; Gough, J. F. *J. Histochem. Cytochem.* **1969**, *17*, 749-750.

(59) Bardez, E.; Devol, I.; Larrey, B.; Valeur, B. *J. Phys. Chem. B* **1997**, *101*, 7786-7793.

(60) Launay, F.; Alain, V.; Destandau, É.; Ramos, N.; Bardez, É.; Baret, P.; Pierre, J.-L. *New. J. Chem.* **2001**, *25*, 1269-1280.

(61) Toroptsev, I. V.; Eshchenko, V. A. *Bull. Exp. Biol. Med.* **1971**, *72*, 968-970.

(62) Frederickson, C. J.; Kasarskis, E. J.; Ringo, D.; Frederickson, R. E. *J. Neurosci. Meth.* **1987**, *20*, 91-103.

(63) Zalewski, P. D.; Millard, S. H.; Forbes, I. J.; Kapaniris, O.; Slavotinek, A.; Betts, W. H.; Ward, A. D.; Lincoln, S. F.; Mahadevan, I. *J. Histochem. Cytochem.* **1994**, *42*, 877-884.

(64) Hendrickson, K. M.; Rodopoulos, T.; Pittet, P.-A.; Mahadevan, I.; Lincoln, S. F.; Ward, A. D.; Kurucsev, T.; Duckworth, P. A.; Forbes, I. J.; Zalewski, P. D.; Betts, W. H. *J. Chem. Soc., Dalton Trans.* **1997**, 3879-3882.

(65) Nasir, M. S.; Fahrni, C. J.; Suhy, D. A.; Kolodsick, K. J.; Singer, C. P.; O'Halloran, T. V. *J. Biol. Inorg. Chem.* **1999**, *4*, 775-783.

(66) Fahrni, C. J.; O'Halloran, T. V. *J. Am. Chem. Soc.* **1999**, *121*, 11448-11458.

(67) Schulman, S. G.; Sanders, L. B. *Anal. Chim. Acta* **1971**, *56*, 83-89.

(68) Chanon, M.; Hawley, M. D.; Fox, M. A. *Photoinduced Electron Transfer*; Elsevier: Amsterdam, 1988; Vol. A.

(69) Rehm, D.; Weller, A. *Isr. J. Chem.* **1970**, *8*, 259-271.

(70) Urano, Y.; Kamiya, M.; Kanda, K.; Ueno, T.; Hirose, K.; Nagano, T. *J. Am. Chem. Soc.* **2005**, *127*, 4888-4894.

(71) Haugland, R. P. *The Handbook: A Guide to Fluorescent Probes and Labeling Technologies*; 10th ed.; Molecular Probes, Inc.: Eugene, OR, 2005.

(72) Martin, J. L.; Stork, C. J.; Li, Y. V. *Cell Calcium* **2006**, *40*, 393-402.

(73) Minta, A.; Kao, J. P. Y.; Tsien, R. Y. *J. Biol. Chem.* **1989**, *264*, 8171-8178.

(74) Gee, K. R.; Brown, K. A.; Chen, W. N.; Bishop-Stewart, J.; Gray, D.; Johnson, I. *Cell Calcium* **2000**, *27*, 97-106.

(75) Gee, K. R.; Zhou, Z.-L.; Qian, W.-J.; Kennedy, R. *J. Am. Chem. Soc.* **2002**, *124*, 776-778.

(76) Gee, K. R.; Zhou, Z.-L.; Ton-That, D.; Sensi, S. L.; Weiss, J. H. *Cell Calcium* **2002**, *31*, 245-251.

(77) Romary, J. K.; Barger, J. D.; Bunds, J. E. *Inorg. Chem.* **1968**, *7*, 1142-1145.

(78) Canzoniero, L. M. T.; Turetsky, D. M.; Choi, D. W. *J. Neurosci.* **1999**, *19*, RC31.

(79) Hirano, T.; Kikuchi, K.; Urano, Y.; Higuchi, T.; Nagano, T. *Angew. Chem. Int. Ed.* **2000**, *39*, 1052-1054.

(80) Hirano, T.; Kikuchi, K.; Urano, Y.; Higuchi, T.; Nagano, T. *J. Am. Chem. Soc.* **2000**, *122*, 12399-12400.

(81) Hirano, T.; Kikuchi, K.; Urano, Y.; Nagano, T. *J. Am. Chem. Soc.* **2002**, *124*, 6555-6562.

(82) Komatsu, K.; Kikuchi, K.; Kojima, H.; Urano, Y.; Nagano, T. *J. Am. Chem. Soc.* **2005**, *127*, 10197-10204.

(83) Brannon, J. H.; Magde, D. *J. Phys. Chem.* **1978**, *82*, 705-709.

(84) Diehl, H.; Ellingboe, J. L. *Anal. Chem.* **1956**, *28*, 882-884.

(85) Walkup, G. K.; Burdette, S. C.; Lippard, S. J.; Tsien, R. Y. *J. Am. Chem. Soc.* **2000**, *122*, 5644-5645.

(86) Burdette, S. C.; Walkup, G. K.; Spingler, B.; Tsien, R. Y.; Lippard, S. J. *J. Am. Chem. Soc.* **2001**, *123*, 7831-7841.

(87) Chang, C. J.; Nolan, E. M.; Jaworski, J.; Burdette, S. C.; Sheng, M.; Lippard, S. J. *Chem. Biol.* **2004**, *11*, 203-210.

(88) Woodroofe, C. C.; Masalha, R.; Barnes, K. R.; Frederickson, C. J.; Lippard, S. J. *Chem. Biol.* **2004**, *11*, 1659-1666.

(89) Tsien, R. Y. *Nature* **1981**, *290*, 527-528.

(90) Goldsmith, C. R.; Lippard, S. J. *Inorg. Chem.* **2006**, *45*, 555-561.

(91) Goldsmith, C. R.; Lippard, S. J. *Inorg. Chem.* **2006**, *45*, 6474-6478.

(92) Nolan, E. M.; Ryu, J. W.; Jaworski, J.; Feazell, R. P.; Sheng, M.; Lippard, S. J. *J. Am. Chem. Soc.* **2006**, *128*, 15517-15528.

(93) Zhang, X.; Hayes, D.; Smith, S. J.; Friedle, S.; Lippard, S. J. *J. Am. Chem. Soc.* **2008**, *130*, 15788-15789.

(94) Burdette, S. C.; Frederickson, C. J.; Bu, W.; Lippard, S. J. *J. Am. Chem. Soc.* **2003**, *125*, 1778-1787.

(95) Chang, C. J.; Nolan, E. M.; Jaworski, J.; Okamoto, K.-I.; Hayashi, Y.; Sheng, M.; Lippard, S. J. *Inorg. Chem.* **2004**, *43*, 6774-6779.

(96) Nolan, E. M.; Jaworski, J.; Racine, M. E.; Sheng, M.; Lippard, S. J. *Inorg. Chem.* **2006**, *45*, 9748-9757.

(97) Nolan, E. M.; Jaworski, J.; Okamoto, K.-I.; Hayashi, Y.; Sheng, M.; Lippard, S. J. *J. Am. Chem. Soc.* **2005**, *127*, 16812-16823.

(98) Wang, H. H.; Gan, Q.; Wang, X.-J.; Xue, L.; Liu, S.-H.; Jiang, H. *Org. Lett.* **2007**, *9*, 4995-4998.

(99) Xue, L.; Wang, H. H.; Wang, X.-J.; Jiang, H. *Inorg. Chem.* **2008**, *47*, 4310-4318.

(100) Loudet, A.; Burgess, K. *Chem. Rev.* **2007**, *107*, 4891-4932.

(101) Wu, Y.; Peng, X.; Guo, B.; Fan, J.; Zhang, Z.; Wang, J.; Cui, A.; Gao, Y. *Org. Biomol. Chem.* **2005**, *3*, 1387-1392.

(102) Koutaka, H.; Kosuge, J.-I.; Fukasaku, N.; Hirano, T.; Kikuchi, K.; Urano, Y.; Kojima, H.; Nagano, T. *Chem. Pharm. Bull.* **2004**, *52*, 700-703.

(103) Tang, B.; Huang, H.; Xu, K.; Tong, L.; Yang, G.; Liu, X.; An, L. *Chem. Commun.* **2006**, 3609-3611.

(104) Kim, H. M.; Seo, M. S.; An, M. J.; Hong, J. H.; Tian, Y. S.; Choi, J. H.; Kwon, O.; Lee, K. J.; Cho, B. R. *Angew. Chem. Int. Ed.* **2008**, *47*, 5167-5170.

(105) Grynkiewicz, G.; Poenie, M.; Tsien, R. Y. *J. Biol. Chem.* **1985**, *260*, 3440-3450.

(106) Maruyama, S.; Kikuchi, K.; Hirano, T.; Urano, Y.; Nagano, T. *J. Am. Chem. Soc.* **2002**, *124*, 10650-10651.

(107) Komatsu, K.; Urano, Y.; Kojima, H.; Nagano, T. *J. Am. Chem. Soc.* **2007**, *129*, 13447-13454.

(108) Xue, L.; Liu, C.; Jiang, H. *Chem. Commun.* **2009**, 1061-1063.

(109) Albota, M.; Beljonne, D.; Brédas, J.-L.; Ehrlich, J. E.; Fu, J.-Y.; Heikal, A. A.; Hess, S. E.; Kogej, T.; Levin, M. D.; Marder, S. R.; McCord-Maughon, D.; Perry, J. W.; Röckel, H.; Rumi, M.; Subramaniam, G.; Webb, W. W.; Wu, X.-L.; Xu, C. *Science* **1998**, *281*, 1653-1656.

(110) Henary, M. M.; Fahrni, C. J. *J. Phys. Chem. A* **2002**, *106*, 5210-5220.

(111) Henary, M. M.; Wu, Y.; Fahrni, C. J. *Chem. Eur. J.* **2004**, *10*, 3015-3025.

(112) Taki, M.; Wolford, J. L.; O'Halloran, T. V. *J. Am. Chem. Soc.* **2004**, *126*, 712-713.

(113) Chang, C. J.; Jaworski, J.; Nolan, E. M.; Sheng, M.; Lippard, S. J. *Proc. Natl. Acad. Sci. USA* **2004**, *101*, 1129-1134.

(114) Woodroofe, C. C.; Lippard, S. J. *J. Am. Chem. Soc.* **2003**, *125*, 11458-11459.

(115) Woodroofe, C. C.; Won, A. C.; Lippard, S. J. *Inorg. Chem.* **2005**, *44*, 3112-3120.

(116) Fierke, C. A.; Thompson, R. B. *BioMetals* **2001**, *14*, 205-222.

(117) Chen, R. F.; Kernohan, J. C. *J. Biol. Chem.* **1967**, *242*, 5813-5823.

(118) Walkup, G. K.; Imperiali, B. *J. Org. Chem.* **1998**, *63*, 6727-6731.

(119) Shults, M. D.; Pearce, D. A.; Imperiali, B. *J. Am. Chem. Soc.* **2003**, *125*, 10591-10597.

(120) Godwin, H. A.; Berg, J. M. *J. Am. Chem. Soc.* **1996**, *118*, 6514-6515.

(121) Hong, S.-H.; Maret, W. *Proc. Natl. Acad. Sci. USA* **2003**, *100*, 2255-2260.

(122) Miyawaki, A.; Llopis, J.; Helm, R.; McCaffery, J. M.; Adams, J. A.; Ikura, M.; Tsien, R. Y. *Nature* **1997**, *388*, 882-887.

(123) Miyawaki, A.; Tsien, R. Y. *Methods Enzymol.* **2000**, *327*, 472-500.

(124) van Dongen, E. M. W. M.; Evers, T. H.; Dekkers, L. M.; Meijer, E. W.; Klomp, L. W. J.; Merkx, M. *J. Am. Chem. Soc.* **2007**, *129*, 3494-3495.

(125) Evers, T. H.; Appelhof, M. A. M.; de Graaf-Heuvelmans, P. T. H. M.; Meijer, E. W.; Merkx, M. *J. Mol. Biol.* **2007**, *374*, 411-425.

(126) Stork, C. J.; Li, Y. V. *J. Neurosci. Meth.* **2006**, *155*, 180-186.

(127) Frederickson, C. J.; Giblin, L. J.; Rengarajan, B.; Masalha, R.; Frederickson, C.; Zeng, Y.; Lopez, E. V.; Koh, J.-Y.; Chorin, U.; Besser, L.; Hershfinkel, M.; Li, Y.; Thompson, R. B.; Krezel, A. *J. Neurosci. Meth.* **2006**, *154*, 19-29.

(128) Qian, J.; Noebels, J. L. *J. Physiol.* **2005**, *566*, 747-758.

(129) Kay, A. R. *J. Neurosci.* **2003**, *23*, 6847-6855.

(130) Kay, A. R. *Trends Neurosci.* **2006**, *29*, 200-206.

(131) Ketterman, J. K.; Li, Y. V. *J. Neurosci. Res.* **2008**, *86*, 422-434.

(132) Minami, A.; Sakurada, N.; Fuke, S.; Kikuchi, K.; Nagano, T.; Oku, N.; Takeda, A. *J. Neurosci. Res.* **2006**, *83*, 167-176.

(133) Lin, W.; Mohandas, B.; Fontaine, C. P.; Colvin, R. A. *BioMetals* **2007**, *20*, 891-901.

(134) Gyulkhandanyan, A. V.; Lee, S. C.; Bikopoulos, G.; Dai, F.; Wheeler, M. B. *J. Biol. Chem.* **2006**, *281*, 9361-9372.

(135) Priel, T.; Hershfinkel, M. *Biochem. Biophys. Res. Commun.* **2006**, *346*, 205-212.

(136) Hermanson, G. T. *Bioconjugate techniques*; Elsevier Academic Press: Boston, 2008.

(137) Aslam, M.; Dent, A. *Bioconjugation: Protein Coupling Techniques for the Biomedical Sciences*; MacMillan Reference Ltd.: London, 1998.

(138) Chen, I.; Ting, A. Y. *Curr. Opin. Biotech.* **2005**, *16*, 35-40.

(139) Marks, K. M.; Nolan, G. P. *Nat. Meth.* **2006**, *3*, 591-596.

(140) O'Hare, H. M.; Johnsson, K.; Gautier, A. *Curr. Opin. Struct. Biol.* **2007**, *17*, 488-494.

(141) Giepmans, B. N. G.; Adams, S. R.; Ellisman, M. H.; Tsien, R. Y. *Science* **2006**, *312*, 217-224.

(142) Griffin, B. A.; Adams, S. R.; Tsien, R. Y. *Science* **1998**, *281*, 269-272.

(143) Martin, B. R.; Giepmans, B. N. G.; Adams, S. R.; Tsien, R. Y. *Nat. Biotech.* **2005**, *23*, 1308-1314.

(144) Bhunia, A. K.; Miller, S. C. *ChemBioChem* **2007**, *8*, 1642-1645.

(145) Goldsmith, C. R.; Jaworski, J.; Sheng, M.; Lippard, S. J. *J. Am. Chem. Soc.* **2006**, *128*, 418-419.

(146) Guignet, E. G.; Hovius, R.; Vogel, H. *Nat. Biotech.* **2004**, *22*, 440-444.

(147) Howarth, M.; Takao, K.; Hayashi, Y.; Ting, A. Y. *Proc. Natl. Acad. Sci. USA* **2005**, *102*, 7583-7588.

(148) Howarth, M.; Ting, A. Y. *Nat. Protocols* **2008**, *3*, 534-545.

(149) Chen, I.; Howarth, M.; Lin, W.; Ting, A. Y. *Nat. Meth.* **2005**, *2*, 99-104.

(150) Fernández-Suarez, M.; Baruah, H.; Martínez-Hernández, L.; Xie, K. T.; Baskin, J. M.; Bertozzi, C. R.; Ting, A. Y. *Nat. Biotech.* **2007**, *25*, 1483-1487.

(151) Saxon, E.; Bertozzi, C. R. *Science* **2000**, *287*, 2007-2010.

(152) Agard, N. J.; Baskin, J. M.; Prescher, J. A.; Lo, A.; Bertozzi, C. R. *ACS Chem. Biol.* **2006**, *1*, 644-648.

(153) Baskin, J. M.; Prescher, J. A.; Laughlin, S. T.; Agard, N. J.; Chang, P. V.; Miller, I. A.; Lo, A.; Codelli, J. A.; Bertozzi, C. R. *Proc. Natl. Acad. Sci. USA* **2007**, *104*, 16793-16797.

(154) Keppler, A.; Gendreizig, S.; Gronemeyer, T.; Pick, H.; Vogel, H.; Johnsson, K. *Nat. Biotech.* **2003**, *21*, 86-89.

(155) Keppler, A.; Pick, H.; Arrivoli, C.; Vogel, H.; Johnsson, K. *Proc. Natl. Acad. Sci. USA* **2004**, *101*, 9955-9959.

(156) Palmer, A. E.; Tsien, R. Y. *Nat. Protocols* **2006**, *1*, 1057-1065.

(157) Tour, O.; Adams, S. R.; Kerr, R. A.; Meijer, R. M.; Sejnowski, T. J.; Tsien, R. W.; Tsien, R. Y. *Nat. Chem. Biol.* **2007**, *3*, 423-431.

(158) Tomat, E.; Nolan, E. M.; Jaworski, J.; Lippard, S. J. *J. Am. Chem. Soc.* **2008**, *130*, 15776-15777.

(159) Crivat, G.; Kikuchi, K.; Nagano, T.; Priel, T.; Hershfinkel, M.; Sekler, I.; Rosenzweig, N.; Rosenzweig, Z. *Anal. Chem.* **2006**, *78*, 5799-5804.

(160) Dittmer, P. J.; Miranda, J. G.; Gorski, J. A.; Palmer, A. E. *J. Biol. Chem.* **2009**, *284*, 16289-16297.

Chapter 2. Solution and Fluorescence Properties of Symmetric Dipicolylamine-Containing Dichlorofluorescein-Based Zn(II) Sensors

Introduction

The past several years have seen substantial growth in the field of ion-selective fluorescence sensing, including the detection of transition metal ions,[1-5] alkali and alkaline earth metal cations,[6,7] protons,[8-10] and anions.[11-13] Because of the biological relevance of these species, many detection efforts have focused on the use of fluorescent sensors in cells and tissues.[14-16] Interest in biological Zn^{2+} is especially high, particularly loosely bound, mobile populations of the ion in various human tissues including, but not limited to, the pancreas,[17,18] intestine,[19,20] retina,[21,22] and brain.[23-26] Although the application of fluorescence-based functional imaging in a biological setting is the ultimate goal, the continued development of improved sensors depends on achieving a thorough understanding of the underlying chemical properties of the available constructs.

Many ion sensors are based on the well-known fluorophore–spacer–receptor design, in which an alkyl spacer separates the fluorescent component from the analyte-binding receptor.[1] "Turn-on" sensors are often described as functioning by means of a photoinduced electron transfer (PET) mechanism,[27] whereby the receptor unit serves as an electron donor in the absence of analyte, quenching the fluorophore excited state. Upon binding of the analyte to the receptor, electron transfer is prevented and the quenching mechanism is blocked. Descriptions of this process are usually qualitative in nature, although some worthy efforts have been directed toward quantifying the energetics of electron transfer by employing redox potentials[28-30] or through theoretical computations.[10,31]

When the receptor component of such a fluorescent sensor is composed of a single heteroatom or small chemical unit, the quenching behavior of the compound is easily identified.[32] One recent study explored the possibility that more distal heteroatoms in a complex

fluorescein derivative might serve as electron donors in the quenching process.[33] In our previous descriptions of sensors bearing the 2,2-dipicolylamine (2,2-DPA) moiety as the receptor, the tertiary nitrogen atom has been cited as the electron donor in the metal-free state;[34] however, some experiments have linked the fluorescence change of related pyridyl-appended sensors at low pH values to protonation of the pyridyl group (Figure 2.1).[9,35] Other reports, using sensors with an extended receptor group that includes 2,2-DPA, ignore any potential quenching contribution from this unit, focusing instead on a more proximal electron donor.[36,37]

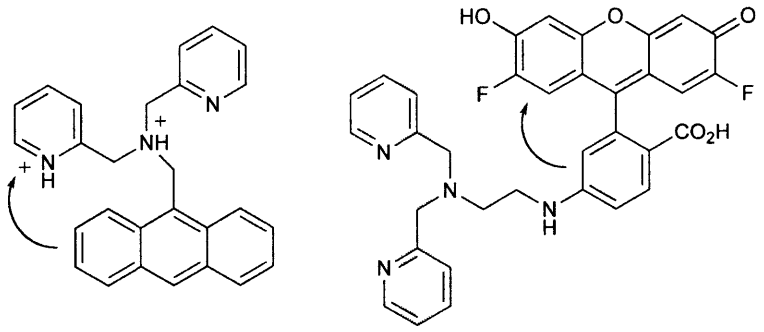

Figure 2.1. Examples of fluorescent sensors with DPA receptors that exhibit a quenching mode other than electron transfer from the tertiary nitrogen atom. (Left) A protonated pyridyl group acts as an electron acceptor from the excited anthracene ring.[9] (Right) Quenching is ascribed to donation from the aminobenzoate group into the fluorophore.[37]

Since the report of our first fluorescent Zn^{2+} sensor, Zinpyr-1 (**1**, Figure 2.2),[38] we have prepared a variety of analogues with a range of receptor units, binding affinities, and fluorescent responses.[39-41] During the same interval, we evaluated their ability to detect labile zinc in cells and neuronal tissue.[42,43] Although many compounds can provide qualitative images of mobile zinc in live cells, it is desirable to identify and quantitate subcellular zinc pools as part of the process of understanding the role of this important metal ion. This goal cannot be realized without thorough knowledge of the fluorescence behavior of the sensors in relation to their ion-binding properties.

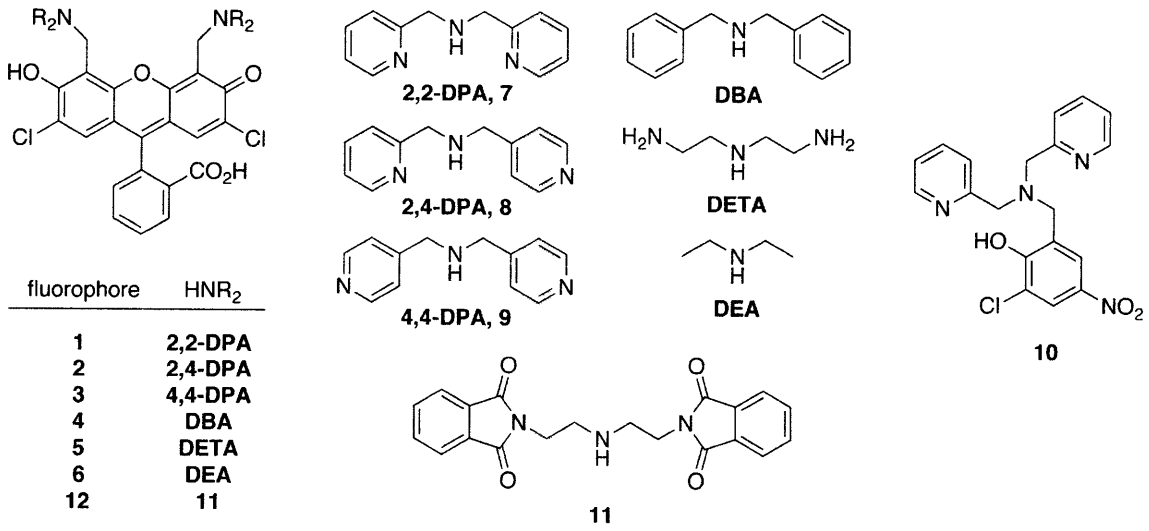

fluorophore	HNR_2
1	2,2-DPA
2	2,4-DPA
3	4,4-DPA
4	DBA
5	DETA
6	DEA
12	11

Figure 2.2. Compounds Studied and Synthetic Precursors

Despite their relative ease of synthesis, symmetrical members of the Zinpyr family of sensors are fairly complex in terms of structure, with two separate metal-binding pockets and several potential protonation sites (Figure 2.2). Although a few properties were identified that led to improvements to reduce proton-based background fluorescence and to tune the Zn^{2+} affinity,[44] a complete understanding of the solution equilibria and photophysical behavior of these compounds is lacking. To address this deficiency, a series of new ZP1 analogues was synthesized, modifying the receptor groups to tune both the proton affinity and contribution to fluorophore quenching. As described here, by using a combination of spectrophotometric and potentiometric pH titration methods, we obtained a complete set of pK_a values for ZP1 and, using this information, have been able to identify the protonated and zinc-bound species in solution responsible for fluorescence turn-on over a wide pH range. This analysis has also led us to revise some previously reported properties of this sensor, including the Zn^{2+} affinity and extent of fluorescence response to increasing equivalents of both Zn^{2+} and protons. The results represent a significant step forward in elucidating the solution chemistry of complex ion-responsive fluorescent probes and provide a paradigm for future work in this area.

Experimental Section

Reagents. 2′,7′-Dichlorofluorescein (DCF) was purchased from Avocado and recrystallized from EtOH before use. Solvents were supplied by Mallinckrodt and used as received. Piperazine-N,N′-bis(2-ethanesulfonic acid) (PIPES) and 99.999% KCl were purchased from Calbiochem. The synthesis of 1,5-bis(phthalimido)-3-azapentane (**11**) was previously described.[45] All other reagents were purchased from Aldrich and used as received.

General Methods. NMR spectra were obtained on a Bruker 400 MHz spectrometer at ambient temperature and referenced to the residual proton resonance of the deuterated solvent. Low-resolution mass spectra were obtained by using an Agilent 1100 series LC/MSD mass spectrometer. High-resolution mass spectra were provided by staff at the MIT Department of Chemistry Instrumentation Facility using a Bruker Daltonics APEXIV 4.7 T FT-ICR mass spectrometer.

Spectroscopic Measurements. Optical absorption spectra were collected with a Cary 1E spectrophotometer, and fluorescence emission spectra were recorded with a Photon Technology International QM-4/2003 fluorometer. Measurements at pH 7.0 were performed in aqueous buffer containing 50 mM PIPES and 100 mM KCl. Solutions for quantum yield measurements under basic conditions contained 0.1 M NaOH with no additional electrolyte. Extinction coefficients were obtained at pH 7.0 using dye solutions in the range 0.1−1.0 μM. All quantum yield measurements were performed with a dye concentration of 0.3 μM, exciting each fluorophore at its wavelength of maximal absorbance. Emission spectra were integrated from 490 to 700 nm after subtracting the signal caused by scattered excitation light. Fluorescence pH titration curves were acquired using a solution containing 10 mM KOH, 100 mM KCl, and 1.0 μM dye, to which were added aliquots of dilute aqueous HCl. Readings at several points between

pH 2 and 10 were recorded using an Orion 720A pH meter. Samples were maintained at 25 ± 1 °C using a circulating water bath for all spectroscopic measurements.

Potentiometric Titrations. A Mettler Toledo T70 automated titrator equipped with a DG-111-SG glass electrode, calibrated against standard buffers, was used for all potentiometric titrations. Solutions were prepared from Millipore water that had been degassed by boiling under low pressure for at least 3 h.[46] Samples were maintained at 25 ± 1 °C by circulating temperature-regulated water through the jacketed titration vessel during all experiments. Initial solutions of ligands **7**–**10** contained 1 mM of the neutral molecule and 3 equiv of HCl. Compounds **1**–**3** (0.6–1 mM) were predissolved in 1 mL of 1.0 M HCl and diluted with water. Samples were titrated with ca. 0.1 M NaOH, which was standardized against potassium hydrogen phthalate before each series of titrations. Analysis of the data was performed by using the HYPERQUAD2006 v3.1.48 computer program.[47] For each compound, the proton dissociation constants (pK_a values) were determined from three separate titrations. The number of protonation equilibria was allowed to vary during the construction of computer models for titrations of **1**–**3**. In each case, the best fit was obtained for a six-proton system. Titrations of **1** and **10** in the presence of 1 equiv of $ZnCl_2$ were used to calculate dissociation constants (K_d values) for Zn^{2+}. The previously determined pK_a values were held constant during refinement of the K_d values. In all cases, the triplicate data sets for each compound were combined for determination of the dissociation constants, which in turn were used to compute theoretical titration curves for comparison with the experimental ones. Titration solutions contained 100 mM KCl as the electrolyte to maintain constant ionic strength, and $\log(K_w)$ was defined as 13.78, which is appropriate for these conditions.[48]

X-ray Crystallographic Studies. Single crystals were coated with paratone-N oil, mounted at room temperature on the tips of glass fibers or nylon loops (Oxford magnetic mounting system), and cooled under a stream of cold N_2 maintained by a KRYO-FLEX low-temperature apparatus. Intensity data were collected on a Bruker APEX CCD diffractometer with graphite-monochromated Mo Kα radiation (λ = 0.71073 Å) controlled by a Pentium-based PC running the SMART software package.[49] A total of 2800 frames were acquired for each measurement. The structures were solved by direct methods and refined on F^2 by using the SHELXTL software.[50,51] Empirical absorption corrections were applied with SADABS,[52] and the structures were checked for higher symmetry with PLATON.[53] All non-hydrogen atoms were refined anisotropically. In general, hydrogen atoms were assigned idealized positions and given thermal parameters equivalent to either 1.5 (methyl hydrogen atoms) or 1.2 (all other hydrogen atoms) times the thermal parameter of the atom to which they were attached. The hydrogen atoms of O1 and O3 of the hydroxyl groups in all three structures were located from the electron density map, respectively, as were the hydrogen atoms of the water molecule in the structure of **1**.

Compound **6** crystallizes without solvent, whereas compound **1** crystallizes with one molecule each of MeCN and water. There are two independent molecules in the asymmetric unit of crystalline **2**. A pyridine ring in one of these molecules was modeled as disordered over two positions with relative occupancies of 69:31.

(2-Pyridylmethyl)(4-pyridylmethyl)amine (2,4-DPA, 8). A solution of 4-(aminomethyl)-pyridine (0.95 mL, 9.4 mmol) and 2-pyridyl-carboxaldehyde (0.95 mL, 9.9 mmol) in 10 mL of MeOH was stirred for 5 min before addition of $NaBH_4$ (403 mg, 10.6 mmol) slowly over 5 min. The resulting red solution was stirred overnight, followed by addition of 10 drops of

concentrated HCl. The solution was concentrated to afford a red oil and then diluted with 50 mL of H_2O. Extraction into $CHCl_3$, washes with saturated aqueous $NaHCO_3$, drying over $MgSO_4$, and evaporation of solvent yielded an amber oil. Flash chromatography on a silica column (CH_2Cl_2:MeOH gradient from 40:1 to 20:1) gave 872 mg (48%) of a yellow oil. ^{1}H NMR (CD_2Cl_2, 400 MHz): δ 3.82 (2H, s), 3.86 (2H, s), 7.14–7.18 (1H, m), 7.27–7.31 (3H, m), 7.61–7.67 (1H, dt, J = 2.0 Hz, 8.0 Hz), 8.47–8.54 (3H, m). LRMS (ESI): calcd for $[M + H]^+$, 200.1; found, 199.9.

9-(o-Carboxyphenyl)-2,7-dichloro-4,5-bis[2-(pyridylmethyl)-4-(pyridylmethyl)-amino-methyl]-6-hydroxy-3-xanthenone (ZP1B, 2). A mixture of 2,4-DPA (239 mg, 1.20 mmol) and paraformaldehyde (31.0 mg, 1.03 mmol) in 11 mL of MeCN was heated at 70 °C for 20 min before addition of a suspension of DCF (150 mg, 0.374 mmol) in 12 mL of MeCN. The solution was stirred at 65 °C for 2 d and then cooled to room temperature. Crystals slowly formed upon standing. The material was filtered and washed with MeCN, Et_2O, and pentane, yielding 218 mg (71%) of pink crystalline blocks, mp = 188 °C (dec). ^{1}H NMR (DMSO-d_6, 400 MHz): δ 3.79 (4H, s), 3.94 (4H, s), 4.10 (4H, s), 6.50 (2H, s), 7.24 (4H, d, J = 4.8 Hz), 7.30 (1H, d, J = 7.6 Hz), 7.33–7.40 (4H, m), 7.70 (1H, app t, J = 7.6 Hz), 7.78 (1H, app t, J = 7.6 Hz), 7.84 (2H, app t, J = 7.6 Hz), 7.96 (1H, d, J = 8.0 Hz), 8.41 (4H, d, J = 4.8 Hz), 8.61 (2H, d, J = 4.0 Hz). ^{13}C NMR (DMSO-d_6, 100 MHz) δ 49.44, 57.08, 58.25, 82.83, 110.55, 112.72, 116.92, 123.56, 124.15, 124.80, 125.70, 126.73, 127.32, 131.20, 136.47, 138.35, 147.62, 148.84, 149.03, 150.24, 151.82, 155.97, 157.34, 168.86. HRMS (ESI): calcd for $[M + H]^+$, 823.2197; found, 823.2204.

Di(4-pyridylmethyl)amine (4,4-DPA, 9). To a solution of 4-pyridylcarboxaldehyde (0.95 mL, 10 mmol) and 4-aminomethylpyridine (0.91 mL, 9.0 mmol) in 10 mL of MeOH was added $NaBH_4$ (360 mg, 9.5 mmol) slowly over 2 min. The resulting red solution was stirred overnight

before being quenched with 10 drops of concentrated HCl. The solution was concentrated to give an oil and then diluted with 20 mL of H_2O and made basic with additions of solid Na2CO$_3$. The material was extracted into $CHCl_3$, washed with saturated aqueous $NaHCO_3$, dried over $MgSO_4$, and concentrated to an oil. Flash chromatography on a silica column (CH_2Cl_2:MeOH gradient from 20:1 to 9:1) yielded 450 mg (25%) of a yellow oil. ^{1}H NMR (CD_2Cl_2, 400 MHz): δ 1.72 (1H, br s), 3.84 (4H, s), 7.32 (4H, d, J = 6.4 Hz), 8.53 (4H, d, J = 6.4 Hz). LRMS (ESI): calcd for $[M + H]^+$, 200.1; found, 200.0.

9-(o-Carboxyphenyl)-2,7-dichloro-4,5-bis[di(4-pyridylmethyl)aminomethyl]-6-hydroxy-3-xanthenone (4-DPA-DCF, 3). A suspension of di(4-pyridylmethyl)amine (159 mg, 0.797 mmol) and paraformaldehyde (24.4 mg, 0.813 mmol) in 6 mL of MeCN was stirred at 80 °C for 20 min before addition of a suspension of DCF (102 mg, 0.254 mmol) in 12 mL of MeCN. After being stirred overnight at 80 °C, the mixture was allowed to cool to room temperature and filtered. The resulting solid was washed with MeCN, Et_2O, and pentane, yielding 162 mg (77%) of pink powder, mp = 196 °C (dec). ^{1}H NMR (CD_2Cl_2/MeOD, 400 MHz): δ 3.72–3.90 (8H, m), 4.01–4.15 (4H, m), 6.66 (2H, s), 7.18 (1H, d, J = 7.6 Hz), 7.37 (8H, d, J = 6.0 Hz), 7.68–7.82 (2H, m), 8.04 (1H, d, J = 7.6 Hz), 8.60 (8H, d, J = 6.0 Hz). ^{13}C NMR (DMSO-d_6, 100 MHz): δ 49.83, 57.34, 82.35, 111.25, 112.50, 116.77, 124.66, 125.77, 126.61, 127.32, 131.23, 136.49, 146.38, 148.58, 150.30, 151.74, 155.22, 168.81. HRMS (ESI): calcd for $[M + H]^+$, 823.2197; found 823.2192.

9-(o-Carboxyphenol)-2,7-dichloro-4,5-bis(dibenzylaminomethyl)-6-hydroxy-3-xanthenone (DBA-DCF, 4). A suspension of dibenzylamine (250 μL, 1.30 mmol) and paraformaldehyde (39.7 mg, 1.32 mmol) in 7 mL of MeCN was stirred at 80 °C for 30 min before addition of a suspension of DCF (168 mg, 0.419 mmol) in 12 mL of 1:1 MeCN:H_2O. The reaction mixture

was stirred at 80 °C for 48 h and cooled to room temperature, and the resulting precipitate was filtered and washed with 1:1 MeCN:H_2O. The solid was mixed with boiling EtOH, cooled, filtered, and washed with Et2O and hexanes, yielding 282 mg (82%) of a pink powder, mp = 242 °C (dec). ^{1}H NMR (CD_2Cl_2, 400 MHz): δ 3.70–3.83 (8H, m), 3.95–4.05 (4H, m), 6.63 (2H, s), 7.15 (1H, d, J = 7.6 Hz), 7.31–7.45 (20H, m), 7.68–7.74 (2H, m), 8.06 (1H, d, J = 7.6 Hz). HRMS (ESI): calcd for $[M + H]^+$, 819.2387; found, 819.2369.

9-(o-Carboxyphenol)-2,7-dichloro-4,5-bis{di[2-ethyl(2-methyl-isoindole-1,3-dione)]-aminomethyl}-6-hydroxy-3-xanthenone (12). A suspension of 11 (280 mg, 0.771 mmol) and paraformaldehyde (25 mg, 0.83 mmol) in 12 mL of 1:1 DMF:MeCN was stirred at 70 °C for 20 min, forming a homogeneous solution. A suspension of DCF (100 mg, 0.249 mmol) in 8 mL of MeCN was added, and the mixture was stirred at 70 °C for 48 h. After cooling to room temperature, the resulting solid was filtered and washed thoroughly with MeCN, Et_2O, and pentane, yielding 154 mg of pink powder (54%). ^{1}H NMR (DMSO-d_6, 400 MHz): δ 2.94–3.06 (8H, m), 3.73–3.83 (8H, m), 4.22 (4H, s), 6.40 (2H, s), 7.32 (1H, d, J = 8.0 Hz), 7.53–7.60 (1H, m), 7.62–7.74 (16H, m), 7.88 (1H, t, J = 8.0 Hz), 7.96 (1H, d, J = 7.6 Hz).

9-(o-Carboxyphenol)-2,7-dichloro-4,5-bis[di(2-aminoethyl)aminomethyl]-6-hydroxy-3-xanthenone (DETA-DCF, 5). Hydrazine monohydrate (0.50 mL, 10 mmol) was added to a suspension of 12 (60 mg, 52 μmol) in 10 mL of EtOH, changing the color to bright pink. The mixture was heated at 80 °C for 4 h, cooled to room temperature, filtered, and washed with MeCN, Et_2O, and pentane. The solid was mixed with MeOH for 1 h before being filtered and dissolved in MeOH with a minimal amount of concentrated HCl. The solvent was removed, and the solid was thoroughly washed with MeOH, yielding 32 mg (96%) of a glassy orange solid. ^{1}H NMR (D_2O, 400 MHz): δ 2.92 (8H, t, J = 6.2 Hz), 3.10 (8H, t, J = 6.2 Hz), 3.98 (4H, s),

7.17–7.22 (3H, m), 7.61–7.72 (2H, m), 8.12 (1H, d, J = 8.0 Hz). HRMS (ESI): calcd for $[M + H]^+$, 631.2197; found, 631.2185.

9-(o-Carboxyphenyl)-2,7-dichloro-4,5-bis(diethylaminomethyl)-6-hydroxy-3-xanthenone (DEA-DCF, 6). A solution of diethylamine (125 mg, 1.71 mmol) and paraformaldehyde (47.3 mg, 1.58 mmol) in 8 mL of MeCN was stirred at 60 °C for 30 min before addition of a suspension of DCF (160 mg, 0.398 mmol) in 15 mL of MeCN. After being stirred overnight at 60 °C, the mixture was allowed to cool to room temperature and filtered. The resulting pink powder was washed with MeCN, Et_2O, and pentane, yielding 118 mg (52%) of pure product. X-ray diffraction-quality crystals were obtained by diffusion of Et_2O into a CH_2Cl_2 solution, mp = 230 °C (dec). ^{1}H NMR (CD_2Cl_2, 400 MHz): δ 1.22 (12H, t, J = 7.2 Hz), 2.74–2.86 (8H, m), 4.06–4.20 (4H, m), 6.62 (2H, s), 7.32 (1H, d, J = 7.6 Hz), 7.67–7.81 (2H, m), 8.01 (1H, d, J = 7.6 Hz). ^{13}C NMR (DMSO-d_6, 100 MHz): δ 10.91, 46.99, 50.50, 83.21, 109.39, 109.69, 116.97, 124.22, 125.29, 127.19, 127.35, 130.28, 135.36, 148.23, 151.72, 157.65, 168.84. HRMS (ESI): calcd for $[M + H]^+$, 571.1761; found, 571.1762.

2-[(Di{2-pyridylmethyl}amino)methyl]-6-chloro-4-nitrophenol (10). A suspension of 7 (235 mg, 1.18 mmol) and paraformaldehyde (36 mg, 1.2 mmol) in 10 mL of MeCN was stirred at 75 °C for 20 min before addition of a solution of 2-chloro-4-nitrophenol (179 mg, 1.03 mmol) in 8 mL of MeCN. Heating was continued overnight, followed by removal of the solvent. Purification by flash chromatography on silica (30:1 CH_2Cl_2:MeOH) yielded 165 mg (43%) of a bright yellow glassy solid. ^{1}H NMR (D_2O, 400 MHz): δ 3.87 (2H, s), 3.91 (4H, s), 7.17–7.23 (2H, m), 7.27 (2H, d, J = 8.0 Hz), 7.63–7.68 (2H, m), 7.95 (1H, d, J = 2.8 Hz), 8.19 (1H, d, J = 2.8 Hz), 8.55 (2H, d, J = 4.8 Hz). ^{13}C NMR (MeOD, 100 MHz): δ 56.06, 58.55, 122.89, 123.44, 124.84,

124.86, 125.10, 137.79, 148.10, 157.33. HRMS (ESI): calcd for $[M + H]^+$, 385.1062; found, 385.1052.

Results and Discussion

Syntheses. In order to investigate the role of various heteroatoms in zinc-binding receptors used to image mobile Zn^{2+} by fluorescence, we prepared analogues of ZP1 (**1**, Figure 2.2) as the most attractive targets for study. The synthesis from commercially available DCF is more straightforward than that required for non-chlorinated analogues such as ZP2.[34] The route to fluorophores **2**–**6** (Figure 2.2) employs standard Mannich-like reaction conditions and affords symmetric probes. Extra steps to protect and then deprotect the primary amine groups of DETA were required to prepare **6** (Scheme 2.1). Previous protocols employed H_2O and MeCN solvent mixtures, but in most cases MeCN alone provides better results and in some cases diffraction-quality crystals grow by slow evaporation of the solvent from the reaction solution.

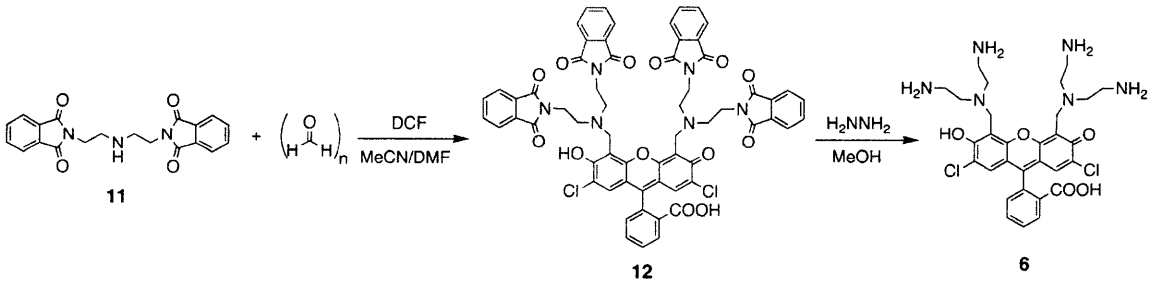

Scheme 2.1. Synthesis of Fluorophore **6**

The secondary amine precursors to **2** and **3** were prepared by following a procedure for a similar compound,[54] although the yields were unexpectedly low, there being at least one other major, unidentified product in each case. Diethylamine is commercially available, and the target **6** was synthesized in adequate yield (52%) and excellent purity. Dibenzylamine is also commercially available, but it and the corresponding fluorophore **4** have rather poor solubility at

and below pH 7, making potentiometric titrations impractical and preventing complete characterization. Intermediate **12** also suffered from poor solubility, as did final compound **6**.

Table 2.1. Spectroscopic Properties of Fluorophores **1-6**

	Absorbance maximum (nm)	Extinction Coefficient, ε ($M^{-1}cm^{-1}$)	Emission maximum (nm)	Fluorescence pK_a	Quantum Yield, Φ[a] (pH 7.0)	Quantum Yield, Φ[a] (0.1 M NaOH)
6	504	100,400	521	10.2	0.86	0.009
5	509	61,900	526	9.6	0.095	--[b]
4	510	--[b]	527	8.6	0.65	0.006
1[c]	515	79,500[d]	528	7.0, 4.0	0.17	0.009
2	516	68,000	531	5.6	0.034	0.012
3	519	90,100	543	5.0	0.024	0.019

[a]Referenced to fluorescein in 0.1 M NaOH (Φ = 0.95).[55] [b]Lack of solubility prevents accurate measurement. [c]Values for the apo form. [d]Value from ref. 34

Spectroscopic Properties. Pertinent spectroscopic properties of compounds **1**–**6** are summarized in Table 2.1. Unless otherwise noted, all measurements were performed at pH 7. Each of these compounds absorbs strongly in the visible range, with λ_{max} between 504 and 519 nm and a spectrum characteristic of fluorescein derivatives. All of the compounds display fluorescent turn-on in response to protons, and a fluorescence-based pK_a value was determined for each (Figures 2.3 and 2.4), with **1** displaying a two-step turn-on. The latter observation is inconsistent with our previously reported titration curve for **1**[34] but is believed to be correct for several reasons. The new curve was constructed from a set of titrations with many more data points than previous ones, yielding more detail. Additionally, this curve matches quite well those for ZP1(5-CO_2H) and ZP1(6-CO_2H),[42] as expected since addition of a carboxyl group to the "bottom ring" should not have a significant effect on the basicity of the binding pockets. Finally, the new titration curve agrees with expectations from the speciation model derived from potentiometric titrations (vide infra).

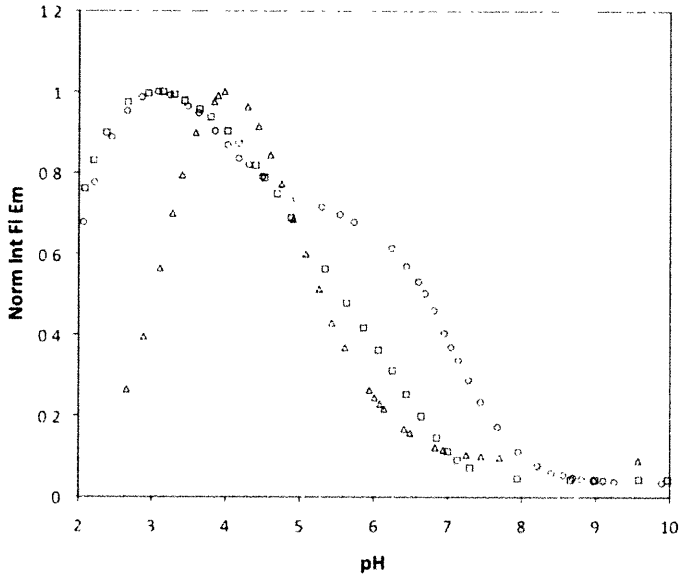

Figure 2.3. Normalized and integrated fluorescence emission of compounds **1** (circles), **2** (squares), and **3** (triangles) over the pH range 2–10. Each solution contains 1.0 μM of the fluorophore and 100 mM KCl as the electrolyte. The fluorescence "turns on" as the pH is lowered due to protonation of the quenching units. The decrease in fluorescence at the lower end of the pH scale is caused by formation of the non-fluorescent lactone isomer.

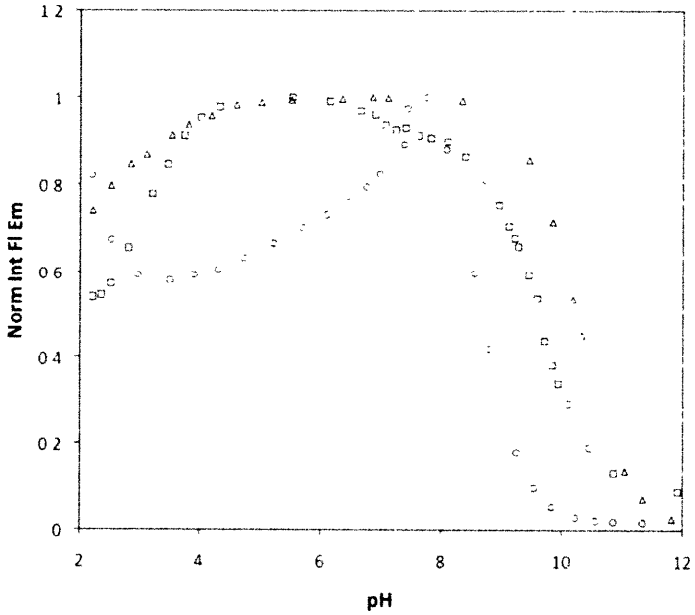

Figure 2.4. Normalized and integrated fluorescence emission of compounds **4** (circles), **5** (squares), and **6** (triangles) over the pH range 2-12. Each solution contains 1.0 μM of the fluorophore and 100 mM KCl as the electrolyte. The fluorescence "turns on" as the pH is lowered due to protonation of the quenching units. The decrease in fluorescence at the lower end of the pH scale is caused by formation of the non-fluorescent lactone isomer. The drop in emission from **4** below pH 8 is due to partial precipitation.

Under basic conditions (0.1 M NaOH), **1** and **6** have the same low quantum yield (Φ) of 0.009. Since the electron-donating ethyl groups of DEA make its nitrogen atom a strong electron donor, significant quenching is expected according to the Rehm–Weller model of PET.[28] Electron donation from the DPA tertiary nitrogen atom is expected to be weaker due to the proximity of the electron-withdrawing pyridyl groups. Since these two compounds exhibit the same Φ value, it would appear that all four pyridyl groups of **1** contribute to its quenching, a conclusion supported by the potentiometry results below. The low Φ value for **4** in basic solution also suggests that its phenyl units play a role in the quenching process. It seems more likely, however, that the greater hydrophobicity of the aromatic rings in this latter compound promotes π-stacking interactions that disrupt the fluorescence.[56]

Although there are only three compounds to compare, there is a noticeable trend in Φ values for the pyridyl-based sensors in basic solution. The quantum yield is lowest for **1**, which has four 2-pyridyl groups, and highest for **3**, which has four 4-pyridyl groups. The value for **2**, with an equal mixture of substitution positions, is intermediate. This trend suggests that the pendant pyridyl arms participate in fluorescence quenching. Further evidence of such pyridyl-based quenching is presented below in the section discussing potentiometric results.

Potentiometric Titrations, Model Compounds. Since **1**–**6** are relatively complex molecules, each having two identical Zn^{2+} binding sites and many potential protonation sites, we began this part of our study by analyzing the properties of a simpler set of compounds. Potentiometric titrations were performed on the three parent DPA ligands, **7**–**9** (Figures 2.2 and 2.5), and the derived pK_a values are reported in Table 2.2. We were unable to assign a value to pK_{a1} for **7** under our experimental conditions, so values from a previous study[57] are listed.

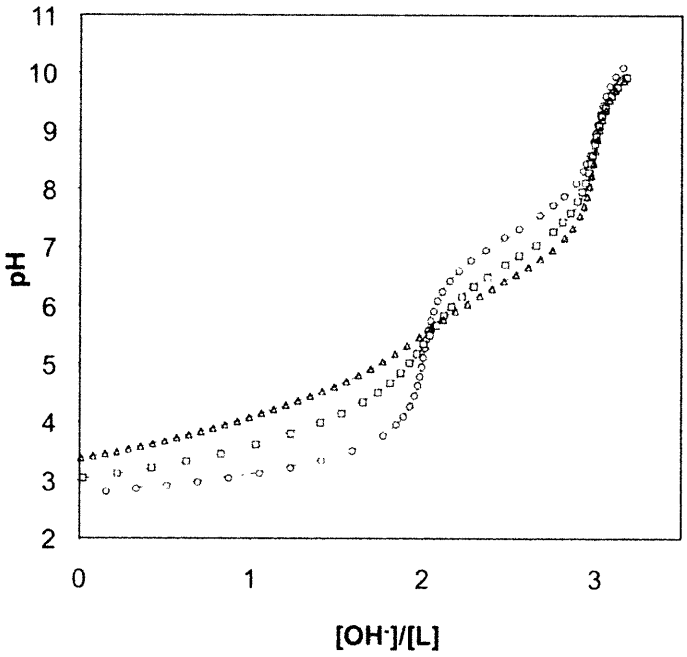

Figure 2.5. Potentiometric titration curves of DPA ligands **7** (circles), **8** (squares), and **9** (triangles) in aqueous solution containing 100 mM KCl at 25 °C. At the beginning of the titration, each solution contained 1.0 mM of the neutral molecule with 3 equiv of added HCl. The abscissa reports equivalents of base added per mole of ligand. The solid lines overlying the data points represent theoretical curves from calculated pK_a values.

Table 2.2. Proton and Zinc Dissociation Constants for Compounds **7-10**

Compound	pK_{a3}	pK_{a2}	pK_{a1}	K_d
7[a]	7.27	2.41	1.75	160 nM
8	6.79 (7)	4.099 (4)	2.20 (1)	--
9	6.47 (1)	4.530 (9)	3.415 (4)	--
10	7.99 (3)	4.61 (5)	2.87 (15)	0.29 (9) pM

[a]Values from ref. 57. Numbers in parentheses represent standard deviations in the last significant digit.

For the DPA ligands, pK_{a3} shifts to lower values as the pyridyl nitrogen atoms are directed away from the central amine nitrogen atom. This trend indicates that, although the first proton is expected to bind to the electron-rich central nitrogen atom, the 2-pyridyl groups participate as hydrogen bond acceptors for that proton. Since 4-pyridyl groups cannot contribute in this manner, the associated pK_a values are shifted higher, toward the value for free pyridine (pK_a =

5.17),[58] but do not reach that value because of the nearby positive charge from the protonated central nitrogen atom.

Before attempting an analysis of **1** by potentiometry, we also synthesized and studied model compound **10** (Figure 2.2 and Table 2.2). Its para-nitro substituent enhances the acidity of the phenol group and the pK_{a3} value is 7.99, making this compound a reasonable mimic for one of the binding pockets in **1**. The 0.29 pM K_d value for Zn^{2+} calculated from potentiometric titrations of a 1:1 metal:ligand mixture seems unusually high until one considers related compounds from the literature (Figure 2.6). Diethylenetriamine has a K_d value for Zn^{2+} of 1.6 nM,[59] and addition of a pendant phenolic group to the central nitrogen atom increases that affinity by several orders of magnitude (K_d = 0.85 fM), despite only a modest increase in basicity.[60] Since the dissociation constant of Zn^{2+} for DPA is 160 nM,[56] the affinity for phenol-appended model **10** should be much higher, as observed.

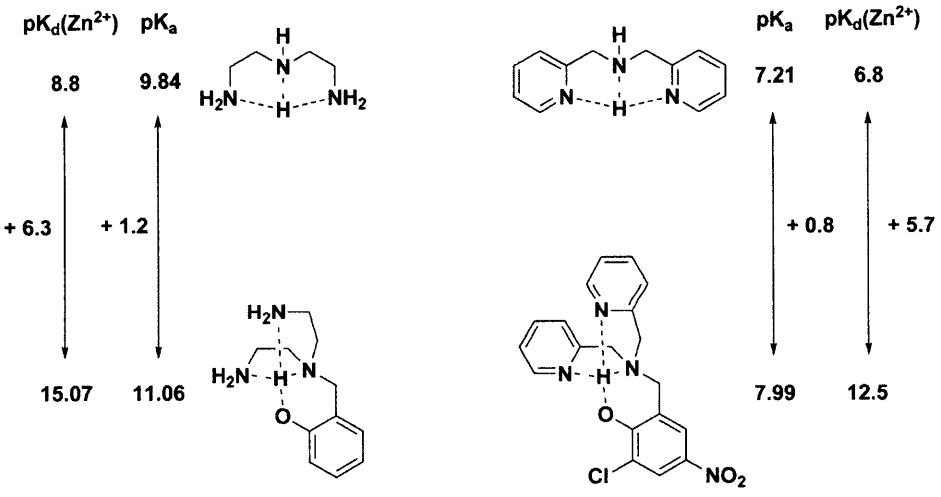

Figure 2.6. Comparison of dissociation constants for dien and **7** and the effects of adding a methylene-tethered phenolate appendage. A small increase in proton affinity portends a large increase in zinc affinity. Values from refs 57, 59, 60 and this work.

Potentiometric Titrations, Fluorophores. Representative titration data and the corresponding model curves for **1**–**3** are shown in Figure 2.7, and the calculated pK_a values are reported in

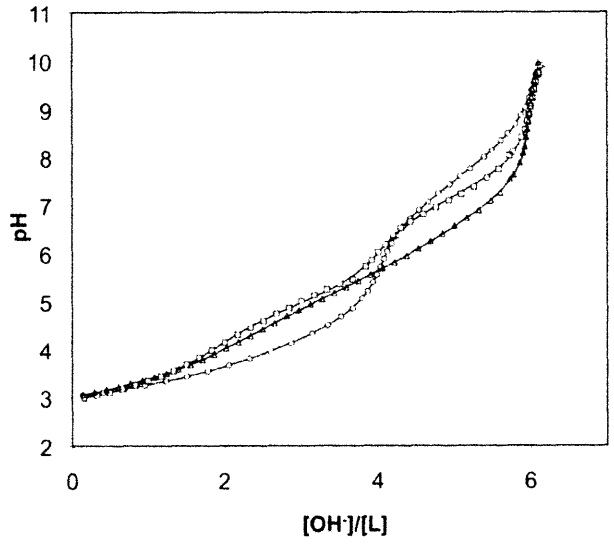

Figure 2.7. Potentiometric titration curves of fluorophores **1** (circles), **2** (squares), and **3** (triangles) in aqueous solution containing 100 mM KCl at 25 °C. Each trial started with 0.6–1.0 mM of the neutral molecule, dissolved in excess HCl. The abscissa is measured in equivalents of base added per mole of ligand. The solid lines overlying the data points represent theoretical curves from calculated pK_a values.

Table 2.3. Proton and Zinc Dissociation Constants for Fluorophores **1-3**

Equation				-logK^a		
				1	**2**	**3**
HL^-	⇌	$L^{2-} + H^+$	pK_{a6}	8.12 (2)	7.473 (5)	7.04 (1)
H_2L	⇌	$HL^- + H^+$	pK_{a5}	6.96 (1)	6.35 (1)	6.06 (1)
H_3L^+	⇌	$H_2L + H^+$	pK_{a4}	4.59 (3)	5.205 (8)	5.261 (9)
H_4L^{2+}	⇌	$H_3L^+ + H^+$	pK_{a3}	3.810 (9)	4.51 (2)	4.57 (3)
H_5L^{3+}	⇌	$H_4L^{2+} + H^+$	pK_{a2}	2.8 (3)	3.10 (3)	3.47 (2)
H_6L^{4+}	⇌	$H_5L^{3+} + H^+$	pK_{a1}	2.3 (2)	2.67 (5)	2.99 (2)
LZn	⇌	$L^{2-} + Zn^{2+}$		13.4 (3)		
$HLZn^+$	⇌	$LZn + H^+$		6.57 (7)		
H_2LZn^{2+}	⇌	$HLZn^+ + H^+$		4.02 (4)		
H_3LZn^{3+}	⇌	$H_2LZn^{2+} + H^+$		3.19 (9)		
LZn_2^{2+}	⇌	$LZn + Zn^{2+}$		8.9 (3)		

[a] K represents the dissociative equilibrium constant for the equations displayed on the left, corresponding to the loss of either a proton or zinc ion from the ligand (L) or ligand complex. No zinc-binding data are available for **2** or **3** due to precipitation of free Zn^{2+} during these experiments. Numbers in parentheses represent standard deviations in the last significant digit.

Table 2.3. Limited solubility affected our ability to model the lowest two dissociation constants for **1**–**3** since the calculated K_a values are on the same order as the concentrations used in the titrations.[46] In such cases, the relevant dissociation constants have questionable physical validity, but the quality of the fit to the titration data is improved, especially in the low pH range, by their inclusion. Like the structurally similar compound TPEN, which can support a 4+ charge from protonation at pH 3 (pK_{a1} = 2.85),[61] larger, dianionic **1** can accommodate six protons to achieve the same charge at a similar pH. Separate models containing from four to seven protonation events were evaluated, and the best fit was obtained for the six-proton model. Although a mixed solvent system utilizing MeOH or DMSO together with water would probably have increased the solubility of these compounds, we chose to maintain purely aqueous conditions so that the results from these titrations could be directly related to those from spectroscopic measurements of these and related compounds. Fortunately, the most important fluorescence behavior occurs at higher pH values, and the overall analysis is not affected by uncertainty in the lowest two pK_a values. The solubilities of **4** and **5** were insufficient over the desired pH range to perform a meaningful analysis. The dissociation constants of **6** are expected to be higher than that of diethylamine (pK_a = 10.93)[58] and were outside of the range of measurement under our conditions.

Two opposing trends emerge from the results in Table 2.3. The two highest pK_a values decrease as 4-pyridyl groups substitute for 2-pyridyl groups. The trend reverses for pK_{a4} through pK_{a1}, with the values increasing as more pyridyl groups are substituted in the 4-position. The reason for these trends becomes clear with the assignment of the dissociation constants to specific protonation sites (vide infra).

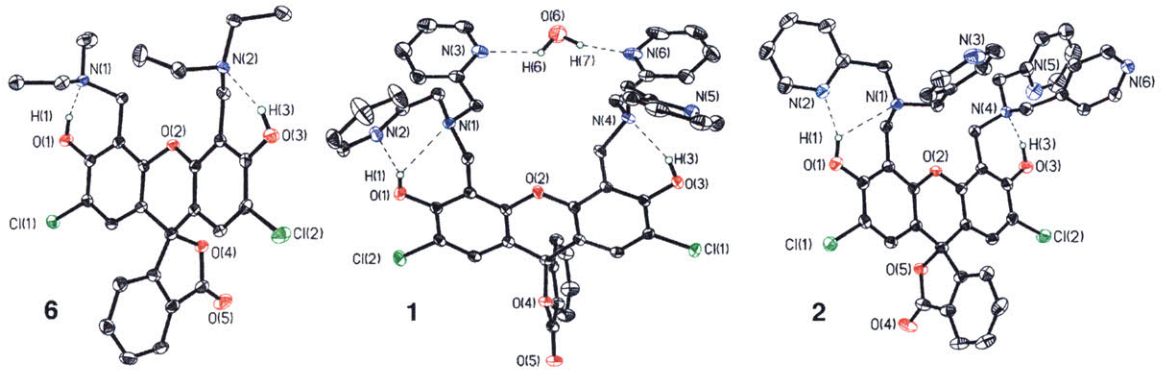

Figure 2.8. ORTEP diagrams showing 50% probability thermal ellipsoids on all non-hydrogen atoms. Short hydrogen bond contacts are shown as dotted lines.

Crystallographic Insights. As with the parent ligand arms, **7**–**9**, the pyridyl groups of **1**–**3** are also expected to help stabilize protons in the two binding pockets, with an additional contribution from the phenolic oxygen atoms. The crystal structures of **1**, **2**, and **6** (Figure 2.8 and Table 2.4) clearly reveal protons, located from difference electron density maps, bound to the phenolic oxygen atoms of both pockets. For **1** and **6**, these protons are within reasonable hydrogen bonding distance (Table 2.5) of the tertiary nitrogen atoms. Additionally, each binding pocket of **1** has one pyridyl nitrogen atom in reasonably close contact with the bound proton, lending support to the idea that all of the atoms in the N_3O binding group help to stabilize protons in the pockets. The other two pyridyl arms of **1** interact with one another through a bridging water molecule in the crystal structure. In solution, the equivalent pyridyl arms would contribute equally, although modestly, to proton stabilization. Two different conformations were found in the asymmetric unit of the crystal lattice of **2**, with an intermolecular interaction reducing the number of hydrogen bonds within the binding pockets (Figure 2.9). Any such intermolecular bonding feature is expected to be minimal in solution, however, where in-pocket bonding should dominate.

Table 2.4. Crystallographic parameters for **1**, **2**, and **6**

	1·MeCN·H$_2$O	**2·MeCN·0.25H$_2$O**	**6**
Empirical formula	$C_{48}H_{41}N_7O_6Cl_2$	$C_{48}H_{39}N_7O_{5.25}Cl_2$	$C_{30}H_{32}N_2O_5Cl_2$
Formula weight	882.78	868.76	571.48
Crystal System	Triclinic	Triclinic	Triclinic
Space group	$P\bar{1}$	$P\bar{1}$	$P\bar{1}$
a (Å)	13.023(3)	14.766(3)	10.521(2)
b (Å)	13.385(4)	14.851(3)	11.825(3)
c (Å)	14.076(4)	22.573(4)	12.749(3)
a (deg)	80.980(4)	92.659(3)	90.430(3)
b (deg)	86.683(4)	105.087(2)	111.283(3)
g (deg)	61.886(3)	117.641(3)	111.419(3)
V (Å^3)	2136.9(10)	4152.4(14)	1357.8(5)
Z	2	4	2
r_{calc}, g/cm^3	1.372	1.390	1.398
Temperature (K)	110	110	110
μ (Mo Ka), mm^{-1}	0.212	0.216	0.283
q range (deg)	2.11 to 27.88	1.99 to 26.14	2.30 to 26.37
Crystal size (mm)	0.23 x 0.20 x 0.16	0.45 x 0.20 x 0.10	0.15 x 0.15 x 0.10
Total no. of data	36729	51063	21002
No. of unique data	10110	16307	5524
Completeness to *q*	99.2 %	98.5 %	99.5 %
max, min peaks, e/Å^3	0.575 and -0.358	0.686 and -0.420	0.825 and -0.718
Goodness-of-fit on	1.052	1.039	1.061
R_1 (%)[a]	4.87	5.11	4.77
wR_2 (%)[b]	11.92	12.61	11.66

[a] $R_1 = \sum||F_o|-|F_c||/\Sigma|F_o|$, [b] $wR_2 = \{\Sigma[w(F_o^2-F_c^2)^2]/\Sigma[w(F_o^2)^2]\}^{1/2}$

Table 2.5. Summary of Distances (Å) between Hydrogen Bond Donor and Acceptor Atoms in the X-ray Crystal Structures of **1**, **2**, and **6**.

	Bond Lengths[a]	Å
Compound **1**	O1–H1...N1	3.0036(19)
	O1–H1...N2	2.935(2)
	O3–H3...N4	2.712(2)
	O3–H3...N5	3.385(2)
	O6–H6...N3	2.938(3)
	O6–H7...N6	2.931(3)
Compound **2**	O1–H1...N1	3.118(3)
	O1–H1...N2	2.648(3)
	O3–H3...N4	2.624(3)
	O3–H3...N5	3.414(3)
Compound **6**	O1–H1...N1	2.580(3)
	O3–H3...N2	2.644(2)

[a]Atoms are labeled as indicated in Figure 2.8.

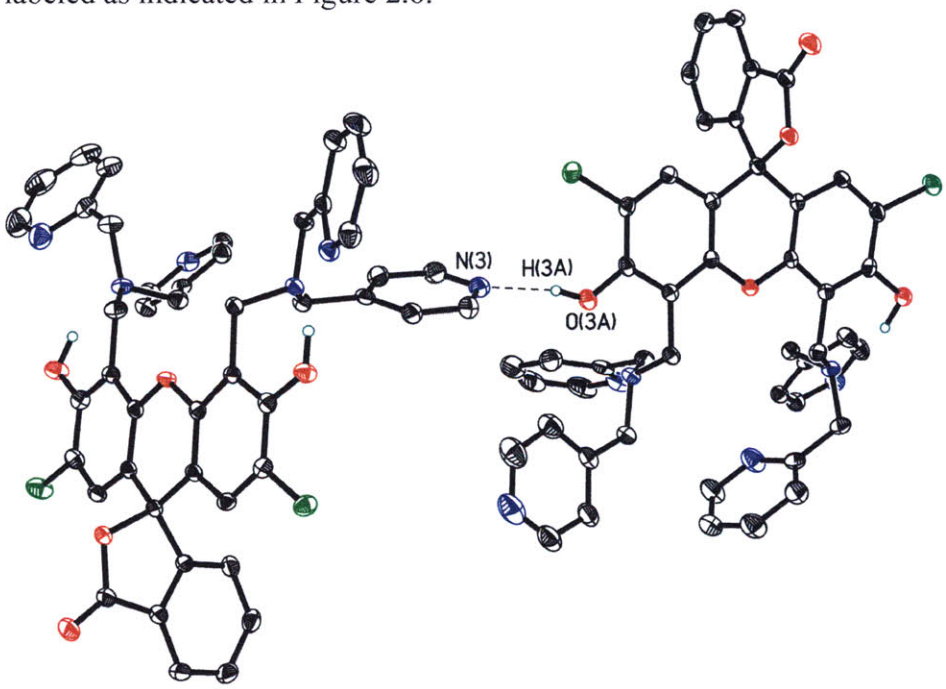

Figure 2.9. ORTEP diagram of the two independent molecules in the structure of **2** (40% probability thermal ellipsoids on all non-hydrogen atoms) showing intermolecular hydrogen bonding (O3A–H3A...N3 = 2.673(3) Å).

Determination of Protonation Sites. Protons occupying the binding pockets draw electron density from the phenolic oxygen atoms, reducing conjugation through the xanthenone π-system. This electronic effect is exhibited as a small (ca. 10 nm) shift in the optical spectrum as the pH is lowered. For **1**, this hypsochromic shift occurs over the pH range bracketing the two highest pK_a values (Figure 2.10), reinforcing the conclusions that the two phenolic oxygen atoms are involved in proton binding and that the tertiary nitrogen atoms are not the sole sites of protonation. The same spectral shift occurs for **2** (Figure 2.11) but not for **3** (Figure 2.12), the least basic of the set. Since the unprotonated molecule is completely symmetrical, the highest pK_a value represents a statistical combination of two equally basic sites. A single binding pocket would be expected to have a pK_a value approximately 0.3 unit lower.[62] Once the first proton is bound, however, electronic communication through the xanthenone system lowers the basicity of the other pocket, contributing to the separation between these two acid dissociation constants.

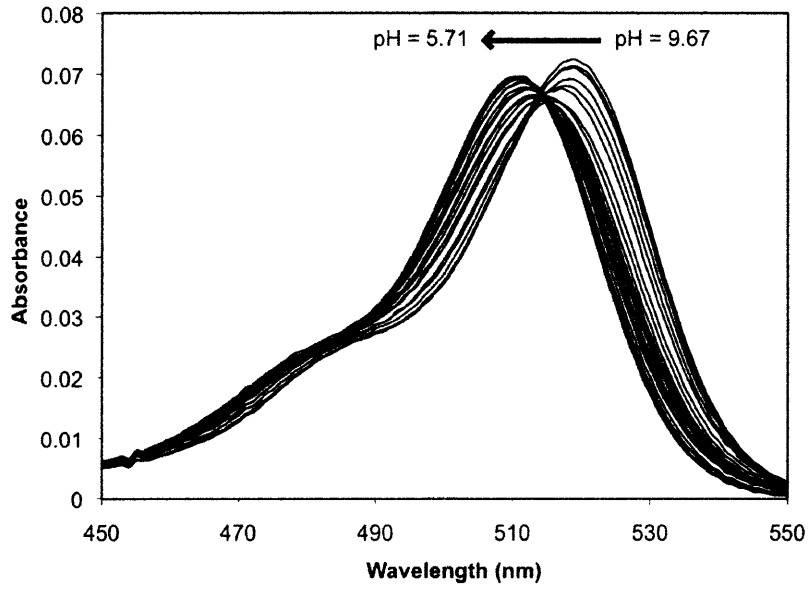

Figure 2.10. Absorbance spectra of a 1.0 μM solution of **1** containing 100 mM KCl over the pH range 9.67–5.71. An overall hypsochromic shift (519 to 511 nm) occurs as the pH is lowered due to protonation of the binding pockets, resulting in reduced conjugation through the π-system of the xanthenone group.

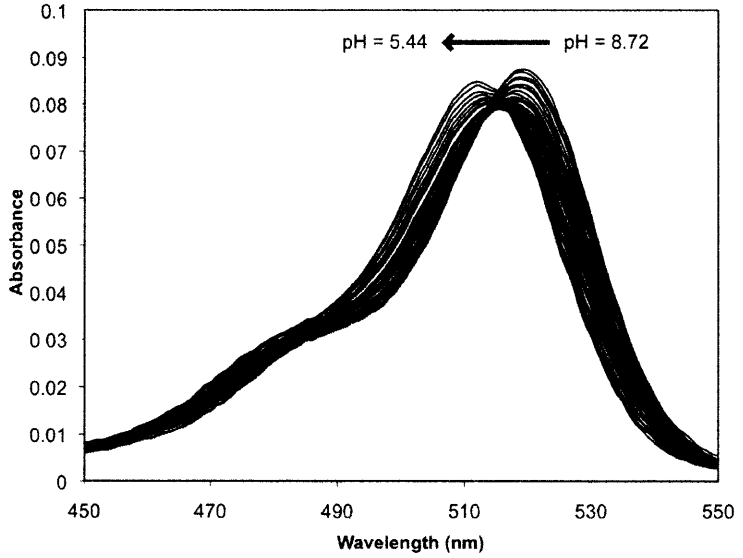

Figure 2.11. Absorbance spectra of a 1.0 μM solution of **2** containing 100 mM KCl over the pH range 8.72-5.44. A hypsochromic shift (519 nm to 512 nm) occurs as the pH is lowered due to protonation of the binding pockets, resulting in reduced conjugation through the π-system of the xanthenone group.

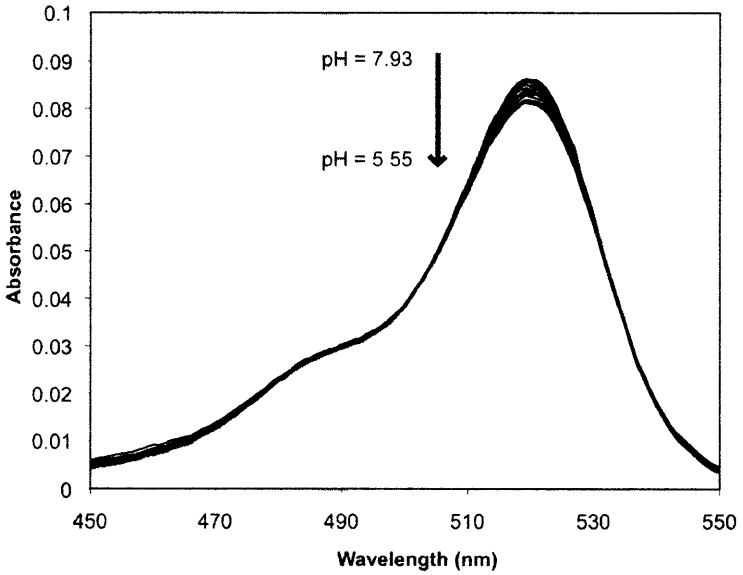

Figure 2.12. Absorbance spectra of a 1.0 μM solution of **3** containing 100 mM KCl over the pH range 7.93-5.55. No wavelength shift occurs as the pH is lowered, only a slight decrease in absorbance. The difference in first proton affinities between the fluorophore (pK_{a6} = 7.02) and the parent amine (pK_{a3} = 6.47) is not very large, therefore the hydrogen bonding interaction with the phenolic oxygen of the absorbing xanthenone moiety is not sufficient to perturb the absorption spectrum.

The third proton binds to any one of the four equivalent pyridyl groups. The pK_a value associated with this event, despite being increased by a statistical factor, is lower than that for free pyridine owing to the weak interaction with the proton already present in the binding pocket. The next three protonation sites are assigned to the remaining pyridyl groups, with gradually decreasing pK_a values due to the buildup of positive charge in the vicinity of the binding pockets.

Another potential protonation site that was considered is the carboxylate group on the "bottom ring" of **1**, which has been discussed for both anionic and neutral forms of fluorescein.[63] In the pH range covering the lowest two pK_a values, however, there is a simultaneous decrease in the absorbance and emission intensities (Figure 2.13). This observation suggests that the unprotonated carboxylate group has closed to form the lactone isomer, which neither absorbs in the same spectral range as the ring-open form nor fluoresces. Ab initio calculations have revealed such a preference for the lactone isomer over the quinoid, carboxylate-protonated form.[64] Although some amount of solvation energy is lost with lactone formation, the negative charge on the free carboxylate group gets redistributed to the phenolic oxygen atoms, where positive charge has accumulated due to nitrogen atom protonation. At any rate, the absorption and emission bands are only diminished, not extinguished, such that an equilibrium exists between the ring-open and -closed forms.

Combining the various results and observations from crystallography, spectroscopy, and potentiometry, we have been able to construct a fairly detailed picture of the protonation states of **1** over a wide pH range (Scheme 2.2). The number of potential protonation sites, along with the narrow spread of dissociation constants, makes a definitive assignment of all the microstates in this system difficult, but we find this model to represent the data reasonably well.

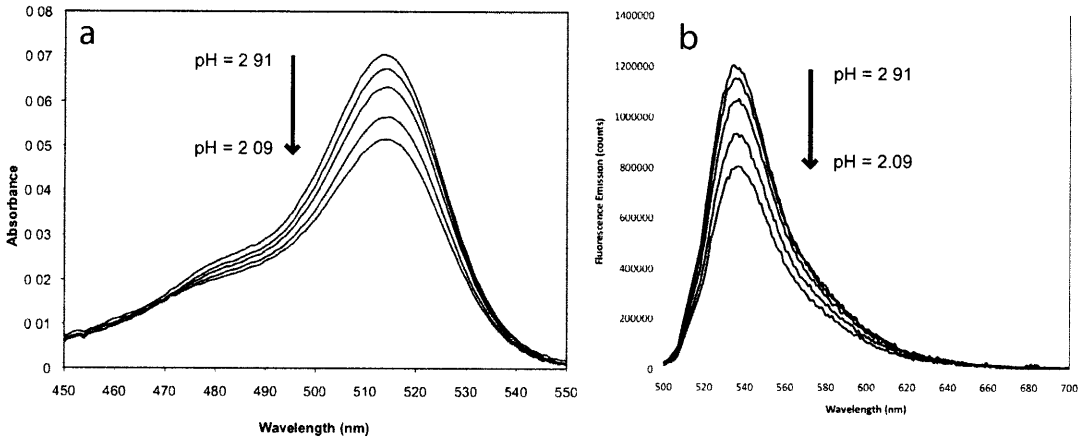

Figure 2.13. Absorbance (a) and fluorescence (b) spectra of a 1.0 μM solution of **1** containing 100 mM KCl over the pH range 2.91-2.09. Both absorbance and emission decrease in unison as the pH is lowered, suggesting formation of the ring-closed lactone isomer.

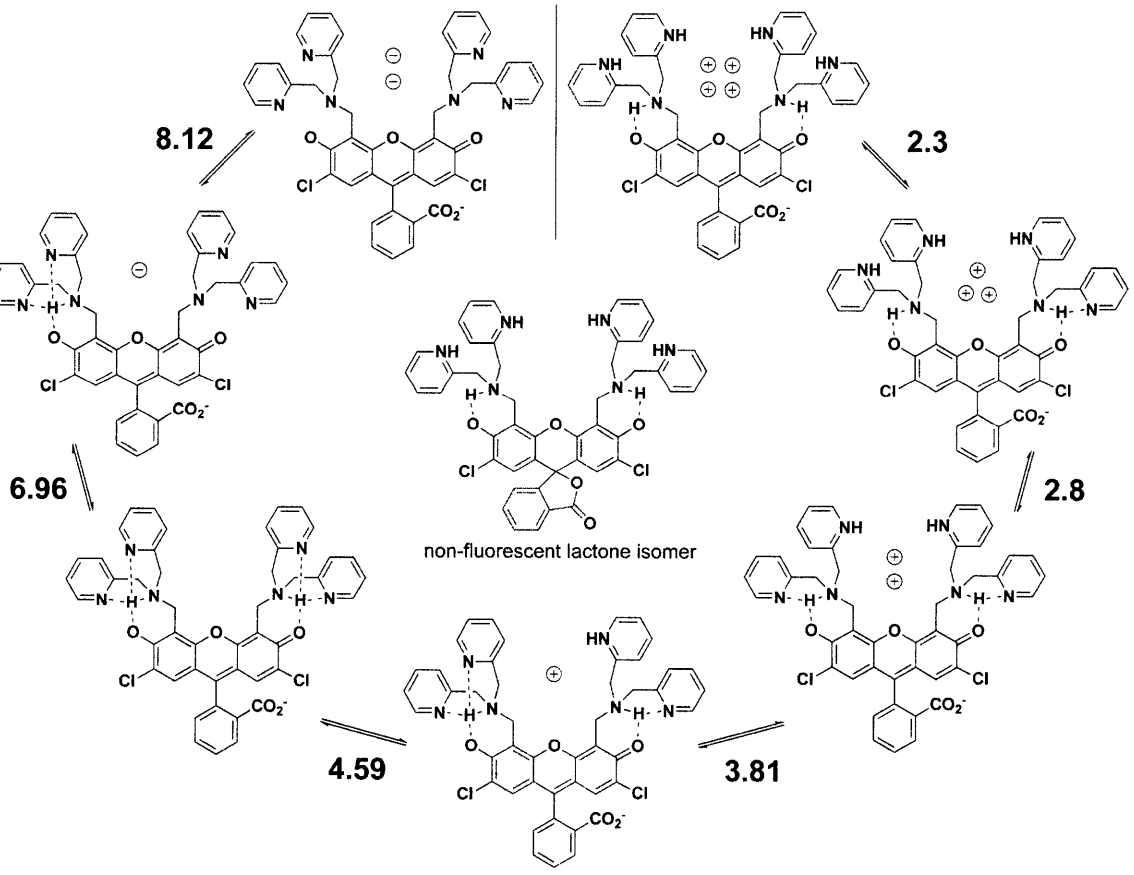

Scheme 2.2. Protonation equilibria of ZP1 (**1**). The number adjacent to each set of equilibria arrows represents the corresponding pK_a value. Charges within the binding pockets have been omitted for clarity.

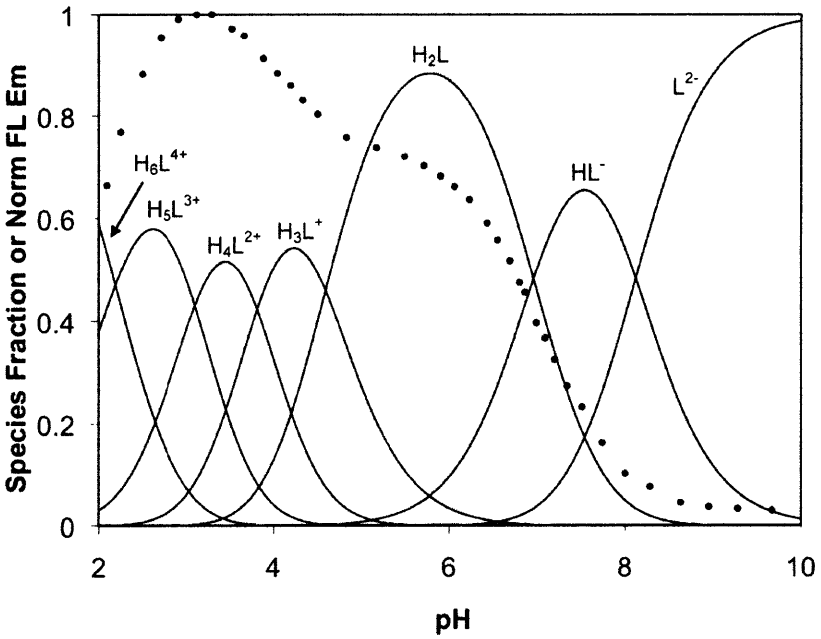

Figure 2.14. Fluorescence pH titration data (points) for **1** overlaid on a speciation plot created from calculated acid dissociation constants.

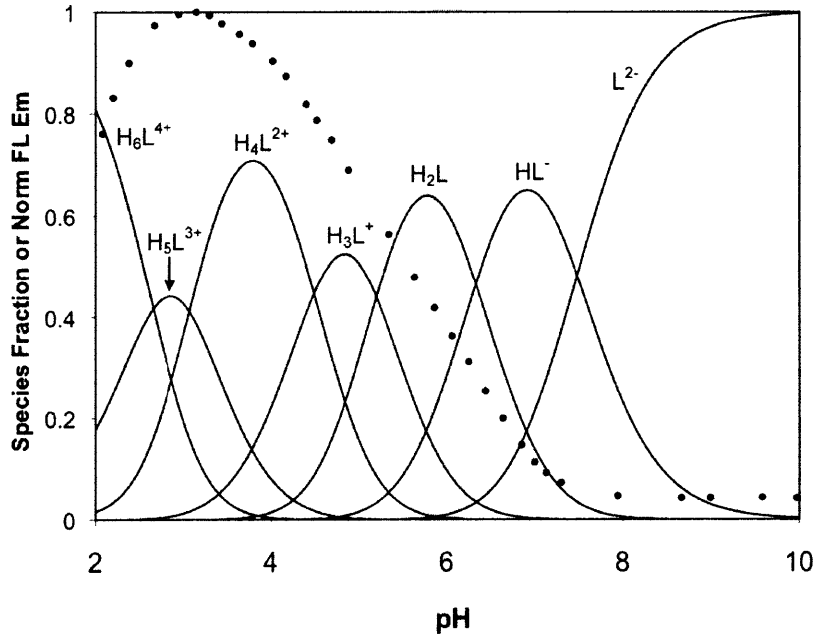

Figure 2.15. Fluorescence pH titration data (points) for **2** overlaid on a speciation plot created from calculated acid dissociation constants.

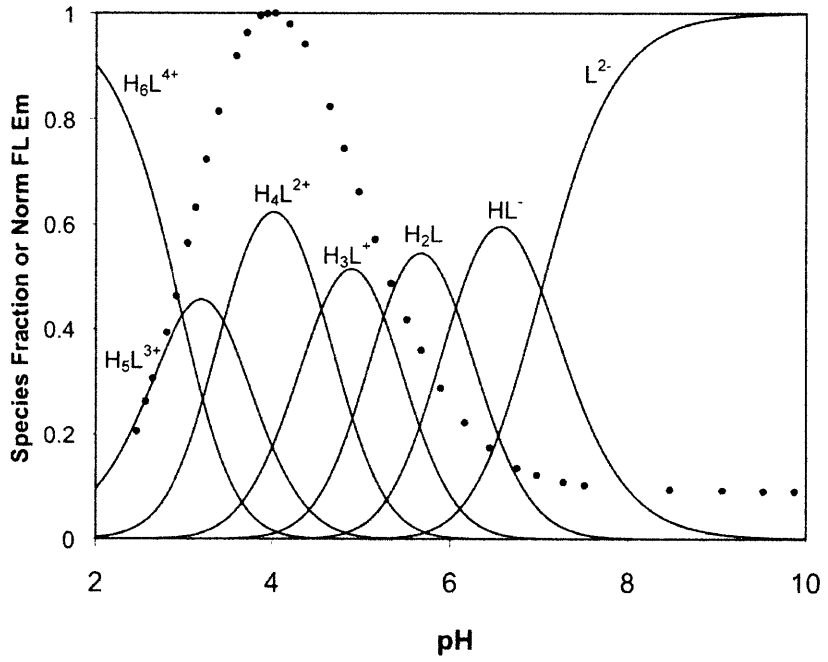

Figure 2.16. Fluorescence pH titration data (points) for **3** overlaid on a speciation plot created from calculated acid dissociation constants.

Correlation of Fluorescence Behavior with Proton Equilibria. Using the calculated pK_a values for **1**–**3**, speciation plots were constructed and overlaid with the fluorescence pH titration curves for each compound (Figures 2.14-2.16). For **1**, the initial fluorescence increase occurs upon binding of the second proton, corresponding to occupancy of both binding pockets. A second, smaller increase occurs during the binding of two additional protons. Since the binding sites for these two protons are assigned as pyridyl groups, we conclude that the pyridyl arms of DPA are not innocent bystanders in the quenching mechanism of these compounds. In fact, the main "turn-on" for **3** does not occur concurrently with formation of the diprotonated species, which is expected to have both tertiary nitrogen atoms bound to protons. Instead, the fluorescence of **3** begins to increase significantly only when the third and fourth protons bind to

pyridyl groups. At lower pH values, the absorbance spectra of **3** diminish along with the emission spectra (not shown), suggesting formation of the lactone isomer. If not for this isomerization, protonation of the remaining pyridyl groups might allow for an even greater increase in fluorescence emission. The same pattern is evident for **2**, but with approximately equivalent turn-on contributions from protonation of the binding pockets and the subsequent pyridyl protonation.

Our results indicate a clear trend between the protonation state of the pyridyl arms of these fluorophores and their fluorescence response, but the mechanism for this behavior remains to be determined. Although a pyridinium group can act as an electron acceptor, quenching the emission of an attached fluorophore,[9,29,35] we know of no previous examples of a free pyridyl group acting as a quenching unit in a PET-based sensor, and it is unlikely that PET is the underlying cause for this secondary turn-on behavior. There are examples of fluorophores that are quenched through a process involving hydrogen bond formation with pyridine,[65,66] and such bonds exist in the diprotonated forms of **1** and **2**. No intramolecular pyridyl-to-fluorophore hydrogen bonds are possible in **3**, however, so this mechanism for quenching from the pyridyl units can be dismissed. An analysis based on the Rehm−Weller formalism[28] and the utilization of electrochemistry, transient absorption spectroscopy, and computational methods may help explain this pyridyl-based quenching behavior - topics for future investigations.

Zinc Coordination. With the pK_a values for **1** in hand, further titrations were performed in the presence of $ZnCl_2$ in order to determine the relevant dissociation constants. The solubility of these mixtures was insufficient to complete all of the desired titrations, and solutions containing greater than a 1:1 metal-to-ligand ratio became cloudy over the course of the experiment,

rendering the experimental results unsuitable for analysis. Therefore, we were limited to experiments containing 1 equiv of $ZnCl_2$, and data from these trials were used to determine K_{d1} and to approximate K_{d2} (Figure 2.17). In addition to protonated and zinc-bound species, the mixed species $(HLZn)^+$, $(H_2LZn)^{2+}$, and $(H_3LZn)^{3+}$ were included in our computer model. A complete set of $-\log K$ values from our calculations for **1** are reported in Table 3. Very tight binding values are difficult to model accurately by potentiometry, but the consistency between multiple data sets, as reflected in the small standard deviation values, gives us confidence in the reported binding constants. From these values, a speciation plot was constructed for **1** in the presence of 1 equiv of Zn^{2+} over the pH range 2–10 (Figure 2.18). A titration using the same 1:1 metal-to-ligand ratio was also monitored by fluorescence, and the normalized, integrated emission curve was overlaid on the speciation plot. The result is similar to the proton-only system; that is, significant fluorescence turn-on does not occur until species are formed having both binding pockets occupied. The species LZn has one unoccupied pocket, which causes significant fluorescence quenching, and the primary turn-on only occurs with formation of the mixed species $(HLZn)^+$ as the pH is lowered. The small amount of dizinc complex that forms under this model leads us to report the second dissociation constant as only an estimated value. A secondary turn-on at low pH occurs with the formation of the pyridyl-protonated species $(H_2LZn)^{2+}$ and $(H_3LZn)^{3+}$.

The previously determined Zn^{2+} affinity of **1**,[34] measured by fluorescence titration (K_d = 0.7 nM), more closely matches the binding affinity for a second Zn^{2+} ion determined in this study. The fluorescence-based affinity value was obtained by titrating **1** with zinc in a dual-buffer system to control levels of the "free" ion. Although appropriate for ligands with very high affinities, this approach did not allow for determination of the binding stoichiometry. In order to

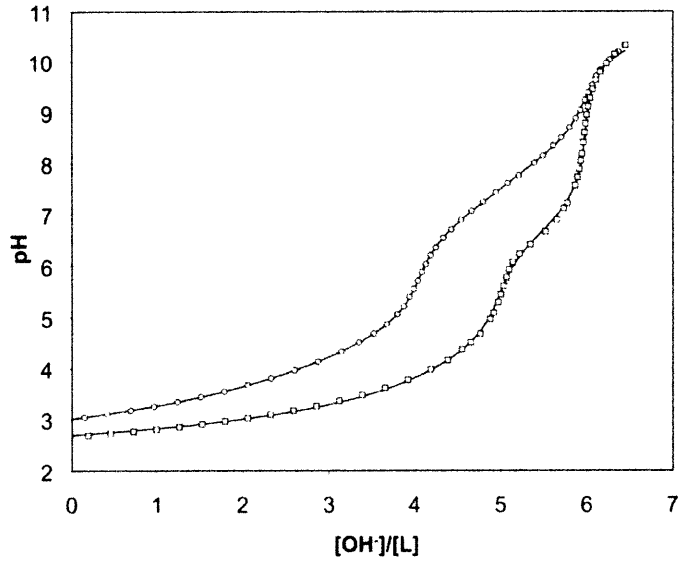

Figure 2.17. Potentiometric titration curves of **1** in the absence of $ZnCl_2$ (circles) and in the presence of 1 equivalent of $ZnCl_2$ (squares) in aqueous solution containing 100 mM KCl at 25 °C. Each trial started with 0.6 mM of the neutral molecule, dissolved in excess HCl. The abscissa is measured in equivalents of base added per mole of ligand. The solid lines overlaying the data points represent model curves from calculated pK_a values.

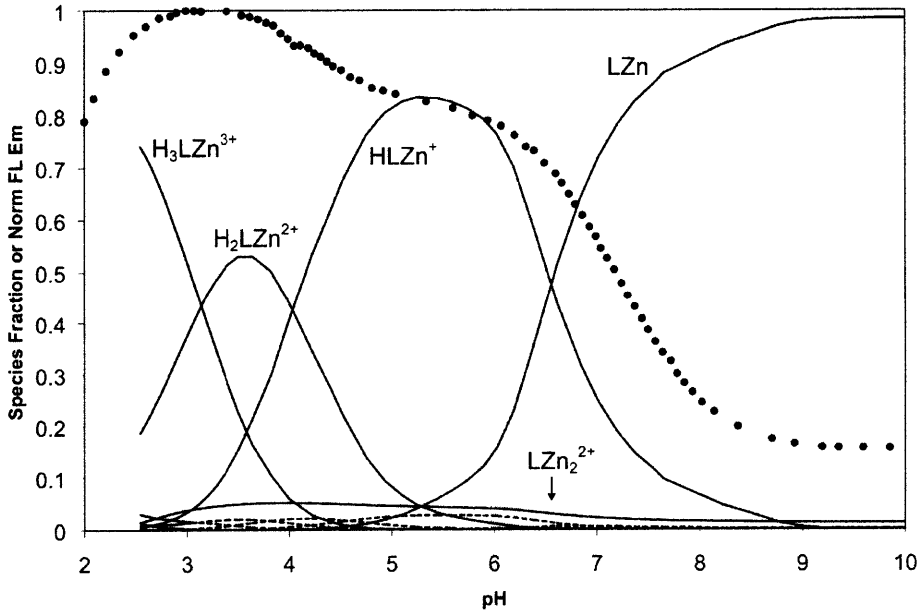

Figure 2.18. Fluorescence pH titration data (circles) for a 1:1 mixture of **1** and $ZnCl_2$ overlaid on a speciation plot created from the calculated proton and Zn^{2+} dissociation constants. The species containing zinc are represented with solid lines and those without zinc are represented with dashed lines. Labels for the minor species are omitted for clarity.

distinguish the degree of fluorescence turn-on induced by the binding of one versus two zinc ions, a solution of the sensor was titrated with small aliquots of $ZnCl_2$ (Figure 2.19). There is an initial, small turn-on in the range of 0–1 equiv of Zn^{2+}, caused by partial alleviation of quenching as one binding pocket is occupied, leaving the other receptor pocket to continue to act as an electron donor. The increase in fluorescence becomes significantly greater upon addition of 1–2 equiv of Zn^{2+} since the zinc affinities for both pockets are very strong and all of the donor groups are occupied, such that quenching influences have been removed.

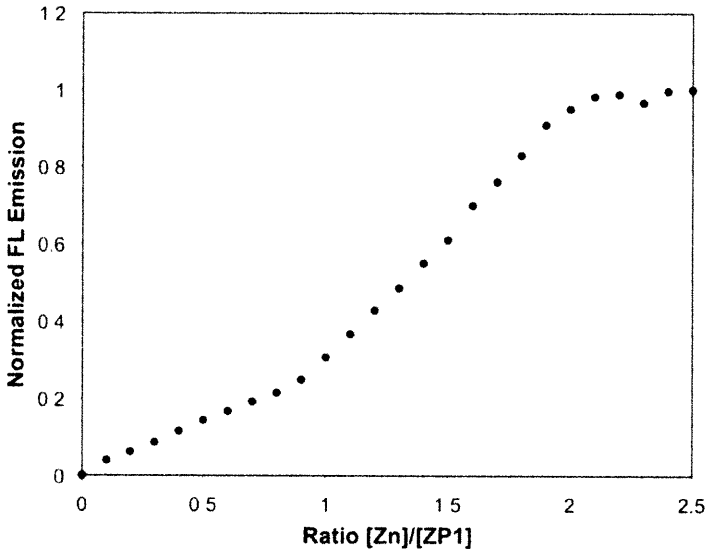

Figure 2.19. Integrated emission response of 0.3 μM **1** at pH 7.0 to increasing amounts of $ZnCl_2$. Binding of the first equivalent of zinc to the sensor does not cause as significant a turn-on as binding the second equivalent.

These observations, taken together, lead to the conclusion that, in order for full fluorescence turn-on to occur, protons and/or Zn^{2+} ions must occupy both binding pockets of **1** (Figure 2.20). This result is consistent with other reports involving PET-based sensors having two separate quenching/binding arms.[7,32,67] Potentiometric titrations of **2** and **3** in the presence of $ZnCl_2$

resulted in the precipitation of unbound zinc at high pH values, suggesting that the metal affinities of these compounds are much lower than those of **1**.

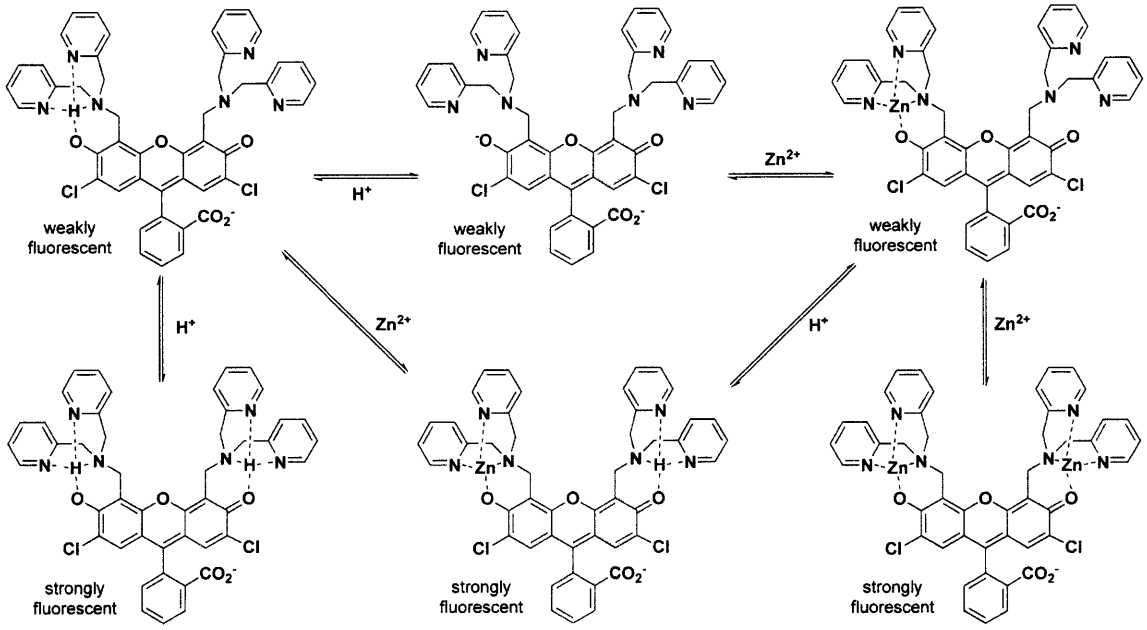

Figure 2.20. Chemical equilibria illustrating the stepwise formation of protonated and zinc-bound complexes of **1**. Significant fluorescence turn-on does not occur until both binding pockets are occupied. Charges are omitted for simplicity.

Summary and Conclusions

We have synthesized a series of Zinpyr-1 (**1**) analogues, **2**–**6**, based on the parent fluorophore 2′,7′-dichlorofluorescein. From a combination of spectrophotometric and potentiometric titrations, as well as X-ray crystallography, a detailed molecular picture of the binding states and fluorescence properties of **1** has emerged. Previous conclusions based purely on fluorometric measurements were revised. We report the direct correlation between the fluorescence emission of these compounds and their proton and zinc equilibria over a wide pH range. The first zinc affinity is much higher than previously thought (K_d = 0.04 pM) because fluorescence-binding titrations actually reveal the affinity for a second zinc ion. The second binding constant

determined in this thesis (K_d = 1.2 nM) is only an estimate due to limitations in solubility, but it matches well the value determined by fluorescence (K_d = 0.7 nM).

Additionally, we present evidence of separate quenching contributions from the tertiary nitrogen atoms and the pyridyl groups of the DPA receptors in **1** and its isomers **2** and **3**. The contribution from the pyridyl groups is of a type not previously reported in PET-based sensors, despite the number of compounds that contain 2,2-DPA as the receptor unit. PET-based quenching by pyridyl groups is unlikely on energetic grounds, and detailed theoretical analyses are required to identify the fluorescence quenching mechanism. Our results again demonstrate the power of potentiometric titrations when used in conjunction with fluorescence spectroscopy to reveal details of the quenching/unquenching mechanisms of complex fluorescent sensors used widely in biological chemistry.[68]

Acknowledgment

This work was supported by a grant from the National Institute of General Medical Sciences, GM065519 (to S.J.L.). Spectroscopic instrumentation at the MIT DCIF is maintained with funding from NIH grant no. 1S10RR13886-01. We thank Simone Friedle for all crystallographic data reported in this chapter.

References

(1) Prodi, L.; Bolletta, F.; Montalti, M.; Zaccheroni, N. *Coord. Chem. Rev.* **2000**, *205*, 59-83.

(2) Kikuchi, K.; Komatsu, K.; Nagano, T. *Curr. Opin. Chem. Biol.* **2004**, *8*, 182-191.

(3) Callan, J. F.; de Silva, A. P.; Magri, D. C. *Tetrahedron* **2005**, *61*, 8551-8588.

(4) Que, E. L.; Domaille, D. W.; Chang, C. J. *Chem. Rev.* **2008**, *108*, 1517-1549.

(5) Nolan, E. M.; Lippard, S. J. *Chem. Rev.* **2008**, *108*, 3443-3480.

(6) Valeur, B.; Leray, I. *Coord. Chem. Rev.* **2000**, *205*, 3-40.

(7) Geue, J. P.; Head, N. J.; Ward, A. D.; Lincoln, S. F. *Dalton Trans.* **2003**, 521-526.

(8) de Silva, A. P.; Rupasinghe, R. A. D. D. *J. Chem. Soc., Chem. Commun.* **1985**, 1669-1970.

(9) de Silva, S. A.; Zavaleta, A.; Baron, D. E.; Allam, O.; Isidor, E. V.; Kashimura, N.; Percarpio, J. M. *Tetrahedron Lett.* **1997**, *38*, 2237-2240.

(10) Fahrni, C. J.; Yang, L.; VanDerveer, D. G. *J. Am. Chem. Soc.* **2003**, *125*, 3799-3812.

(11) Martínez-Máñez, R.; Sancenón, F. *Chem. Rev.* **2003**, *103*, 4419-4476.

(12) Bai, Y.; Zhang, B.-G.; Xu, J.; Duan, C.-Y.; Dang, D.-B.; Liu, D.-J.; Meng, Q.-J. *New J. Chem.* **2005**, *29*, 777-779.

(13) Lee, H. N.; Swamy, K. M. K.; Kim, S. K.; Kwon, J.-Y.; Kim, Y.; Kim, S.-J.; Yoon, Y. J.; Yoon, J. *Org. Lett.* **2007**, *9*, 243-246.

(14) Lim, N. C.; Freake, H. C.; Brückner, C. *Chem. Eur. J.* **2005**, *11*, 38-49.

(15) Domaille, D. W.; Que, E. L.; Chang, C. J. *Nature Chem. Biol.* **2008**, *4*, 168-175.

(16) Palmer, A. E.; Tsien, R. Y. *Nat. Prot.* **2006**, *1*, 1057-1065.

(17) McIsaac, R. J. *Endocrinology* **1955**, *57*, 571-579.

(18) Dunn, M. F. *BioMetals* **2005**, *18*, 295-303.

(19) Giblin, L. J.; Chang, C. J.; Bentley, A. F.; Frederickson, C.; Lippard, S. J.; Frederickson, C. J. *J. Histochem. Cytochem.* **2006**, *54*, 311-316.

(20) Faa, G.; Nurchi, V. M.; Ravarino, A.; Fanni, D.; Nemolato, S.; Gerosa, C.; Van Eyken, P.; Geboes, K. *Coord. Chem. Rev.* **2008**, *252*, 1257-1269.

(21) Wu, S. M.; Qiao, X.; Noebels, J. L.; Yang, X. L. *Vision Res.* **1993**, *33*, 2611-2616.

(22) Redenti, S.; Ripps, H.; Chappell, R. L. *Exp. Eye Res.* **2007**, *85*, 580-584.

(23) Assaf, S. Y.; Chung, S.-H. *Nature* **1984**, *308*, 734-736.

(24) Vogt, K.; Mellor, J.; Tong, G.; Nicoll, R. *Neuron* **2000**, *26*, 187-196.

(25) Galasso, S. L.; Dyck, R. H. *Mol. Med.* **2007**, *13*, 380-387.

(26) Frederickson, C. J.; Koh, J.-Y.; Bush, A. I. *Nat. Rev. Neurosci.* **2005**, *6*, 449-462.

(27) Chanon, M.; Hawley, M. D.; Fox, M. A. *Photoinduced Electron Transfer*; Elsevier: Amsterdam, 1988; Vol. A.

(28) Rehm, D.; Weller, A. *Isr. J. Chem.* **1970**, *8*, 259-271.

(29) de Silva, A. P.; Gunaratne, H. Q. N.; Lynch, P. L. M. *J. Chem. Soc., Perkin Trans. 2* **1995**, 685-690.

(30) Urano, Y.; Kamiya, M.; Kanda, K.; Ueno, T.; Hirose, K.; Nagano, T. *J. Am. Chem. Soc.* **2005**, *127*, 4888-4894.

(31) Lim, M. H.; Wong, B. A.; Pitcock, W. H.; Mokshagundam, D.; Baik, M.-H.; Lippard, S. J. *J. Am. Chem. Soc.* **2006**, *128*, 14364-14373.

(32) Bissell, R. A.; Calle, E.; de Silva, A. P.; de Silva, S. A.; Gunaratne, H. Q. N.; Habib-Jiwan, J.-L.; Peiris, S. L. A.; Rupasinghe, R. A. D. D.; Samarasinghe, T. K. S. D.; Sandanayake, K. R. A. S.; Soumillion, J.-P. *J. Chem. Soc., Perkin Trans. 2* **1992**, 1559-1564.

(33) Sparano, B. A.; Shahi, S. P.; Koide, K. *Org. Lett.* **2004**, *6*, 1947-1949.

(34) Burdette, S. C.; Walkup, G. K.; Spingler, B.; Tsien, R. Y.; Lippard, S. J. *J. Am. Chem. Soc.* **2001**, *123*, 7831-7841.

(35) de Silva, A. P.; Gunaratne, H. Q. N.; McCoy, C. P. *Chem. Commun.* **1996**, 2399-2400.

(36) Hirano, T.; Kikuchi, K.; Urano, Y.; Higuchi, T.; Nagano, T. *J. Am. Chem. Soc.* **2000**, *122*, 12399-12400.

(37) Hirano, T.; Kikuchi, K.; Urano, Y.; Nagano, T. *J. Am. Chem. Soc.* **2002**, *124*, 6555-6562.

(38) Walkup, G. K.; Burdette, S. C.; Lippard, S. J.; Tsien, R. Y. *J. Am. Chem. Soc.* **2000**, *122*, 5644-5645.

(39) Nolan, E. M.; Lippard, S. J. *Inorg. Chem.* **2004**, *43*, 8310-8317.

(40) Nolan, E. M.; Jaworski, J.; Okamoto, K.-I.; Hayashi, Y.; Sheng, M.; Lippard, S. J. *J. Am. Chem. Soc.* **2005**, *127*, 16812-16823.

(41) Nolan, E. M.; Jaworski, J.; Racine, M. E.; Sheng, M.; Lippard, S. J. *Inorg. Chem.* **2006**, *45*, 9748-9757.

(42) Woodroofe, C. C.; Masalha, R.; Barnes, K. R.; Frederickson, C. J.; Lippard, S. J. *Chem. Biol.* **2004**, *11*, 1659-1666.

(43) Nolan, E. M.; Ryu, J. W.; Jaworski, J.; Feazell, R. P.; Sheng, M.; Lippard, S. J. *J. Am. Chem. Soc.* **2006**, *128*, 15517-15528.

(44) Nolan, E. M.; Lippard, S. J. *Acc. Chem. Res.* **2009**, *42*, 193-203.

(45) Teramae, S.; Osako, T.; Nagatomo, S.; Kitagawa, T.; Fukuzumi, S.; Itoh, S. *J. Inorg. Biochem.* **2004**, *98*, 746-757.

(46) Albert, A.; Serjeant, E. P. *Ionization Constants of Acids and Bases*; John Wiley & Sons Inc.: New York, 1962.

(47) Sabatini, A.; Vacca, A.; Gans, P. *Coord. Chem. Rev.* **1992**, *120*, 389-405.

(48) Sweeton, F. H.; Mesmer, R. E.; Baes, C. F., Jr. *J. Soln. Chem.* **1974**, *3*, 191-214.

(49) *SMART v5.626: Software for the CCD Detector System*; Bruker AXS: Madison, WI, 2000

(50) Sheldrick, G. M. *SHELXTL-97*; University of Göttingen: Göttingen, Germany, 2000

(51) Sheldrick, G. M. *Acta Crystallogr. Sect. A* **2008**, *64*, 112-122.

(52) Sheldrick, G. M. *SADABS: Area-Detector Absorption Correction*; University of Göttingen: Göttingen, Germany, 2001

(53) Spek, A. L. *PLATON: A Multipurpose Crystallographic Tool*; Utrecht University: Utrecht, The Netherlands, 2000

(54) Reddig, N.; Pursche, D.; Kloskowski, M.; Slinn, C.; Baldeau, S. M.; Rompel, A. *Eur. J. Inorg. Chem.* **2004**, 879-887.

(55) Brannon, J. H.; Magde, D. *J. Phys. Chem.* **1978**, *82*, 705-709.

(56) Wenska, G.; Paszyc, S. *Can. J. Chem.* **1988**, *66*, 513-516.

(57) Gruenwedel, D. W. *Inorg. Chem.* **1968**, *7*, 495-501.

(58) Christensen, J. J.; Izatt, R. M.; Wrathall, D. P.; Hansen, L. D. *J. Chem. Soc. A* **1969**, 1212-1223.

(59) Smith, R. M.; Martell, A. E. *Critical Stability Constants*; Plenum Press: New York, 1975; Vol. 2.

(60) Berti, E.; Caneschi, A.; Daiguebonne, C.; Dapporto, P.; Formica, M.; Fusi, V.; Giorgi, L.; Guerri, A.; Micheloni, M.; Paoli, P.; Pontellini, R.; Rossi, P. *Inorg. Chem.* **2003**, *42*, 348-357.

(61) Anderegg, G.; Wenk, F. *Helv. Chim. Acta* **1967**, *50*, 2330-2332.

(62) Perrin, D. D.; Dempsey, B.; Serjeant, E. P. *pKa Prediction for Organic Acids and Bases*; Chapman and Hall: London, 1981.

(63) Sjöback, R.; Nygren, J.; Kubista, M. *Spectrochim. Acta A* **1995**, *51*, L7-L21.

(64) Jang, Y. H.; Hwang, S.; Chung, D. S. *Chem. Lett.* **2001**, *30*, 1316-1317.

(65) Martin, M. M.; Ware, W. R. *J. Phys. Chem.* **1978**, *82*, 2770-2776.

(66) Ikeda, N.; Okada, T.; Mataga, N. *Bull. Chem. Soc. Jpn.* **1981**, *54*, 1025-1030.

(67) Zhang, X.; Hayes, D.; Smith, S. J.; Friedle, S.; Lippard, S. J. *J. Am. Chem. Soc.* **2008**, *130*, 15788-15789.

(68) Fahrni, C. J.; O'Halloran, T. V. *J. Am. Chem. Soc.* **1999**, *121*, 11448-11458.

Chapter 3. Subtle Modification of 2,2-Dipicolylamine Lowers the Affinity and Improves the Turn-On of Zn(II)-Selective Fluorescent Sensors

Introduction

The importance of zinc ions in biological systems, including its diverse roles in metalloproteins and structural motifs, has been well established.[1] Of current research interest is to detect and understand the functions of mobile pools of zinc in vertebrate tissues and organs.[2-6] Some resting stores and transient populations of Zn(II) are estimated to reach high micromolar or even millimolar levels.[7-9] Methods for detecting such high concentrations of the ion over more tightly held stores are therefore highly desirable. One relatively non-invasive method of attaining the requisite spatial resolution of Zn(II) localization in vivo is microscopy using Zn(II)-responsive fluorescent sensors. Although a variety of fluorophores have been used to construct such sensors, the metal-binding motifs are less diverse owing to issues of ion selectivity.[10] The di(2-picolyl)amine moiety (2,2-DPA),[11] in particular, has been widely employed because of its specificity for Zn(II) over the physiologically abundant alkali and alkaline earth cations. The first such sensor developed in our laboratory, ZP1, contained 2,2-DPA and has proved to be a useful starting point for fluorescent sensor design.

ZP1 has many favorable features, including intense absorption and emission profiles, water solubility, cell permeability, and reasonable selectivity for Zn(II) over other physiologically abundant metal species.[12] This sensor displays limited fluorescence turn-on because of proton-induced background at pH 7, however, and its high affinity for Zn(II) makes it less valuable for measuring only the labile populations of this ion. One strategy for correcting these deficiencies while keeping the desirable properties is to modify the 2,2-DPA binding units. Previous efforts in this direction yielded sensors with mixed ligand arms, where one picolyl group is substituted by a methyl, benzyl,[13] thioether,[14] or thiophene[15] group, effectively lowering the denticity of the receptor units. In each of these cases, the affinity for Zn(II) was significantly reduced but the pK_a

of the receptor unit was elevated, increasing proton-induced background fluorescence and diminishing the turn-on. These examples reveal that removal of a donor group from the binding pocket can increase its proton affinity due to electronic influences on the tertiary nitrogen atom. This problem is solved by a simple modification to the 2,2-DPA chelating moiety, namely, altering the connectivity of one pyridyl group to produce (2-picolyl)(4-picolyl)amine (2,4-DPA).[16] Here we describe the replacement of 2,2-DPA units in our ZP1 and ZP3[17] sensors by 2,4-DPA to afford the new sensors ZP1B and ZP3B (Figure 3.1).

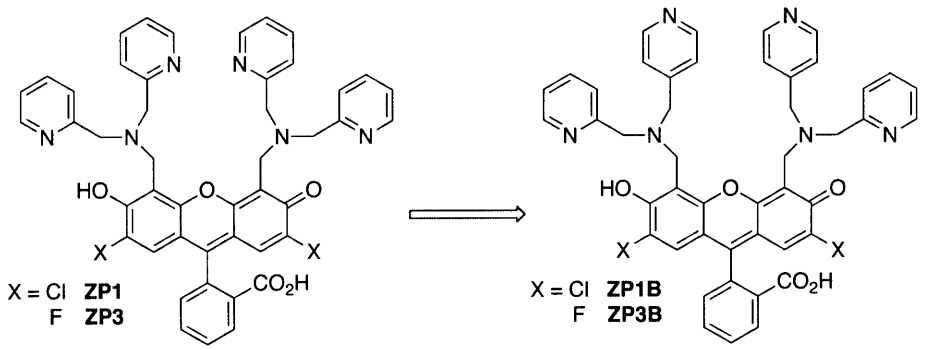

Figure 3.1. Chemical structures of fluorescein-based Zinpyr sensors bearing the 2,2-DPA and 2,4-DPA receptor units

Experimental Section

Synthesis. The syntheses of ZP1, ZP1B, 2',7'-difluorofluorescein (DFF), ZP3, and (2-picolyl)(4-picolyl)amine (2,4-DPA) were previously reported.[12,16,17] Use of pure rather than aqueous MeCN in the Mannich reaction yields high-purity sensors. Solvents were supplied by Mallinckrodt and used as received. All other reagents were purchased from Aldrich and used as received. The X-ray crystal structures of ZP1 and ZP1B were reported previously and the structure of ZP3B is described below.

General Methods. NMR spectra were obtained on a Bruker 400 MHz spectrometer at ambient temperature and referenced to the residual proton resonance of the deuterated solvent. High-resolution mass spectra were provided by staff at the MIT Department of Chemistry

Instrumentation Facility using a Bruker Daltonics APEXIV 4.7 Tesla FT-ICR mass spectrometer.

ZP3B. A suspension of 2,4-DPA (238 mg, 1.20 mmol) and paraformaldehyde (31.0 mg, 1.03 mmol) in 10 mL of MeCN was heated at 70 °C for 30 min before adding a suspension of DFF (138 mg, 0.376 mmol) in 12 mL of MeCN. After heating overnight, the solution was allowed to cool to room temperature and diffraction-quality crystals formed on standing. Filtration and washes with MeCN, Et_2O, and pentane resulted in 237 mg (80 %) of pale ochre crystals. ^{1}H NMR (DMSO-d_6, 400 MHz) δ 3.76 (4H, s), 3.92 (4H, s), 4.08 (4H, s), 6.32 (2H, d, J = 11.2 Hz), 7.21-7.27 (5H, m), 7.29-7.36 (2H, m), 7.38 (2H, d, J = 8.0 Hz), 7.68 (1H, app t, J = 7.2 Hz), 7.72-7.83 (3H, m), 7.93 (1H, d, J = 8.0 Hz), 8.37 (4H, d, J = 6.0 Hz), 8.57 (2H, d, J = 4.8 Hz). ^{13}C NMR (DMSO-d_6, 100 MHz) δ 49.11, 57.15, 58.59, 83.42, 108.36, 112.90, 113.11, 114.06, 123.41, 123.97, 124.03, 124.66, 125.63, 126.73, 131.02, 136.27, 138.20, 146.36, 147.06, 148.09, 148.29, 148.43, 148.93, 149.44, 150.13, 151.97, 157.80, 168.87. ^{19}F NMR (DMSO-d_6, 376.5 MHz) δ -139.7 (2F, d, J = 10.9 Hz). HRMS (ESI) calcd for $[M-H]^-$, 789.2642; found, 789.2616.

X-ray Crystallographic Studies. A single crystal of ZP3B was coated with paratone-N oil, mounted at room temperature on the tip of a glass fiber (Oxford magnetic mounting system), and cooled under a stream of cold N_2 maintained by a KRYO-FLEX low-temperature apparatus. Intensity data were collected on a Bruker APEX CCD diffractometer with graphite-monochromated Mo Kα radiation (λ = 0.71073 Å) controlled by a Pentium-based PC running the SMART software package.[18] A total of 2800 frames were acquired. The structure was solved by direct methods and refined on F^2 by using the SHELXTL software.[19,20] Empirical absorption correction was applied with SADABS[21] and the structure was checked for higher symmetry with PLATON.[22] All non-hydrogen atoms were refined anisotropically. In general, hydrogen atoms

were assigned idealized positions and given thermal parameters equivalent to either 1.5 (methyl hydrogen atoms) or 1.2 (all other hydrogen atoms) times the thermal parameter of the atom to which they were attached. The two hydrogen atoms (H1 and H3) of O1 and O3 of the hydroxyl groups were located from the electron density map. Compound ZP3B crystallizes as pale-yellow blocks with 1.5 molecules of MeCN.

Spectroscopic Measurements. PIPES, piperazine-*N,N'*-bis(2-ethanesulfonic acid), and 99.999% KCl were purchased from Calbiochem. Optical absorption spectra were collected with a Cary 1E spectrophotometer and fluorescence emission spectra were recorded with a Photon Technology International QM-4/2003 fluorimeter. Measurements at pH 7.0 were performed in aqueous buffer containing 50 mM PIPES and 100 mM KCl. Extinction coefficients were obtained at pH 7.0 using dye solutions in the 0.1-1.0 μM range. All quantum yield measurements were performed with a dye concentration of 0.3 μM, exciting each fluorophore at its wavelength of maximal absorbance. Emission spectra were integrated from 490-700 nm after subtracting the signal caused by scattered excitation light. Dissociation constant (K_d) values for Zn(II) were determined at a sensor concentration of 1 μM in the above mentioned pH 7.0 buffer and titrating with aliquots of 1-10 mM $ZnCl_2$. The integrated emission data were treated using a binding equation previously described.[12] Fluorescence pH titration curves were acquired by using a solution containing 10 mM KOH, 100 mM KCl, and 1.0 μM dye, to which was added aliquots of dilute aqueous HCl. Readings at several points between pH 2-10 were recorded with an Orion 720A pH meter. Samples were maintained at 25 ± 1 °C by a circulating water bath for all spectroscopic measurements.

Potentiometric Titrations. A Mettler Toledo T70 Automated Titrator equipped with a DG-111-SG glass electrode, calibrated against standard buffers, was used for all potentiometric titrations.

Solutions were prepared from Millipore water that had been degassed by boiling under low pressure for at least three hours.[23] Titration solutions contained 100 mM KCl as the electrolyte to maintain constant ionic strength and log(K_w) was defined as 13.78, which is appropriate for these conditions.[24] Samples were maintained at 25 ± 1 °C by circulating temperature-regulated water through the jacketed titration vessel during all experiments. ZP3 (0.76 mM) and ZP3B (1 mM) were pre-dissolved in 1 mL of 1.0 M HCl and diluted with water. Samples were titrated with ca. 0.1 M NaOH, standardized against potassium hydrogen phthalate before each series of titrations. Analysis of the data was performed by using the HYPERQUAD2006 v3.1.48 computer program.[25] For each compound, the proton dissociation constants (pK_a values) were determined from three separate titrations. The number of protonation equilibria was allowed to vary during the construction of computer models. In all cases, the triplicate data sets for each compound were combined for determination of the dissociation constants, which in turn were used to compute theoretical titration curves for comparison with the experimental ones.

As described previously, the titration data for ZP1 and ZP1B were best fit to a six proton model,[16] whereas the data for ZP3 and ZP3B were best fit to a five proton model. This difference has little effect on the evaluation of the higher pK_a values, as seen from a comparison between, e.g., pK_{a2} through pK_{a4} of ZP1B and ZP3B. In order to simplify comparison between the various compounds, we assign the lowest dissociation constant for ZP3B and ZP3 as pK_{a2} so that pK_{a6} represents the equilibrium between the monoprotonated (LH^-) and fully deprotonated (L^{2-}) forms in all cases.

Cell culture and Microscopy. Min6 cells were cultured at 37 °C in Dulbecco's Modification of Eagle's Medium (DMEM, Mediatech), containing 4.5 g/L of glucose and L-glutamine and supplemented with 10 % fetal bovine serum (HyClone), penicillin (1 unit/mL), and streptomycin

(1 μg/mL). For live cell imaging, cells were plated onto poly-D-lysine coated glass-bottom culture dishes (MatTek) and grown for 2-3 days. Cells were incubated with 40 μM of either ZP1B or ZP3B and 5 μM Hoechst 33258 (Aldrich) for 1-4 hours at 37 °C, washed with DMEM twice, and imaged in PBS. After collecting images in both the green and blue channels, *N,N,N',N'*-tetrakis(2-pyridylmethyl)-ethylenediamine (TPEN) was added to the dish to a final concentration of 40 μM and cells were imaged again after 5 min.

Microscopy was performed using a Zeiss Axiovert 200M inverted epifluorescence microscope and images were collected with an EM-CCD digital camera (Hamamatsu). Differential Interference Contrast (DIC) and fluorescence images were acquired with an oil-immersion 63x objective lens. An EXFO metal-halide lamp was used for fluorescence excitation, with a GFP filter (450-490 nm excitation, 500-550 nm emission) for the green channel and a DAPI filter (320-380 nm excitation, 420-470 nm emission) used for the blue channel. Microscope operation and image processing were performed using Volocity software (Improvision, Lexington, MA).

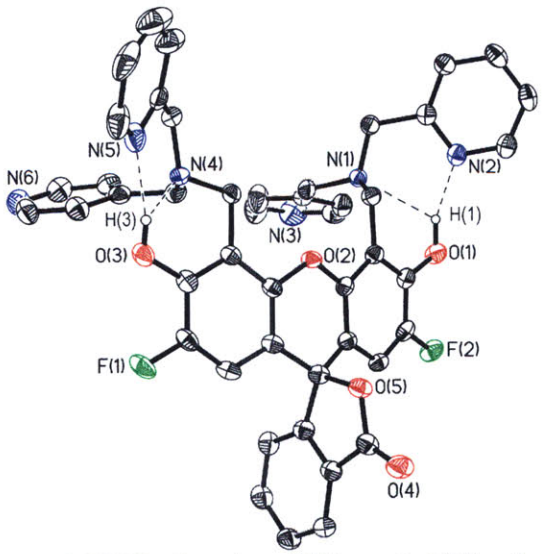

Figure 3.2. ORTEP diagram of ZP3B showing 50% probability thermal ellipsoids on all non-hydrogen atoms. Dashed lines designate hydrogen bonding contacts.

Table 3.1. Crystallographic Parameters for **ZP3B**

	ZP3B•1.5MeCN
Empirical formula	$C_{49}H_{40.5}N_{7.5}O_5F_2$
Formula weight	852.39
Crystal System	Triclinic
Space group	$P\bar{1}$
a (Å)	12.4844(15)
b (Å)	13.9419(17)
c (Å)	14.7210(18)
α (deg)	114.010(2)
β (deg)	103.594(2)
γ (deg)	103.639(2)
V (Å^3)	2110.6(4)
Z	2
ρ_{calc}, g/cm^3	1.341
Temperature (K)	110
μ (Mo Kα), mm^{-1}	0.095
θ range (deg)	2.46 to 26.37
Crystal size (mm)	0.15 x 0.15 x 0.10
Total no. of data	32603
No. of unique data	8583
Completeness to θ	99.5 %
max, min peaks, e/Å^3	0.747 and -0.504
Goodness-of-fit on F^2	1.042
R_1 (%)[a]	6.53
wR_2 (%)[b]	16.14

[a] $R_1 = \sum||F_o|-|F_c||/\Sigma|F_o|$, [b] $wR_2 = \{\Sigma[w(F_o^2-F_c^2)^2]/\Sigma[w(F_o^2)^2]\}^{1/2}$

Results and Discussion

The syntheses of ZP1B and ZP3B apply standard Mannich reaction conditions to link 2,4-DPA to the appropriate dichloro- or difluoro-fluorescein platform, yielding diffraction-quality crystals by slow evaporation of the solvent directly from the reaction solution. As with ZP1B,[16] ZP3B crystallizes as the neutral lactone isomer, with protons bound in both binding pockets

(Figure 3.2 and Table 3.1). The basicity of the binding pockets is determined not just by the tertiary nitrogen atoms but by hydrogen bonding interactions with the pyridyl groups and the phenolic oxygen atoms (Table 3.2).

Table 3.2. Summary of Distances (Å) between Hydrogen Bond Donor and Acceptor Atoms in ZP3B.

Bond Lengths	Å
O1–H1...N1	2.940(3)
O1–H1...N2	2.709(3)
O3–H3...N4	2.932(3)
O3–H3...N5	2.761(3)

Atoms are labeled in Figure 3.2.

The first valuable property of the 2,4-DPA ligand is to lower the pK_a values of the binding pockets of ZP1B and ZP3B, thereby minimizing the proton-induced turn-on. The result is a substantially lower fluorescence quantum yield (Φ) at pH 7 compared to ZP1 and ZP3 (Table 3.3). The quantum yields and pK_a values of ZP1 were remeasured for purposes of comparison to the new sensors for reasons describe elsewhere.[16] Representative fluorescence-based pH titrations for all four sensors are depicted in Figure 3.3. Unlike ZP1 and ZP3, which exhibit a two-step fluorescence turn-on as the pH is lowered, ZP1B and ZP3B display a nearly uniform increase in fluorescence between pH 7.0 and 3.5. This difference in behavior comes from a significant shift in the pK_a values determined from potentiometric titrations (Table 3.4). For all of these compounds, the largest turn-on is caused by binding of the second proton, represented by pK_{a5}; an additional turn-on occurs upon binding of two additional protons (Figure 3.4). The large differences between pK_{a5} and pK_{a4} for ZP1 and ZP3 are responsible for their two-step turn-on. The corresponding differences are much smaller for ZP1B and ZP3B, leading to both a shift in fluorescence pH response and the loss of the two-step feature. The practical result of this

change in proton affinity is that the fluorescence of each of these new sensors exhibits virtually no turn-on at pH ≥ 7.

Table 3.3. Spectroscopic Properties of Sensors Containing the 2,2-DPA and 2,4-DPA Binding Motifs[a]

		Emission λ(nm), Φ[b]				
	Abs λ(nm), ε x10^4 M^{-1}cm^{-1}	free	Zn-bound	pK_a (FL)	K_d (Zn^{2+}) (FL)	DR[c]
ZP1	515, 7.9[d]	531, 0.17	527, 0.70	7.0, 4.0	0.7 nM[d]	4
ZP1B	516, 6.8	530, 0.03	521, 0.70	5.6	12.9(5) mM	23
ZP3[e]	502, 7.5	521, 0.15	516, 0.92	6.8, 4.0	0.7 nM	6
ZP3B	505, 7.3	521, 0.03	512, 0.93	5.7	17(3) mM	31

[a]All measurements made at pH 7.0 (50 mM PIPES, 100 mM KCl). [b]Quantum yield (Φ) referenced to fluorescein in 0.1 M NaOH (Φ = 0.95).[26] [c]Dynamic range (DR) defined as the ratio of Φ_{Zn} to Φ_{apo}. [d]Specific values from ref. 12. Other values for ZP1 have been remeasured for this study. [e]Values from ref. 17.

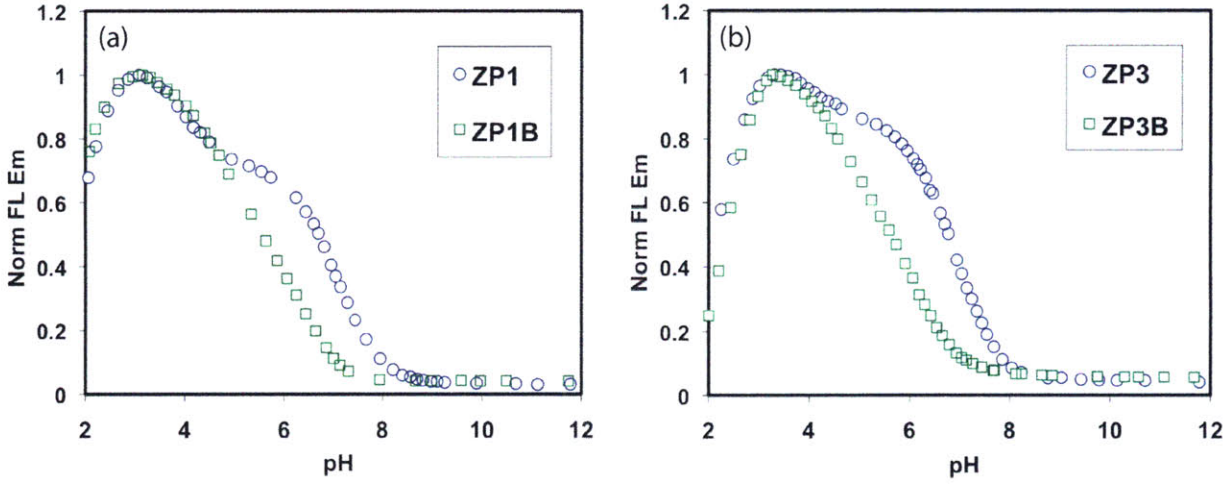

Figure 3.3. Fluorescence-based pH titrations comparing (a) ZP1 with ZP1B and (b) ZP3 with ZP3B. The basicity of the binding pockets is reduced in the compounds bearing 4-pyridyl arms, thereby shifting the fluorescence turn-on to lower pH values.

Table 3.4. Comparison of pK_a values as determined by potentiometric titration

	ZP1B[a]	ZP3B	ZP1[a]	ZP3
pK_{a6}	7.473(5)	7.378(3)	8.12(2)	7.96(2)
pK_{a5}	6.35(1)	6.22(1)	6.96(1)	6.81(2)
pK_{a4}	5.205(8)	5.22(1)	4.59(3)	4.62(4)
pK_{a3}	4.51(2)	4.45(5)	3.810(9)	3.78(1)
pK_{a2}	3.10(3)	3.15(7)	2.8(3)	2.9(2)
pK_{a1}	2.67(5)	--	2.3(2)	--

[a]Values from ref. 16. Numbers in parentheses represent standard deviations in the last significant digit.

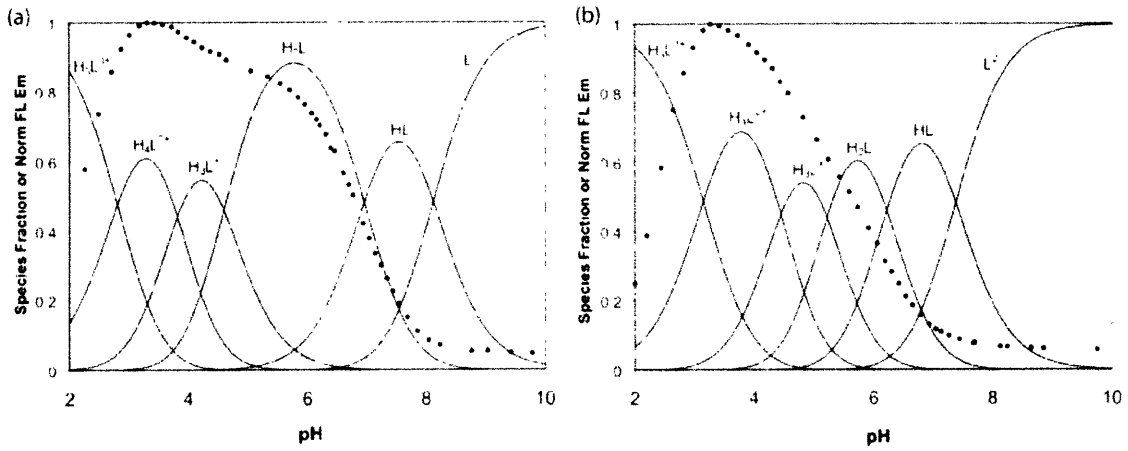

Figure 3.4. Fluorescence pH titration data (points) for (a) ZP3 and (b) ZP3B overlaid on speciation plots created from calculated acid dissociation constants.

With little influence from protons at pH 7, ZP1B and ZP3B each display a large Zn(II)-induced turn-on. Fluorescence titrations with $ZnCl_2$ yield dissociation constants (K_d) in the millimolar range and significantly improved dynamic ranges compared to ZP1 and ZP3 (Figures 3.5a and 3.6a and Table 3.3). Zn(II)-induced changes to the absorption spectra differ from those of our previous sensors (Figures 3.5b and 3.6b). The major peak displays a small hypsochromic shift, as expected from coordination of Zn(II) by the phenolic oxygen atoms, but the intensity of this absorption band is greatly reduced. Additionally, a second band grows in at higher wavelength after the addition of ~8 equiv of $ZnCl_2$. The reason for this behavior is not yet known, but excitation at the peak of the new band yields virtually no fluorescence response and these bands do not appear following a single addition of excess $ZnCl_2$. Furthermore, only Zn(II) binding and not protonation of the receptor units causes these new absorption bands to form. The metal selectivity of these sensors is similar to related compounds like ZS5,[15] with an improved response over ZP1 to Zn(II) in the presence of Fe(II) or Co(II) (Figure 3.7).

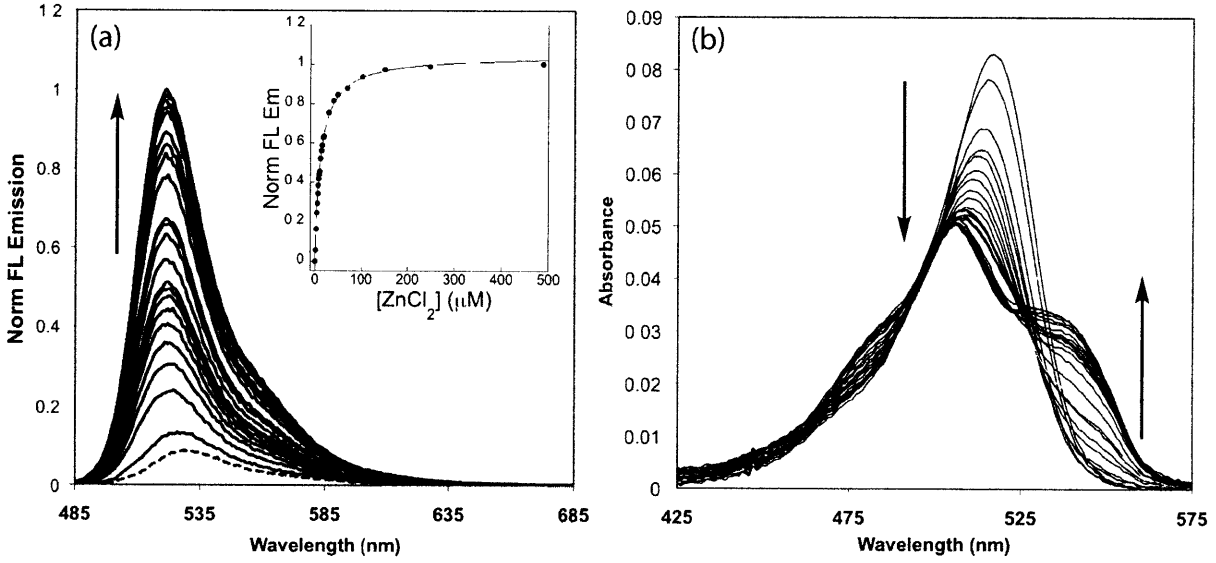

Figure 3.5. Fluorescence (a) and absorbance (b) titration of 1 μM ZP1B with increasing amounts of $ZnCl_2$ at pH 7 (50 mM PIPES, 100 mM KCl). Emission increases from basal fluorescence (dashed line) in the presence of 1, 3, 4, 5, 6, 7, 8, 9, 10, 12, 14, 16, 18, 20, 29, 39, 49, 68, 97, 102, 151, 248, and 489 μM total ZnCl2. The absorption band at 529 nm begins to emerge at ~7 μM $ZnCl_2$.

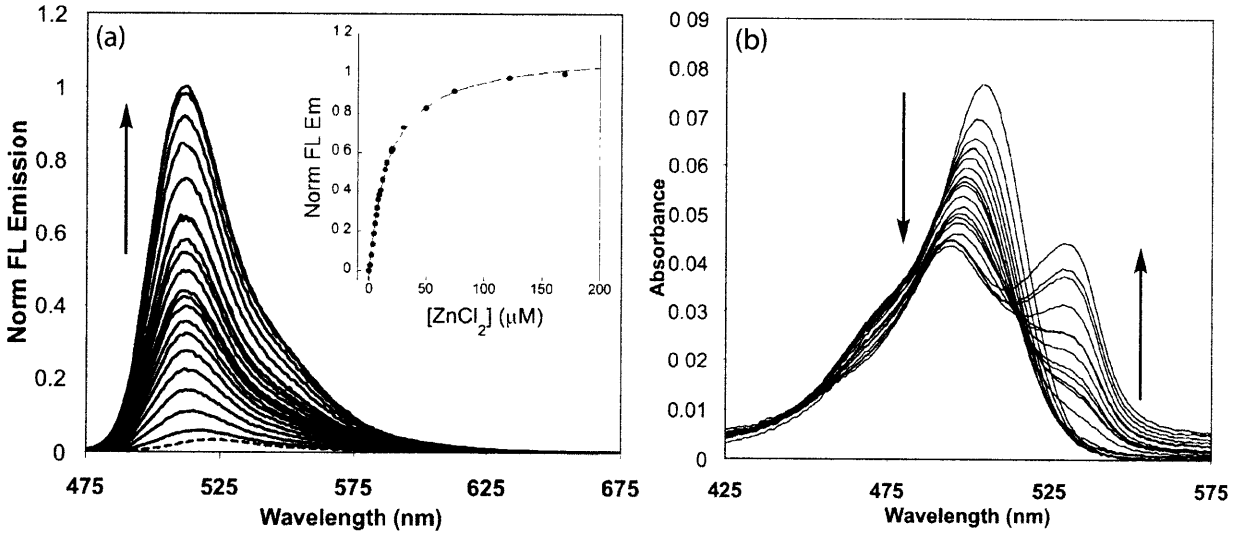

Figure 3.6. Fluorescence (a) and absorbance (b) titration of 1 μM ZP3B with increasing amounts of $ZnCl_2$ at pH 7 (50 mM PIPES, 100 mM KCl). Emission increases from basal fluorescence (dashed line) in the presence of 1, 2, 3, 4, 5, 6, 7, 8, 9, 10, 12, 14, 16, 19, 20, 30, 50, 74, 122, and 170 μM total ZnCl2. The absorption band at 529 nm begins to emerge at 8 mM $ZnCl_2$.

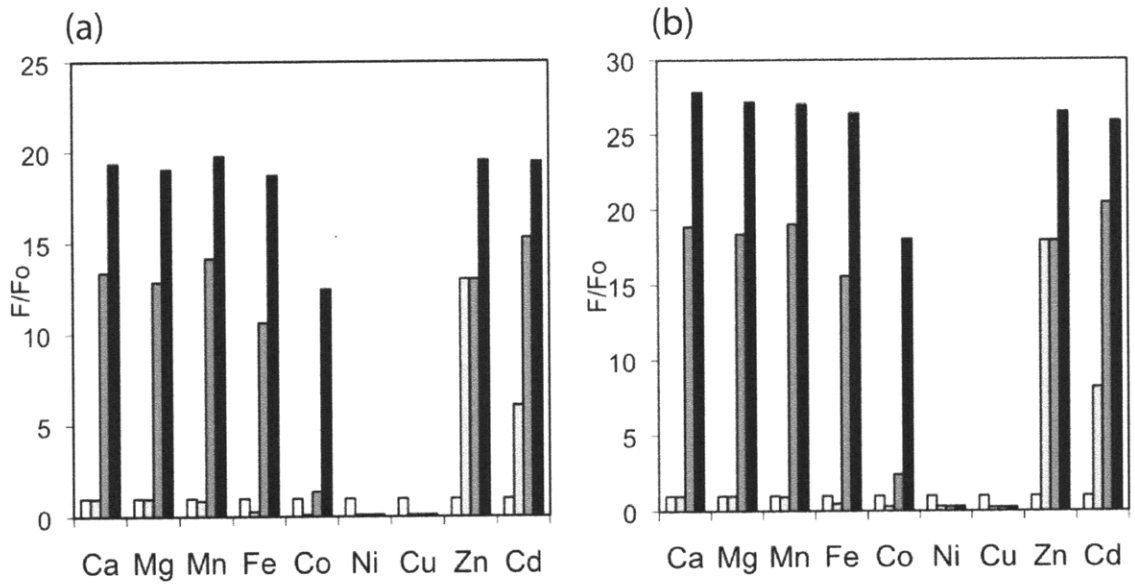

Figure 3.7. Selectivity of (a) ZP1B and (b) ZP3B for Zn(II) in the presence of other metal ions, as measured by fluorescence turn-on. All measurements were normalized to the emission from a 1 μM solution of sensor (white bar) at pH 7 (50 mM PIPES, 100 mM KCl). The light gray bar represents the emission of each solution after addition of 50 equivalents of the divalent cation shown. The dark gray and black bars represent the emission after subsequent addition of 50 and 500 equivalents, respectively, of Zn(II) to the same solution of sensor and the cation of interest.

The relatively high K_d values of ZP1B and ZP3B are appropriate for the detection of labile zinc pools because these values approximate the transient populations of zinc that are estimated in some forms of physiological signaling.[8] Also, the large dynamic range of these new sensors makes them well suited for use in fluorescence microscopy. To highlight the utility of these compounds in a biological application, we examined the fluorescence signal from Min6, a line of pancreatic β-cells.[27]

It is well established that Zn(II) co-localizes with insulin in β-cell secretory vesicles and plays a role in both the synthesis and final structure of the insulin hexamer.[28] These β-cell vesicles exhibit some variability in Zn(II) content, but concentrations reach millimolar levels.[29,30] Although many Zn(II) sensors are touted for their high sensitivity to low ion levels, a more weakly binding sensor will be able to distinguish the most labile Zn(II) populations from more tightly bound stores. Incubation of either ZP1B or ZP3B with Min6 cells yields staining patterns

(Figures 3.8-3.11) that are strikingly similar to those obtained by autometallography, a technique that visualizes only labile, granular Zn(II) in pancreatic cells.[31] No staining is observed in the nuclei, demarcated with the blue dye Hoechst 33258, and the punctate staining of the cytosolic region is suggestive of the distribution of Zn(II)-containing secretory vesicles. Addition of the metal chelator *N,N,N',N'*-tetra(2-picolyl)-ethylenediamine (TPEN) extinguishes the Zn(II)-induced fluorescence. This highly specific fluorescence labeling is an improvement over more diffuse staining patterns obtained with higher-affinity sensors.[32,33]

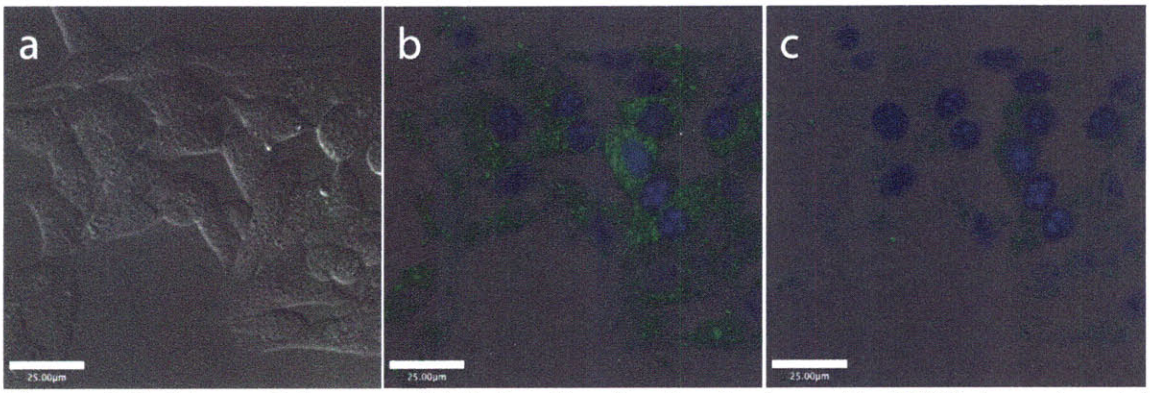

Figure 3.8. Live cell images of Min6 cells after incubating with ZP3B (green) and Hoechst 33258 nuclear stain (blue) for 3 h. DIC image (a) and merged green and blue channels before (b) and after (c) the addition of TPEN.

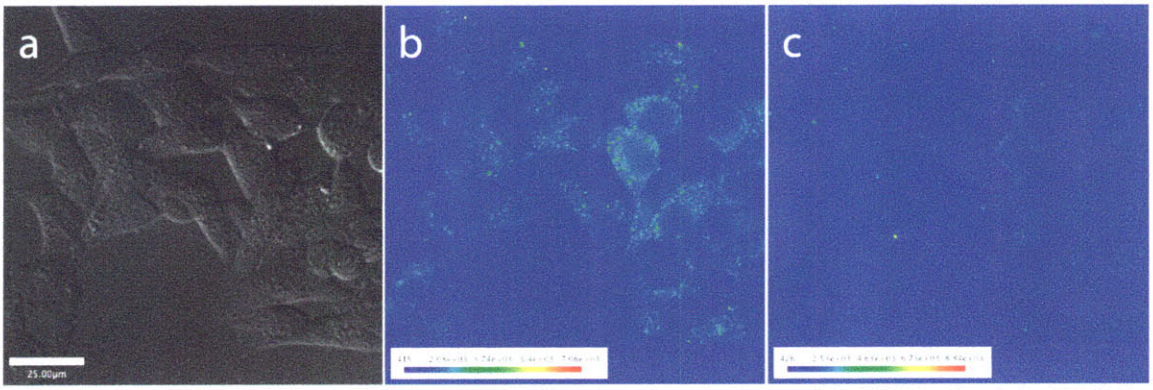

Figure 3.9. Live cell images of Min6 cells after incubating with ZP3B for 3 h. DIC image (a) and green fluorescence channel, depicted on a pseudocolor scale for clarity, before (b) and after (c) the addition of TPEN.

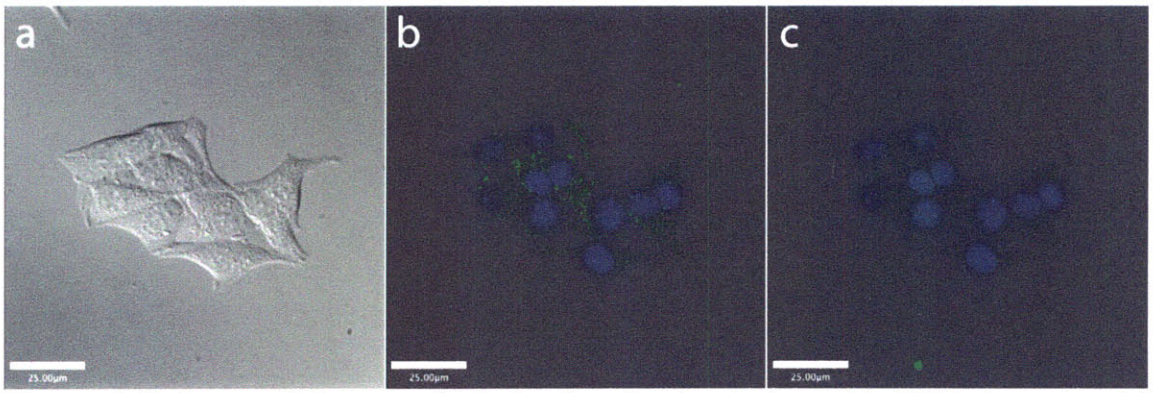

Figure 3.10. Live cell images of Min6 cells after incubating with ZP1B (green) and Hoechst 33258 nuclear stain (blue) for 1 h. DIC image (a) and merged green and blue channels before (b) and after (c) the addition of TPEN.

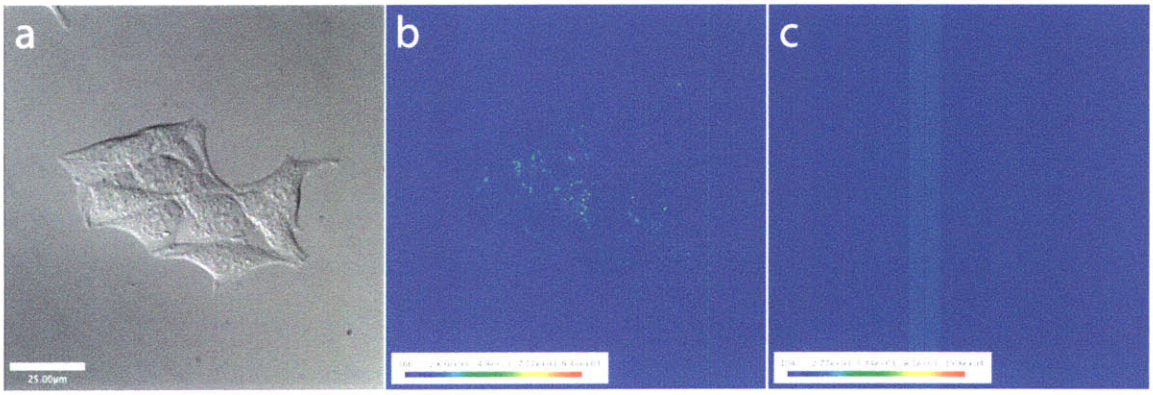

Figure 3.11. Live cell images of Min6 cells after incubating with ZP1B for 1 h. DIC image (a) and green fluorescence channel, depicted on a pseudocolor scale for clarity, before (b) and after (c) the addition of TPEN.

Summary and Conclusions

The variety of receptor groups that have been appended to the fluorescein backbone has yielded Zn(II)-responsive sensors with a wide range of binding affinities, with K_d values from sub-nM to mM.[34] ZP1B and ZP3B are useful additions to the higher end of this binding spectrum, having minimal proton-induced turn-on at physiological pH and large dynamic ranges. Other receptor unit designs provide low Zn(II) affinity with less pH sensitivity, but these constructs also exhibit much lower Φ values in their turned-on states.[35,36] We suggest that introduction of the 2,4-DPA unit in any of the large number of existing fluorescent Zn(II) sensors incorporating 2,2-DPA would create a new sensor that would retain any favorable features of the

original compound but also lower the Zn(II) affinity by several orders of magnitude, allowing for the preferential detection of only the most concentrated stores of Zn(II).

Acknowledgment. This work was supported by a grant from the National Institute of General Medical Sciences, GM065519. Spectroscopic instrumentation at the MIT DCIF is maintained with funding from NIH grant number 1S10RR13886-01. We thank Simone Friedle for all crystallographic data reported in this chapter.

References

(1) Vallee, B. L.; Falchuk, K. H. *Physiol. Rev.* **1993**, *73*, 79-118.

(2) Huang, Y. Z.; Pan, E.; Xiong, Z.-Q.; McNamara, J. O. *Neuron* **2008**, *57*, 546-558.

(3) Palmer, B. M.; Vogt, S.; Chen, Z.; Lachapelle, R. R.; LeWinter, M. M. *J. Struct. Biol.* **2006**, *155*, 12-21.

(4) Redenti, S.; Ripps, H.; Chappell, R. L. *Exp. Eye Res.* **2007**, *85*, 580-584.

(5) Faa, G.; Nurchi, V. M.; Ravarino, A.; Fanni, D.; Nemolato, S.; Gerosa, C.; Van Eyken, P.; Geboes, K. *Coord. Chem. Rev.* **2008**, *252*, 1257-1269.

(6) Gyulkhandanyan, A. V.; Lee, S. C.; Bikopoulos, G.; Dai, F.; Wheeler, M. B. *J. Biol. Chem.* **2006**, *281*, 9361-9372.

(7) Danscher, G.; Stoltenberg, M. *J. Histochem. Cytochem.* **2005**, *53*, 141-153.

(8) Frederickson, C. J.; Koh, J.-Y.; Bush, A. I. *Nat. Rev. Neurosci.* **2005**, *6*, 449-462.

(9) Costello, L. C.; Franklin, R. B. *Mol. Cancer* **2006**, *5*, 17.

(10) Que, E. L.; Domaille, D. W.; Chang, C. J. *Chem. Rev.* **2008**, *108*, 1517-1549.

(11) Romary, J. K.; Barger, J. D.; Bunds, J. E. *Inorg. Chem.* **1968**, *7*, 1142-1145.

(12) Burdette, S. C.; Walkup, G. K.; Spingler, B.; Tsien, R. Y.; Lippard, S. J. *J. Am. Chem. Soc.* **2001**, *123*, 7831-7841.

(13) Goldsmith, C. R.; Lippard, S. J. *Inorg. Chem.* **2006**, *45*, 6474-6478.

(14) Nolan, E. M.; Lippard, S. J. *Inorg. Chem.* **2004**, *43*, 8310-8317.

(15) Nolan, E. M.; Ryu, J. W.; Jaworski, J.; Feazell, R. P.; Sheng, M.; Lippard, S. J. *J. Am. Chem. Soc.* **2006**, *128*, 15517-15528.

(16) Wong, B. A.; Friedle, S.; Lippard, S. J. *J. Am. Chem. Soc.* **2009**, *131*, ASAP.

(17) Chang, C. J.; Nolan, E. M.; Jaworski, J.; Burdette, S. C.; Sheng, M.; Lippard, S. J. *Chem. Biol.* **2004**, *11*, 203-210.

(18) *SMART v5.626: Software for the CCD Detector System*; Bruker AXS: Madison, WI, 2000

(19) Sheldrick, G. M. *SHELXTL-97*; University of Göttingen: Göttingen, Germany, 2000

(20) Sheldrick, G. M. *Acta Crystallogr. Sect. A* **2008**, *64*, 112-122.

(21) Sheldrick, G. M. *SADABS: Area-Detector Absorption Correction*; University of Göttingen: Göttingen, Germany, 2001

(22) Spek, A. L. *PLATON: A Multipurpose Crystallographic Tool*; Utrecht University: Utrecht, The Netherlands, 2000

(23) Albert, A.; Serjeant, E. P. *Ionization Constants of Acids and Bases*; John Wiley & Sons, Inc.: New York, 1962.

(24) Sweeton, F. H.; Mesmer, R. E.; Baes Jr., C. F. *J. Soln. Chem.* **1974**, *3*, 191-214.

(25) Sabatini, A.; Vacca, A.; Gans, P. *Coord. Chem. Rev.* **1992**, *120*, 389-405.

(26) Brannon, J. H.; Magde, D. *J. Phys. Chem.* **1978**, *82*, 705-709.

(27) Miyazaki, J.-I.; Araki, K.; Yamato, E.; Ikegami, H.; Asano, T.; Shibasaki, Y.; Oka, Y.; Yamamura, K.-I. *Endocrinology* **1990**, *127*, 126-132.

(28) Dodson, G.; Steiner, D. *Curr. Opin. Struct. Biol.* **1998**, *8*, 189-194.

(29) Hutton, J. C.; Penn, E. J.; Peshavaria, M. *Biochem. J.* **1983**, *210*, 297-305.

(30) Foster, M. C.; Leapman, R. D.; Li, M. X.; Atwater, I. *Biophys. J.* **1993**, *64*, 525-532.

(31) Søndergaard, L. G.; Brock, B.; Stoltenberg, M.; Flyvbjerg, A.; Schmitz, O.; Smidt, K.; Danscher, G.; Rungby, J. *Horm. Metab. Res.* **2005**, *37*, 133-139.

(32) Lukowiak, B.; Vandewalle, B.; Riachy, R.; Kerr-Conte, J.; Gmyr, V.; Belaich, S.; Lefebvre, J.; Pattou, F. *J. Histochem. Cytochem.* **2001**, *49*, 519-527.

(33) Zhang, X.; Hayes, D.; Smith, S. J.; Friedle, S.; Lippard, S. J. *J. Am. Chem. Soc.* **2008**, *130*, 15788-15789.

(34) Nolan, E. M.; Lippard, S. J. *Acc. Chem. Res.* **2009**, *42*, 193-203.

(35) Komatsu, K.; Kikuchi, K.; Kojima, H.; Urano, Y.; Nagano, T. *J. Am. Chem. Soc.* **2005**, *127*, 10197-10204.

(36) Parkesh, R.; Lee, T. C.; Gunnlaugsson, T. *Org. Biomol. Chem.* **2007**, *5*, 310-317.

Chapter 4. Labeling of the Cell Membrane with Fluorescent Sensors to Track Extracellular Zn(II)

Introduction

In order to effectively utilize fluorescent sensors to detect and monitor changes in biological mobile zinc populations, the probes must have properties that make them useful not only in the cuvette but also in live cells. Although our laboratory has produced a number of sensors that have displayed this function in biological settings,[1-3] many challenges remain. Some of the goals in zinc sensing, such as determining the concentrations and the temporal and spatial dynamics of mobile zinc populations, are complicated by the fact that most sensors are themselves mobile within the cellular environment. In addition, some sensors display a preference to localize within particular subcellular regions[3] – a preference that may change depending upon whether or not the sensor is bound to zinc.

To avoid such complications, a few different strategies have been employed. On a basic level, adding charged functional groups to a sensor will hinder permeability to cell membranes and increase water-solubility. Once internalized, such probes become trapped in the cytosol or selected organelles. Improved solubility may also enhance the dispersion of a sensor, decreasing the chances of binding to particular cellular structures. This strategy is applied in our laboratory by synthesizing variants of our sensors with "bottom-ring" carboxylate groups and their corresponding esters.[4]

To tune the subcellular localization even further, sensors can be covalently attached to specific cellular components. Many techniques have been developed for linking fluorophores or chemical tags to proteins, mostly by expressing a variant of the target protein with a genetically encoded marker or enzyme unit where the attachment is made. This strategy has recently resulted in the coupling of ion-sensitive, small-molecule fluorophores to selected cellular proteins. Roger Tsien's laboratory has developed a fluorescein-based biarsenical sensor for calcium that links to

an artificially expressed tetracysteine tag.[5] In our laboratory, the AGT coupling method has been used to link ZP1 to both mitochondrial and Golgi-localized proteins.[6]

The rationale for designing methods for the subcellular imaging of Zn(II) is the same as for its physiological relative Ca(II).[5,7] Although the various signaling roles of Ca(II) are better established than those of Zn(II), the methods and challenges for studying both ions by fluorescence microscopy are very similar. Labile Zn(II) has been examined by fluorescence in a wide range of tissue and cell types at various magnifications. Light microscopy allows for imaging at a lower resolution limit of ca. 200 nm, which is adequate for the visualization of "microdomains" within eukaryotic cells.[5] Certain cellular structures, such as secretory vesicles[8] and synaptic clefts,[9] are smaller than this resolution limit, however, and distinguishing between different isolated populations of Zn(II) in these "nanodomains" is difficult. Furthermore, since Zn(II) is a tightly regulated species with many known and putative cellular buffers,[10] free zinc concentrations are not expected to remain elevated above background levels very long. Binding by these numerous cellular buffers causes transient release of a Zn(II) store to be highly localized, with free zinc sequestered before it diffuses to fill a large area. Therefore, the spatially averaged concentration determined by a freely diffusing sensor may not accurately reflect local concentrations.

The solution to the problem of imaging events at a scale smaller than the nominal resolution limit of fluorescence microscopy is to fix the reporter to select subcellular locations. For example, the size of a synaptic cleft is sufficiently small (ca. 20 nm) that it is impossible to visually resolve whether a fluorescent signal is originating from the presynaptic cytosol, synaptic cleft, or postsynaptic cytosol. Therefore, when Zn(II) is released from a synaptic vesicle, it becomes difficult to track the fate of this ion using a freely diffusing sensor. By selective

tethering of a fluorescent sensor, it becomes possible to visualize mobile Zn(II) populations through space and time. For instance, localization of the sensor to the postsynaptic membrane ensures that an increase in fluorescent signal is due only to Zn(II) that has crossed the synapse. Likewise, tethering the sensor to the interior of the postsynaptic membrane ensures that only Zn(II) that has been transported into the postsynaptic cytosol is visualized.

Methods for the labeling of cellular components are manifold.[11,12] Some techniques are relatively non-selective, such as the reaction of NHS esters of fluorescent tags with cellular amines, like those of lysine residues on proteins, or the oxidation of cell-surface glycans with sodium periodate, followed by coupling of a functionalized hydrazine tag to the resulting aldehyde moieties.[13] The addition of azide groups to cell-surface structures provides a reaction partner for fluorophore-conjugated alkynes without the aid of a copper catalyst.[14,15] Although these examples do not have single, unique targets on the cell surface, the labeling is accomplished exclusively with small molecules and no genetic manipulation is required. The lack of specificity also allows for extensive fluorophore attachment, yielding high copy numbers and global labeling.

As an initial test of labeling cell membranes with our Zn(II)-responsive probes, an activated ester of ZP1, **ZP1ss**, was synthesized (Scheme 4.1). It was anticipated that this construct would be membrane-impermeable due to the negatively charged sulfonate group and that it would react with free amino groups on cell surface proteins. Since our laboratory has developed sensors with larger dynamic ranges and weaker affinities than those for ZP1, some alternative "bottom-ring" carboxylate sensors were also synthesized.

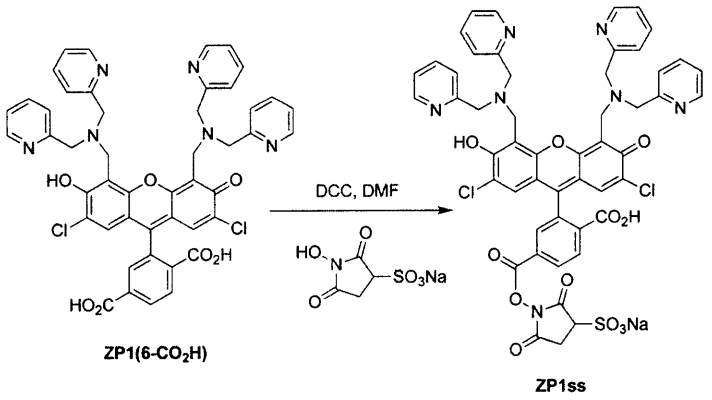

Scheme 4.1 Synthesis of ZP1ss

Experimental Section

Methods and Materials. Solvents were supplied by Mallinckrodt and used as received. All other reagents were purchased from Aldrich and used as received. NMR spectra were obtained on a Bruker 400 MHz spectrometer, and referenced to the residual proton resonance of the deuterated solvent. Low resolution ESI mass spectra were obtained by using an Agilent 1100 Series LC/MSD mass spectrometer.

2',7'-Dichloro-6-(2-(2-(2-(3-iodo-4-(methoxycarbonyl)benzamido)ethoxy)ethoxy)ethyl-carbamoyl)-3-oxo-3H-spiro-3',6'-diyl diacetate (ZP1ss). A solution of **ZP1(6-CO_2H)** (50 mg, 58 μmol), DCC (13 mg, 64 μmol), and sodium N-hydroxysulfosuccinimide (12 mg, 58 μmol) in 2 mL of DMF was stirred overnight. Dilution with 1:1 EtOAc: Et_2O caused precipitation of a pink, flocculent solid which was filtered and washed with Et_2O, yielding 24 mg (39 %) of red powder. ^{1}H NMR (DMSO-d_6, 400 MHz) δ 2.76-2.85 (2H, m), 3.63 (1H, dd, J = 8.8, 2.4 Hz), 3.86-4.01 (8H, m), 4.11 (4H, s), 6.69 (2H, d, J = 4.8 Hz), 7.19-7.27 (4H, m), 7.35 (4H, d, J = 7.6 Hz), 7.68-7.76 (4H, m), 8.09 (1H, br s), 8.15 (1H, d, J = 4.4 Hz), 8.34 (1H, d, J = 4.4 Hz), 8.51 (4H, d, J = 4.8 Hz). LRMS (ESI) calcd for $[M-H]^-$, 1042.2; found, 1042.7.

2-(2,7-dichloro-6-hydroxy-3-oxo-4,5-bis(((pyridin-2-ylmethyl)(pyridin-4-ylmethyl)amino)-methyl)-3H-xanthen-9-yl)terephthalic acid (ZP1B(6-CO_2H), 2). A suspension of 2,4-DPA

(491 mg, 2.46 mmol) and paraformaldehyde (62.4 mg, 2.08 mmol) in 15 mL of MeCN was heated at 70 °C for 30 min before adding a suspension of $Ac_2DCF(6\text{-}CO_2^-)$ pyridinium salt, **1**, (294 mg, 0.484 mmol) in 20 mL of MeCN. After stirring for 48 h, the reaction mixture was cooled to room temperature and a red solid was collected and washed with MeCN. This crude product was suspended in 15 mL of MeCN and added to a fresh mixture of 2/4-DPA (73.7 mg, 0.370 mmol) and paraformaldehyde (16.7 mg, 0.556 mmol) in 12 mL of MeCN at 70 °C. The reaction mixture was heated for 48 h, cooled to room temperature, and filtered. The resulting red solid was washed with MeCN, Et_2O, and pentane, yielding 215 mg (51%) of pure product. ^{1}H NMR (DMSO-d_6, 400 MHz) δ 3.72-3.86 (4H, m), 3.93 (4H, s), 4.10 (4H, s), 6.61 (2H, s), 7.25 (4H, d, J = 6.0 Hz), 7.30-7.42 (4H, m), 7.74 (1H, s), 7.78-7.87 (2H, m), 8.05 (1H, d, J = 8.0 Hz), 8.18 (1H, d, J = 8.0 Hz), 8.42 (4H, d, J = 5.2 Hz), 8.60 (2H, d, J = 3.6 Hz). LRMS (ESI) calcd for $[M\text{-}H]^-$, 865.2; found, 865.8.

2',7'-Difluoro-5/6-carboxyfluorescein (DFF(5/6-CO_2H), 3). A solution of 4-fluororesorcinol (1.99 g, 15.5 mmol) and 1,2,4-benzenetricarboxylic acid (1.65 g, 7.85 mmol) in 15 mL of methanesulfonic acid was sealed in a dry, Teflon-capped flask and heated at 85 °C for 48 h. After cooling to room temperature, the dark purple solution was slowly added to ice water, forming an orange precipitate. The solid was filtered after stirring for 1 h, then dried at 65 °C under vacuum for 3 days, yielding 3.14 g of orange powder (98 %). ^{1}H NMR (MeOD, 400 MHz) δ 6.98-7.11 (4H, m), 7.29-7.40 (4H, m), 7.49 (1H, d, J = 8.0 Hz), 7.97 (1H, s), 8.35-8.47 (3H, m), 8.85 (1H, s). LRMS (ESI) calcd for MH^+, 413.0; found 413.0.

3',6'-Diacetyl-2',7'-difluoro-6-carboxyfluorescein pyridinium salt (Ac_2DFF(6-CO_2H), 4). A suspension of **3** (3.14 g, 7.626 mmol) and pyridine (0.5 mL, 6.18 mmol) in 7 mL of acetic anhydride was stirred at 80 °C, producing a dark purple solution. After 1 h, the solution was

cooled to room temperature then stored at -4 °C. Salt crystals had formed overnight and were removed by filtration. The acetic anhydride was quenched in 25 mL of H_2O and the product was extracted into EtOAc and washed with 3% aq. HCl and brine. Evaporation of the solvent yielded a pale orange solid that was recrystallized from acetic anhydride and pyridine, producing a fine white powder (full yield not determined). ^{1}H NMR (CD_2Cl_2, 400 MHz) δ 2.31 (6H, s), 6.61 (2H, d, J = 10.0 Hz), 7.17 (2H, d, J = 6.4 Hz), 7.37-7.44 (2H, m), 7.77-7.84 (1H, m), 7.92 (1H, s), 8.10 (1H, d, J = 8.0 Hz), 8.38 (1H, d, J = 8.0 Hz), 8.61-8.66 (2H, m).

2-(4,5-bis((bis(pyridin-2-ylmethyl)amino)methyl)-2,7-difluoro-6-hydroxy-3-oxo-3H-xanthen-9-yl)terephthalic acid (ZP3(6-CO_2H), 5). A suspension of di(2-picolyl)amine (256 mg, 1.29 mmol) and paraformaldehyde (15 mg, 0.50 mmol) in 6 mL of MeCN was stirred at 65 °C for 30 min before adding a suspension of **4** (100 mg, 0.202 mmol) in 12 mL of MeCN. Heating continued overnight, with the formation of a dusky pink precipitate. The solid was filtered and washed with MeCN and pentane, yielding 54 mg of pink powder (32 %). ^{1}H NMR (DMSO-d_6, 400 MHz) δ 3.95 (8H, s), 4.10 (4H, s), 6.41 (2H, d, J = 11.2 Hz), 7.19-7.26 (4H, m), 7.34 (4H, d, J = 7.6 Hz), 7.67-7.74 (5H, m), 8.03 (1H, d, J = 8.0 Hz), 8.17 (1H, d, J = 8.0 Hz), 8.47 (4H, d, J = 4.4 Hz). ^{19}F NMR (DMSO-d_6, 376.5 MHz) δ -140.0 (2F, m). LRMS (ESI) calcd for $[M-H]^-$, 833.3; found, 833.3.

4-(4-carboxybutylcarbamoyl)-2-(2,7-dichloro-6-hydroxy-3-oxo-4,5-bis(((pyridin-2-yl-methyl)(pyridin-4-ylmethyl)amino)methyl)-3H-xanthen-9-yl)benzoic acid (ZP1B-valeric acid, 8). A solution of 5-aminovaleric acid (164 mg, 1.40 mmol) in 12 mL of 1:1 CH_2Cl_2:MeOH was added to a solution of **6** (250 mg, 0.40 mmol) in 10 mL of the same solvent mixture. After stirring overnight, the solvent was removed and the solid was redissolved in 24 mL of 5:1 MeCN:MeOH. This solution was added to a mixture of 2,4-DPA (239 mg, 1.20 mmol) and

paraformaldehyde (36 mg, 1.20 mmol) in 12 mL of MeCN that had been heated at 70 °C for 30 min. The reaction mixture was heated for 3 d, cooled to room temperature, and filtered. Slow evaporation of solvent from the filtrate yielded a crystalline solid. Filtration and washes with Et_2O and pentane resulted in 214 mg (54 %) of pure product. ^{1}H NMR (DMSO-d_6, 400 MHz) δ 1.37-1.46 (4H, m), 2.13 (2H, t, J = 6.0 Hz), 3.10-3.17 (2H, m), 3.80 (4H, s), 3.95 (4H, s), 4.11 (4H, s), 6.58 (2H, s), 7.25 (4H, d, J = 6.0 Hz), 7.33-7.41 (4H, m), 7.63 (1H, s), 7.80-7.87 (2H, m), 8.03 (1H, d, J = 8.0 Hz), 8.10 (1H, d J = 8.0 Hz), 8.42 (4H, d, J = 6.0 Hz), 8.61 (2H, d, J = 4.8 Hz). LRMS (ESI) calcd for $[M-H]^-$, 964.3; found, 964.7.

Cell Culture and Microscopy. HeLa cells were plated in either glass-bottomed microscope dishes or on glass cover slips in 24-well plates and grown to 90% confluence in 2.5 mL DMEM supplemented with 10 % FBS and 1 % penicillin. Cells were incubated for 0.5-2 h at 37 °C with a stock solution of 1 mM **ZP1ss** in DMSO, diluting to final concentrations of 10-40 μM. A solution of 4% paraformaldehyde in 0.1 M phosphate buffer, pH 7.4, was used to fix the cells after incubation with the sensor. For exposed samples, imaging was performed in PBS buffer. For sealed samples of fixed cells, the final media consisted of 0.5 % n-propyl gallate and 70 % glycerol in 20 mM Tris buffer, pH 8.0. Imaging was performed using a Zeiss Axiovert 200M inverted fluorescence microscope. Differential Interference Contrast (DIC) and fluorescence images were acquired with an oil-immersion 63x objective lens. An EXFO metal-halide lamp was used for fluorescence excitation at 488 nm, with a GFP filter passing emission from 505-530 nm. The microscope was operated using Volocity software (Improvision, Lexington, MA).

Results and Discussion

Synthesis. Sufficient material for ^{13}C NMR spectra of these compounds is not available, but ^{1}H NMR spectra of each new compound are provided in Appendix 2. Although an NHS ester of ZP1 had been synthesized previously,[16] it was utilized as a precursor for bottom-ring derivatized species rather than as a labeling agent. The sulfonated version, **ZP1ss**, was selected as a target to retain the negatively charged group that makes ZP1(6-CO_2H) cell impermeable. The synthesis of **ZP1ss** (Scheme 4.1) was straightforward, using a simple DCC coupling reaction in DMF.

The 6-carboxy derivatives of both ZP3 and ZP1B were also synthesized (Scheme 4.2) in order to produce the corresponding sulfosuccinimidyl esters to compare labeling with **ZP1ss**. ZP1B derivative **2** was synthesized by Mannich reaction from **1**, using 2,4-DPA in place of 2,2-DPA. The syntheses of **3** and **4** were modified from a published procedure[17] and **5** was also produced by Mannich reaction. Unfortunately, the protocol that yielded **ZP1ss** failed to convert **2** and **5** to the desired esters.

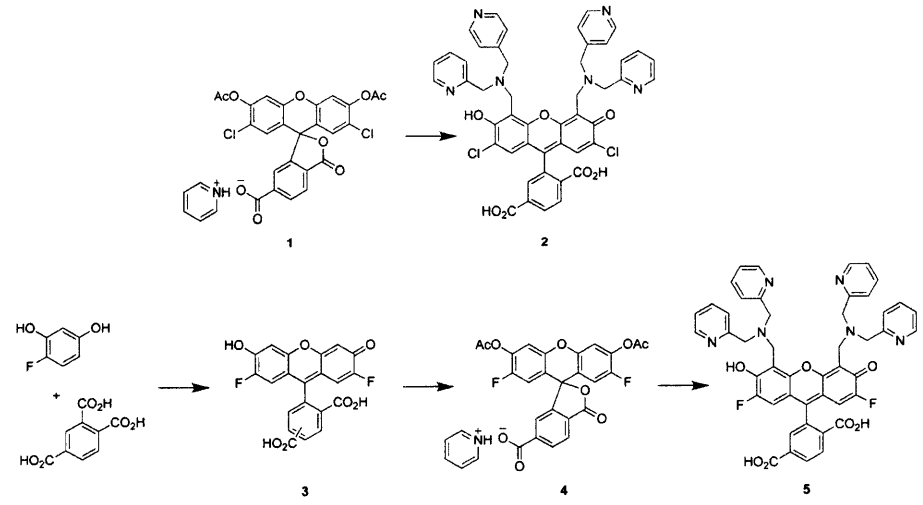

Scheme 4.2 Synthesis of carboxylate-derivatized Zinpyr sensors

In order to increase the distance between the sensor and the labeled protein, a version of **2** with a short spacer was also constructed (Scheme 4.3). Addition of 5-aminovaleric acid to **6** yielded intermediate **7**, which was converted to **8** without purification.

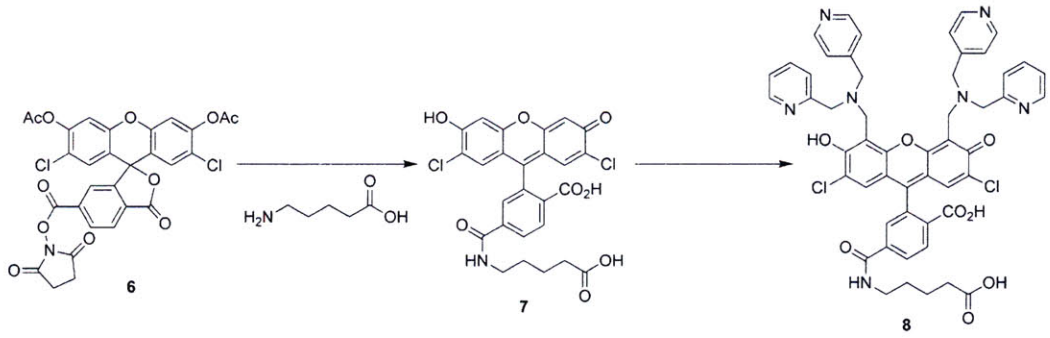

Scheme 4.3 Synthesis of valeric acid-derivatized ZP1B

Cell studies and imaging. Cell labeling with **ZP1ss** was tested using HeLa cells in three different formats. First, live cell imaging was performed, which yielded the promising result of cells with a distinctive fluorescent outline (Figure 4.1). Although some internal fluorescence was observed, which may have been caused by non-specific uptake by the cell, the cell membrane was clearly labeled, unlike in cells treated with the non-esterified ZP1(6-CO_2H) (not shown). Unfortunately, addition of $ZnCl_2$ did not elicit any increase in fluorescence emission, even at concentrations where visible precipitation occurred ($\geq$ 60 μM). Since high concentrations of zinc can be toxic, the morphologies of the cells may have changed, affecting the quality of the final image of Figure 4.1.

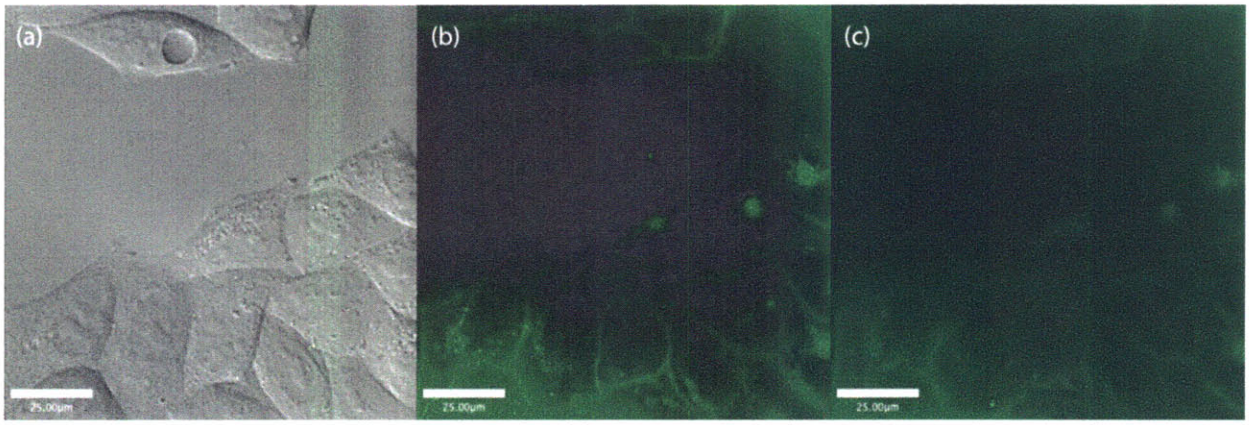

Figure 4.1 Live HeLa cells incubated with **ZP1ss**. DIC image (a) and green fluorescence channel before (b) and after (c) the addition of $ZnCl_2$.

Imaging was also performed using fixed cells prepared in two different ways. Using a common approach, HeLa cells were grown on glass microscope covers at the bottom of the wells of a 24-well plate. After incubation with the sensor, the cells were fixed and varying amounts of $ZnCl_2$ were added to some samples. The covers, with the attached cells, were then sealed against microscope slides with nail polish. Sealing in this fashion seemed to affect the morphology of the cells; none of the previously observed fluorescent outlining of cells was seen. Instead, the prevalent fluorescence pattern was a uniform emission over the majority of the cell body (Figure 4.2), which might be interpreted as a flattening of the upper portion of the membrane into a single focal plane.

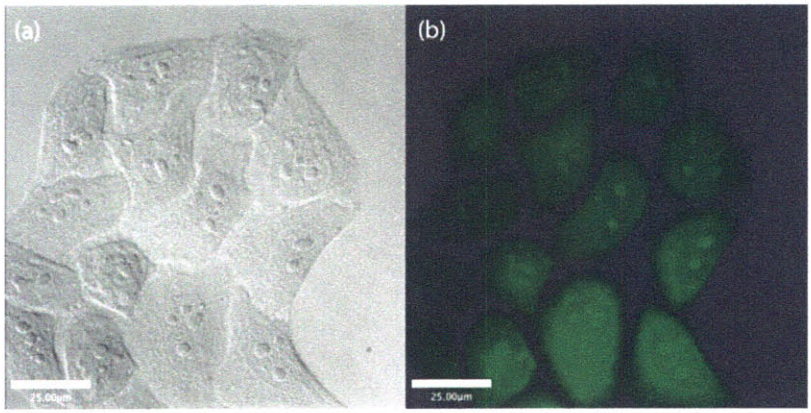

Figure 4.2 HeLa cells fixed and sealed after incubation with **ZP1ss**. DIC image (a) and green fluorescence channel (b).

As a compromise between using living cells, where the same sample can be imaged before and after addition of zinc, and permanently fixed and sealed cells, a third cell preparation method was used. HeLa cells were grown in microscope dishes as for live cell preparations, followed by incubation with the sensor. The cells were then fixed in the dishes, keeping them bathed in PBS medium, which allowed for later addition of zinc and did not artificially compress the cells. The resulting images resembled those from live cell imaging but still did not display any zinc-induced increase in fluorescence intensity (Figure 4.3).

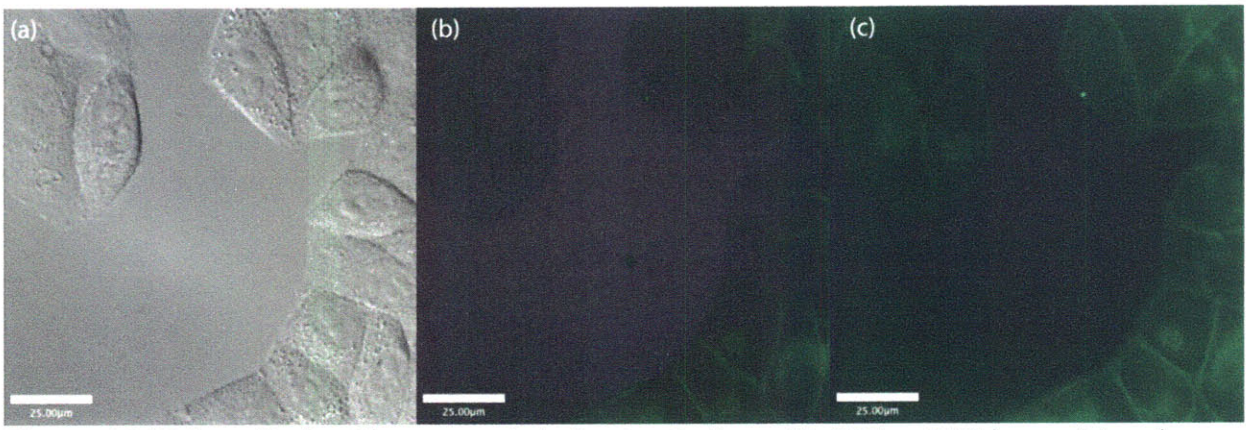

Figure 4.3 HeLa cells fixed but not sealed after incubation with **ZP1ss**. DIC image (a) and green fluorescence channel before (b) and after (c) the addition of $ZnCl_2$.

In order to overcome the lack of observed fluorescence increase in these cell experiments, the syntheses of analogs of **ZP1ss** were attempted, using either the fluorinated ZP3 platform or the 2,4-DPA binding group, both of which lower the proton affinity of the sensor and therefore the background fluorescence signal. The corresponding esters were not successfully obtained using the same procedure that yielded **ZP1ss**, however.

Another possible explanation for the lack of dynamic fluorescence signal is the direct attachment of the sensor to protein targets, with no intervening linker. Protein-sensor interactions may inhibit operation of the sensor. To eliminate this possibility, a spacer of some sort can be added between the sensor and the activated ester. In order to keep the synthesis as simple as possible, some type of linear amino acid is desirable as the spacer, so that the amino group can conjugate to the carboxyl unit of the sensor and the free acid end can be used to form the activated ester. As a first step in this direction, 5-aminovaleric acid was selected as the spacer unit. Formation of the final sulfonated NHS ester was attempted exactly as for **ZP1ss**, but with no success thus far.

It remains to be seen whether the sulfonate group of the NHS moiety is necessary to keep the sensors cell-impermeable. The purification of NHS esters lacking a sulfonate group would likely

be simplified due to the difference in charge between the product and the carboxylate-bearing starting material. Other spacer units may also be employed, perhaps bearing polar groups to increase solubility in water, or having a greater length to increase sensor-protein separation.

Conclusions

Although an activated NHS ester of ZP1 was capable of labeling the membrane of HeLa cells, no change in fluorescence signal was observed upon addition of zinc. There are several possible explanations for this behavior. First, direct coupling to proteins may interfere with the response of the sensor. This interference may be caused by quenching of the fluorophore or interaction of the receptor units with the protein, resulting in an artificial turn-on response even in the absence of zinc. Alternatively, the sensor density may be sufficiently high that the background fluorescence washes out the signal change upon zinc binding. Lastly, the incubation time with the sensor may be long enough for significant endocytosis to occur, causing the fluorescence signal to originate from just inside the cell membrane. In this case, no fluorescence change would be observed since added Zn(II) remains in the bathing medium and could not be intercepted by the sensor. More tests need to be performed to determine if this method of cell labeling is worth pursuing.

References

(1) Burdette, S. C.; Frederickson, C. J.; Bu, W.; Lippard, S. J. *J. Am. Chem. Soc.* **2003**, *125*, 1778-1787.

(2) Chang, C. J.; Nolan, E. M.; Jaworski, J.; Burdette, S. C.; Sheng, M.; Lippard, S. J. *Chem. Biol.* **2004**, *11*, 203-210.

(3) Nolan, E. M.; Ryu, J. W.; Jaworski, J.; Feazell, R. P.; Sheng, M.; Lippard, S. J. *J. Am. Chem. Soc.* **2006**, *128*, 15517-15528.

(4) Woodroofe, C. C.; Masalha, R.; Barnes, K. R.; Frederickson, C. J.; Lippard, S. J. *Chem. Biol.* **2004**, *11*, 1659-1666.

(5) Tour, O.; Adams, S. R.; Kerr, R. A.; Meijer, R. M.; Sejnowski, T. J.; Tsien, R. W.; Tsien, R. Y. *Nat. Chem. Biol.* **2007**, *3*, 423-431.

(6) Tomat, E.; Nolan, E. M.; Jaworski, J.; Lippard, S. J. *J. Am. Chem. Soc.* **2008**, *130*, 15776-15777.

(7) Lim, N. C.; Freake, H. C.; Brückner, C. *Chem. Eur. J.* **2005**, *11*, 38-49.

(8) Shtrahman, M.; Yeung, C.; Nauen, D. W.; Bi, G.-Q.; Wu, X.-L. *Biophys. J.* **2005**, *89*, 3615-3627.

(9) Savtchenko, L. P.; Rusakov, D. A. *Proc. Natl. Acad. Sci. USA* **2007**, *104*, 1823-1828.

(10) Bozym, R. A.; Thompson, R. B.; Fierke, C. A. In *Reviews in Fluorescence*; Geddes, C. D., Lakowicz, J. R., Eds.; Springer: New York, 2006.

(11) Marks, K. M.; Nolan, G. P. *Nat. Meth.* **2006**, *3*, 591-596.

(12) O'Hare, H. M.; Johnsson, K.; Gautier, A. *Curr. Opin. Struct. Biol.* **2007**, *17*, 488-494.

(13) Hermanson, G. T. *Bioconjugate techniques*; Elsevier Academic Press: Boston, 2008.

(14) Agard, N. J.; Baskin, J. M.; Prescher, J. A.; Lo, A.; Bertozzi, C. R. *ACS Chem. Biol.* **2006**, *1*, 644-648.

(15) Baskin, J. M.; Prescher, J. A.; Laughlin, S. T.; Agard, N. J.; Chang, P. V.; Miller, I. A.; Lo, A.; Codelli, J. A.; Bertozzi, C. R. *Proc. Natl. Acad. Sci. USA* **2007**, *104*, 16793-16797.

(16) Woodroofe, C. C. Ph.D. Dissertation, Massachusetts Institute of Technology, 2004.

(17) Sun, W.-C.; Gee, K. R.; Klaubert, D. H.; Haugland, R. P. *J. Org. Chem.* **1997**, *62*, 6469-6475.

Appendix 1. Synthesis of Components for the Construction of Tethered Zn(II)-Responsive Fluorophores

Introduction

The previous chapter described the most direct method attempted in our laboratory for the extracellular labeling of living cells with our Zn(II)-responsive probes. Unfortunately, although the plasma membrane of HeLa cells was illuminated by incubation with the ZP1ss active ester probe, no significant increase in fluorescence was observed upon addition of $ZnCl_2$. Additional routes toward membrane labeling have been initiated using methods developed in the laboratory of Carolyn Bertozzi.[1,2]

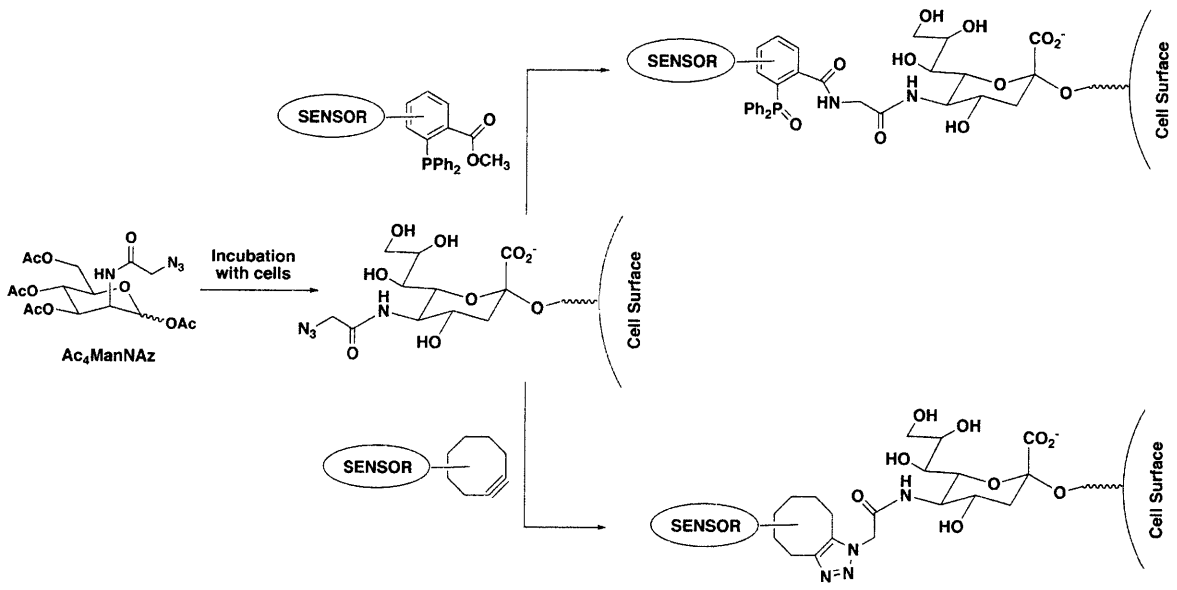

Scheme A1.1. Phosphine- and cyclooctyne-based routes to labeling cell-surface azidosugars

Both methods start with the expression of an azidosugar on the cell surface. The azide functionality is tolerated by the metabolic machinery that converts the sugar mannosamine into a sialic acid residue that is expressed as part of a cell surface glycoprotein. The coupling partner to this azide can be either a specially designed phosphine, which reacts through the Staudinger ligation mechanism, or a strained cyclooctyne unit, which reacts through a strained [3+2] cycloaddition. Either of these moieties can be linked to a fluorescent sensor in a modular fashion. The overall scheme for utilizing this technique to attach zinc-responsive sensors to the cell

surface is shown in Scheme A1.1. The advantages of this method include lack of genetic manipulation in order to express the chemical label, the small size of the complete target-sensor conjugates, and the potential for a high density of labeling due to the large number of sialic acid residues on both cancer cells and neurons.

Work in our laboratory has demonstrated the versatility of ZP1 as a starting point for synthetic modification. For this reason, in addition to its favorable photophysical properties, the ZP1 platform is generally used for initial studies involving coupling to other chemical units.[3-5] Therefore, the initial targets for both the phosphine and cyclooctyne probes incorporated ZP1 tethered by a short, water-soluble diamine spacer to the functional coupling unit (Figure A1.1). Progress towards the synthesis of these full probes is described here. In addition, the modular nature of these constructs was explored by synthesizing a ZP1B-based intermediate.

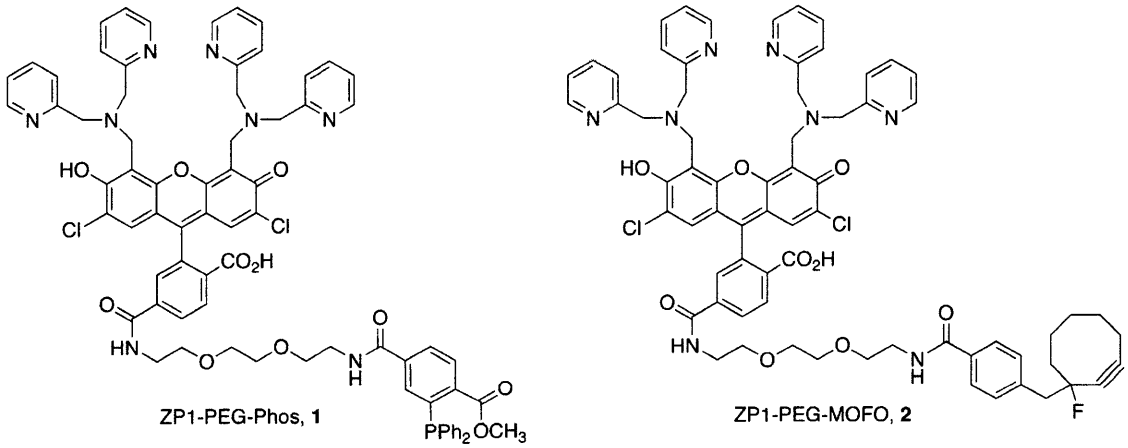

Figure A1.1. ZP1-based synthetic targets

Experimental Section

Materials and Methods. Solvents were supplied by Mallinckrodt and used as received. All other reagents were purchased from Aldrich and used as received. NMR spectra were obtained on a Bruker 400 MHz spectrometer, and referenced to the residual proton resonance of the

deuterated solvent. Low resolution mass spectra were obtained by using an Agilent 1100 Series LC/MSD mass spectrometer.

1-Methyl-2-iodoterephthalate succinimidyl ester (NHS-PP, 3). To a stirred solution of 1-methyl-2-iodoterephthalate (161 mg, 0.525 mmol) and N-hydroxysuccinimide (70.6 mg, 0.613 mmol) in 40 mL THF was added DCC (115 mg, 0.558 mmol). After 20 h, a white precipitate had formed. The mixture was concentrated, added to CH_2Cl_2, and the solution was filtered and concentrated to form a yellow oil. Purification by flash chromatography on a silica column (33:1 CH_2Cl_2:MeOH) yielded 170 mg (80.3%) of a viscous yellow oil. ^{1}H NMR ($CDCl_3$, 400 MHz) δ 2.94 (4H, br s), 3.99 (3H, s), 7.87 (1H, d), 8.15 (1H, dd), 8.71 (1H, d).

Methyl 4-(2-(2-(2-aminoethoxy)ethoxy)ethylcarbamoyl)-2-iodobenzoate (PEG-PP, 4). A solution of **3** (348 mg, 0.862 mmol) in 12 mL of CH_2Cl_2 was added to a solution of 3,6-dioxa-1,8-diamine (766 mg, 5.17 mmol) in 3 mL of CH_2Cl_2 while stirring over 20 min. Stirring was continued overnight before diluting with 50 mL of CH_2Cl_2 and extracting with 1 M HCl. The aqueous phase was neutralized with solid $NaHCO_3$ and extracted with CH_2Cl_2. Washes with satd. aq. $NaHCO_3$, drying over $MgSO_4$, and removal of solvent in vacuo yielded 195 mg (52 %) of a yellow oil. ^{1}H NMR (MeOD, 400 MHz) δ 2.79 (2H, t), 3.52 (2H, t), 3.57 (2H, t), 3.63-3.70 (6H, m), 3.94 (3H, s), 7.79 (1H, d), 7.89 (1H, dd), 8.43 (1H, d). LRMS (ESI) Calcd for MH^+ 437.1, found 437.1.

2',7'-dichloro-6-(2-(2-(2-(3-iodo-4-(methoxycarbonyl)benzamido)ethoxy)ethoxy)ethyl-carbamoyl)-3-oxo-3H-spiro[isobenzofuran-1,9'-xanthene]-3',6'-diyl diacetate (Ac_2DCF-PEG-PP, 5). A solution of **4** (195 mg, 0.448 mmol) in 6 mL of CH_2Cl_2 and 2 mL of MeOH was added to a solution of **Ac_2DCF-NHS** (94 mg, 0.149 mmol) in 3 mL of CH_2Cl_2, yielding a bright orange mixture. The solution was stirred overnight before concentrating to a red film and

redissolving in 5 mL of acetic anhydride and 5 drops of Et_3N. After 1 h, the reaction was quenched by stirring with 50 mL of 0.5 M HCl. The product was extracted into CH_2Cl_2, washed with satd. aq. $NaHCO_3$, dried over $MgSO_4$, filtered, and concentrated to a yellow oil. Flash chromatography on a silica column (33:1 $CHCl_3$:MeOH) yielded 117 mg (83 %) of a pale yellow glassy solid. ^1H NMR (CD_2Cl_2/MeOD, 400 MHz) δ 2.37 (6H, s), 3.49 (2H, t), 3.54-3.65 (10H, m), 3.95 (3H, s), 6.93 (2H, s), 7.17 (2H, s), 7.74-7.83 (3H, m), 8.10 (1H, d), 8.20 (1H, dd), 8.37 (1H, d). LRMS (ESI) Calcd for MNa^+ 969.0, found 968.9.

2',7'-Dichloro-6-(2,2-dimethyl-4-oxo-3,8,11-trioxa-5-azatridecan-13-ylcarbamoyl)-3-oxo-3H-spiro[isobenzofuran-1,9'-xanthene]-3',6'-diyl diacetate (Ac_2DCF-PEG-Boc, 8). A solution of **Ac_2DCF-NHS** (369 mg, 0.662 mmol) in 20 mL of 1:1 CH_2Cl_2:MeOH was added dropwise to a solution of **7** (769 mg, 3.10 mmol) in 4 mL of 1:1 CH_2Cl_2:MeOH. The resulting bright orange solution was stirred for 24 h, then concentrated to form a glassy, red solid. This solid was redissolved in 15 mL of acetic anhydride and Et_3N (0.5 mL, 3.6 mmol) was added to the solution, which was stirred overnight. The resulting pale yellow solution was diluted with 75 mL of CH_2Cl_2, washed with 0.5 M HCl (75 mL) and satd. aq. $NaHCO_3$ (2x75 mL), dried over $MgSO_4$, filtered, and concentrated to a yellow oil. Flash chromatography on a silica column (7:1 EtOAc:Hex) yielded 189 mg (37.6%) of a glassy white solid. ^1H NMR ($CDCl_3$/CD_3OD, 400 MHz) δ 1.25 (9H, s), 2.20 (6H, s), 3.03 (2H, t), 3.32 (2H, t), 3.39-3.47 (8H, m), 6.70 (2H, s), 7.04 (2H, s), 7.54 (1H, s), 7.97 (1H, d), 8.04 (1H, d).

4-(2-(2-(2-Aminoethoxy)ethoxy)ethylcarbamoyl)-2-(2,7-dichloro-6-hydroxy-3-oxo-3H-xanthen-9-yl)benzoic acid (DCF-PEG, 10). A solution of **8** (100mg, 0.132 mmol) in 4 mL of MeOH, 1 mL of CH_2Cl_2, and 4 drops of Et_3N was stirred overnight and then concentrated to form a red film. The material was redissolved in 5 mL of CH_2Cl_2 containing 2 % TFA. After 4 h,

the resulting yellow precipitate was filtered and washed with pentane, yielding 33.5 mg (44 %) of a yellow powder. ^{1}H NMR (MeOD, 400 MHz) δ 3.02 (2H, t), 3.50 (2H, t), 3.55-3.63 (8H, m), 6.64 (2H, s), 6.82 (2H, s), 7.61 (1H, s), 8.08-8.16 (2H, m). LRMS (ESI) Calcd for MH^+ 575.1, found 575.0.

2-(4,5-Bis((bis(pyridin-2-ylmethyl)amino)methyl)-2,7-dichloro-6-hydroxy-3-oxo-3H-xanthen-9-yl)-4-(2,2-dimethyl-4-oxo-3,8,11-trioxa-5-azatridecan-13-ylcarbamoyl)benzoic acid (ZP1-PEG-Boc, 11). A solution of **8** (251 mg, 0.330 mmol) in a combination of 10 mL of MeOH, 2 mL of CH_2Cl_2, and 10 drops of Et_3N was stirred overnight before evaporating the solvents, to afford a deep red glass, **9**. This material was redissolved in 8 mL of MeCN and added to a solution of 2-dipicolylamine (209 mg, 1.05 mmol) and paraformaldehyde (31.0 mg, 1.03 mmol) in 12 mL of MeCN that had been stirred at 70 °C for 20 min. Heating continued for 24 h, and the mixture was cooled to -24 °C. The cold mixture was filtered and washed with MeCN, Et_2O, and pentane, yielding 173 mg of opaque pink crystals (48 %). ^{1}H NMR (CD_2Cl_2/MeOD, 400 MHz) δ 1.34 (9H, s), 3.10-3.17 (2H, m), 3.37-3.45 (2H, m), 3.45-3.57 (8H, m), 3.90-4.03 (8H, m), 4.19 (4H, s), 6.59 (2H, s), 7.17-7.22 (4H, m), 7.35 (4H, d, J = 8.0 Hz), 7.63-7.69 (5H, m), 8.02 (1H, d, J = 8.4 Hz), 8.08 (1H, d, J = 8.4 Hz), 8.48-8.53 (4H, m).

4-(2-(2-(2-Aminoethoxy)ethoxy)ethylcarbamoyl)-2-(4,5-bis((bis(pyridin-2-ylmethyl)amino)-methyl)-2,7-dichloro-6-hydroxy-3-oxo-3H-xanthen-9-yl)benzoic acid (ZP1-PEG, 12). A solution of **11** (145 mg, 0.132 mmol) in 5 mL of CH_2Cl_2 containing 2 % TFA was stirred at room temperature overnight. Another 0.1 mL of TFA was added, stirring for 3 h before storing the solution at -24 °C overnight. No precipitate formed, so the CH_2Cl_2 was removed and the oily material was washed with MeCN, Et_2O, pentane, and THF. Drying yielded 173 mg of a pasty red solid (131 %, crude). ^{1}H NMR (MeOD, 400 MHz) δ 3.06 (2H, t, J = 4.8 Hz), 3.54-3.72 (10H,

m), 4.43-4.56 (12H, m), 6.68 (2H, s), 7.42-7.52 (8H, m), 7.62 (1H, s), 7.90-7.97 (4H, m), 8.14 (1H, d, J = 8.0 Hz), 8.28 (1H, d, J = 8.0 Hz), 8.60 (4H, d, J = 5.2 Hz).

2-(2,7-Dichloro-6-hydroxy-3-oxo-4,5-bis(((pyridin-2-ylmethyl)(pyridin-4-ylmethyl)amino)-methyl)-3H-xanthen-9-yl)-4-(2,2-dimethyl-4-oxo-3,8,11-trioxa-5-azatridecan-13-yl-carbamoyl)benzoic acid (ZP1B-PEG-Boc, 13). A suspension of 2,4-DPA (223 mg, 1.12 mmol) and paraformaldehyde (34.7 mg, 1.16 mmol) in 12 mL of MeCN was heated at 70 °C for 30 min before adding a solution of **9** (247 mg, 0.366 mmol) in 8 mL of MeCN. The solution was heated at 70 °C for 3 d, then cooled to room temperature. The solvent was removed by slow evaporation and the resulting solid was broken up and washed with MeCN, Et_2O, and pentane, yielding 169 mg (42 %) of pink, crystalline powder. ^{1}H NMR (CD_2Cl_2, 400 MHz) δ 1.34 (9H, s), 3.14 (2H, t, J = 5.2 Hz), 3.40 (2H, t, J = 4.4 Hz), 3.46-3.58 (8H, m), 3.74-3.92 (4H, m), 3.96 (4H, s), 6.18 (4H, s), 6.59 (2H, s), 7.26 (2H, d, J = 8.0 Hz), 7.28-7.35 (6H, m), 7.64 (1H, s), 7.71-7.80 (2H, m), 8.02 (1H, d, J = 8.0 Hz), 8.10 (1H, d, J = 8.0 Hz), 8.37 (4H, d, J = 6.0 Hz), 8.67 (2H, d, J = 4.4 Hz).

4-(2-(2-(2-Aminoethoxy)ethoxy)ethylcarbamoyl)-2-(2,7-dichloro-6-hydroxy-3-oxo-4,5-bis(((pyridin-2-ylmethyl)(pyridin-4-ylmethyl)amino)methyl)-3H-xanthen-9-yl)benzoic acid (ZP1B-PEG, 14). A solution of **13** (87 mg, 79 μmol) in 5 mL of CH_2Cl_2 containing 4 % TFA was stirred overnight. The solvent was evaporated and the resulting oil was washed thoroughly with Et_2O, yielding a red paste (final yield not measured). ^{1}H NMR (CD_2Cl_2, 400 MHz) δ 3.01 (2H, t, J = 5.2 Hz), 3.50 (2H, t, J = 4.8 Hz), 3.54-3.62 (8H, m), 4.11 (4H, s), 4.23 (4H, s), 4.29 (4H, s), 6.66 (2H, s), 7.46-7.52 (4H, m), 7.66 (1H, s), 7.80 (4H, d, J = 6.8 Hz), 7.94-8.00 (2H, m), 8.13 (2H, s), 8.48 (4H, d, J = 5.2 Hz), 8.75-8.79 (2H, m). LRMS (ESI) calcd for $[M+H]^+$, 997.3; found, 997.4.

Results and Discussion

Synthesis. Sufficient material for ^{13}C NMR spectra of these compounds is not available, but ^{1}H NMR spectra of each new compound are provided in Appendix 2.

Staudinger Ligation Components. A few different synthetic routes toward phosphine probe **1** were considered. In order to minimize phosphine oxidation, the Pd-catalyzed conversion of the phenyl iodide precursor was avoided until the other components were assembled. In the end, the most successful route is that described in Scheme A1.2. Synthesis of the free acid version of **3** was described previously[1] and formation of the NHS ester was performed by a standard method. Addition of an excess of 3,6-dioxa-1,8-diamine yielded **4** in sufficient purity to couple with our established dichlorofluorescein-based synthon **Ac_2DCF-NHS**. Reprotection of the xanthenone phenolate groups, followed by flash chromatography yielded **5**. Rather than install the DPA receptor units in pursuit of the full target probe, formation of the final triaryl phosphine moiety was tested using $Pd(OAc)_2$ and diphenylphosphine. The expected product was not observed in the reaction mixture by ESI-MS. Since acetylated fluorescein compounds like **5** are normally amenable to purification by chromatography, protection using acetic anhydride was attempted. This method usually produces a colorless solution but the reaction mixture remained deep red and no identifiable product could be isolated.

The synthesis of Ac_4ManNAz was undertaken as described elsewhere,[6] although final purification by HPLC was not performed due to incomplete synthesis of the fluorophore-labeled phosphine construct.

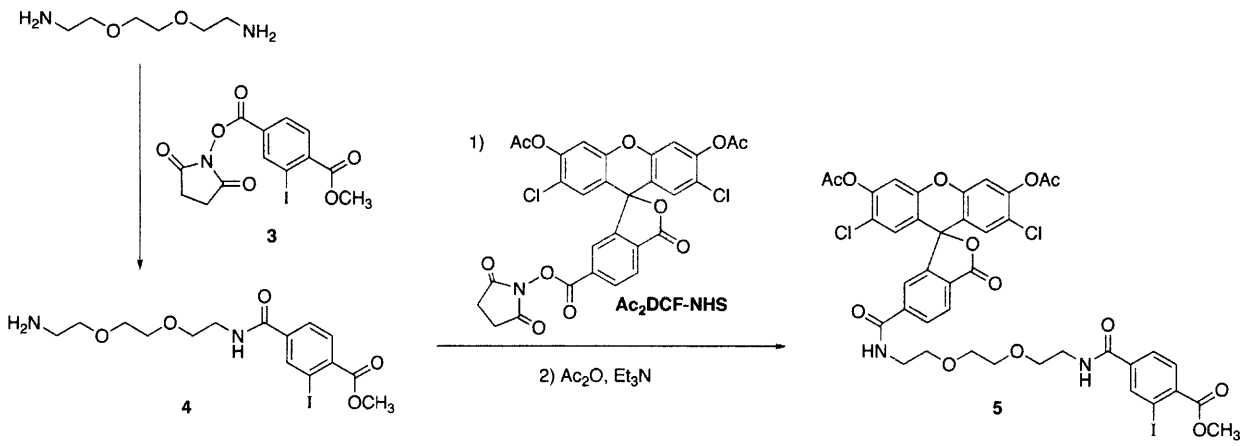

Scheme A1.2. Synthesis of Staudinger ligation probe precursor

Fluorescent monofluorinated octyne (MOFO) Construct. Like phosphine target **1**, the design for MOFO-based target **2** is entirely modular. In this case, construction of the octyne coupling component was completed apart from the fluorophore and tether components. Synthesis of the activated pentafluorophenyl ester of MOFO, **6**, was performed based on the published protocol (Scheme A1.3);[2] however, the overall yield was only ca. 2%.

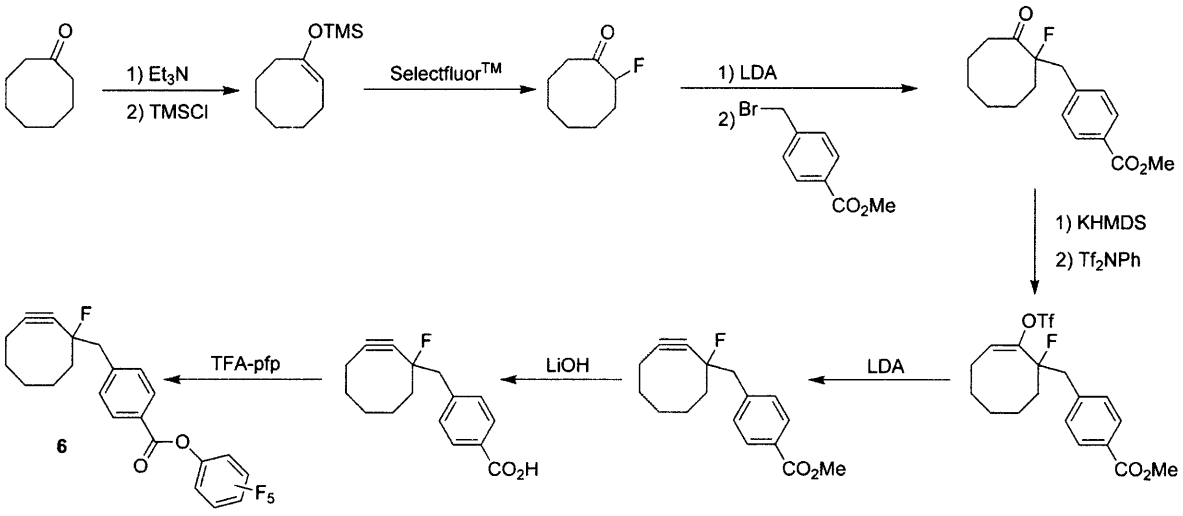

Scheme A1.3. Synthesis of MOFO-pfp ester

The synthesis of several fluorophore-tether components was accomplished as shown in Scheme A1.4. Addition of excess **7** to **Ac_2DCF-NHS**, followed by reprotection with acetic anhydride, yielded **8**. After purification by chromatography, the acetyl groups were removed

with base, resulting in flexible precursor **9**. Removal of the Boc group with dilute TFA produced a Zn(II)-insensitive test dye, **10**. Alternatively, a Mannich reaction can potentially install a variety of secondary amine ligands prior to Boc deprotection. Both the 2,2-DPA and 2,4-DPA receptor groups were successfully attached, resulting in tether-bearing probes **12** and **14**, although adequate purification of these two compounds has not been completed.

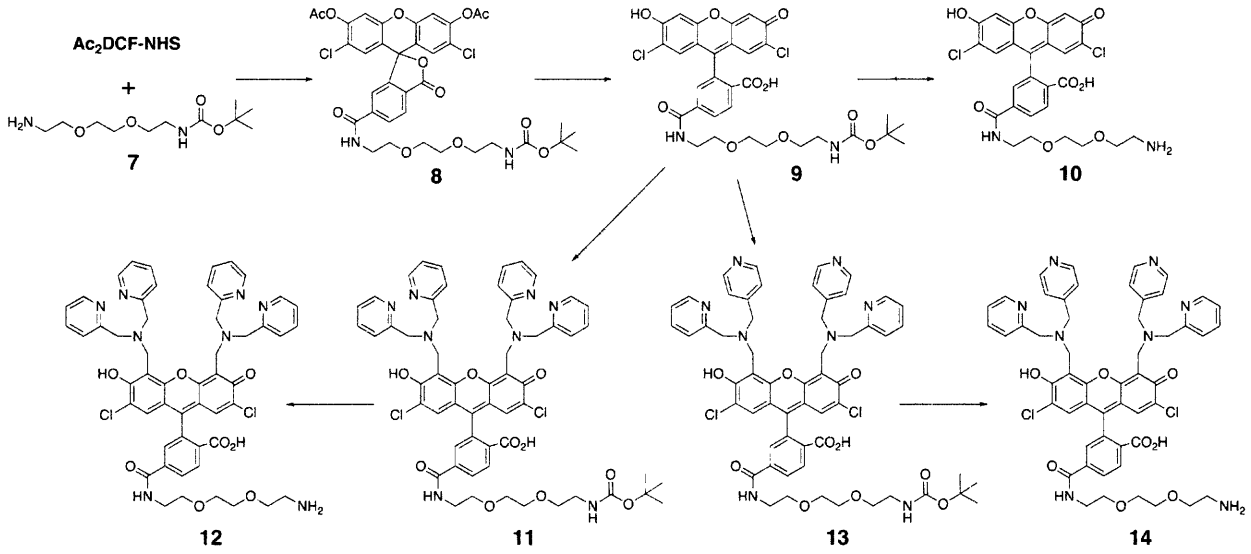

Scheme A1.4. Synthesis of fluorophores with an amine tethering group

The coupling of a tethered fluorophore to MOFO was tested by combining MOFO ester **6** with **10** in MeOH with stoichiometric Et_3N. Upon observing no product formation by ESI-MS after 1 h, excess Et_3N was added and the solution was allowed to stir for 2 d at ambient temperature, occasionally monitoring the reaction by ESI-MS. The only identifiable component during this time was the starting material **10**. No trace of even the hydrolyzed acid from **6** was observed, although it is possible that the methyl ester formed instead. After evaporation of the methanol, no significant amount of non-polar material was recovered from extractions using a water/ethyl acetate combination. The aqueous phase retained all observable fluorescent material. The reason why such a normally facile reaction between an activated ester and a primary amine failed is unknown at this point.

Conclusions

Despite the initial attractiveness of the bioorthogonal azide-phosphine and azide-octyne coupling schemes, the syntheses of both target compounds **1** and **2** proved to be challenging. Although the planned route to **1** required relatively few steps, incompatibility of functional groups with the phosphine coupling reaction may block this pathway. Synthesis of **2**, while requiring more steps, seems within reach. In addition, the octyne reaction with azides is more efficient than the phosphine reaction, making **2** a more attractive target for cell labeling.

References

(1) Saxon, E.; Bertozzi, C. R. *Science* **2000**, *287*, 2007-2010.

(2) Agard, N. J.; Baskin, J. M.; Prescher, J. A.; Lo, A.; Bertozzi, C. R. *ACS Chem. Biol.* **2006**, *1*, 644-648.

(3) Woodroofe, C. C. Ph.D. Dissertation, Massachusetts Institute of Technology, 2004.

(4) Woodroofe, C. C.; Won, A. C.; Lippard, S. J. *Inorg. Chem.* **2005**, *44*, 3112-3120.

(5) Tomat, E.; Nolan, E. M.; Jaworski, J.; Lippard, S. J. *J. Am. Chem. Soc.* **2008**, *130*, 15776-15777.

(6) Luchansky, S. J.; Hang, H. C.; Saxon, E.; Grunwell, J. R.; Yu, C.; Dube, D. H.; Bertozzi, C. R. *Methods Enzymol.* **2003**, *362*, 249-272.

Appendix 2. Miscellaneous NMR Spectra

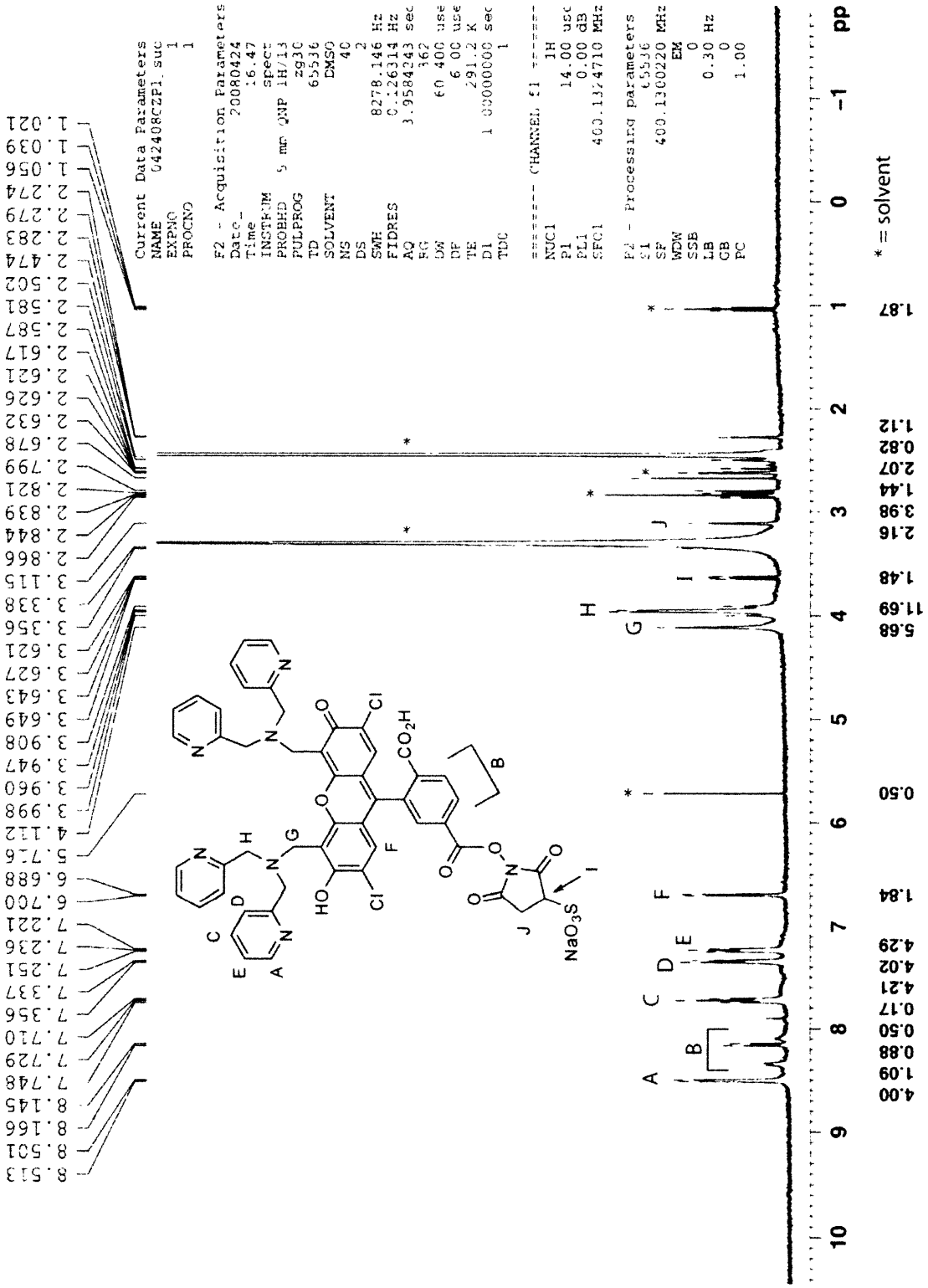

Figure A2.1. ^{1}H NMR Spectrum of ZP1ss

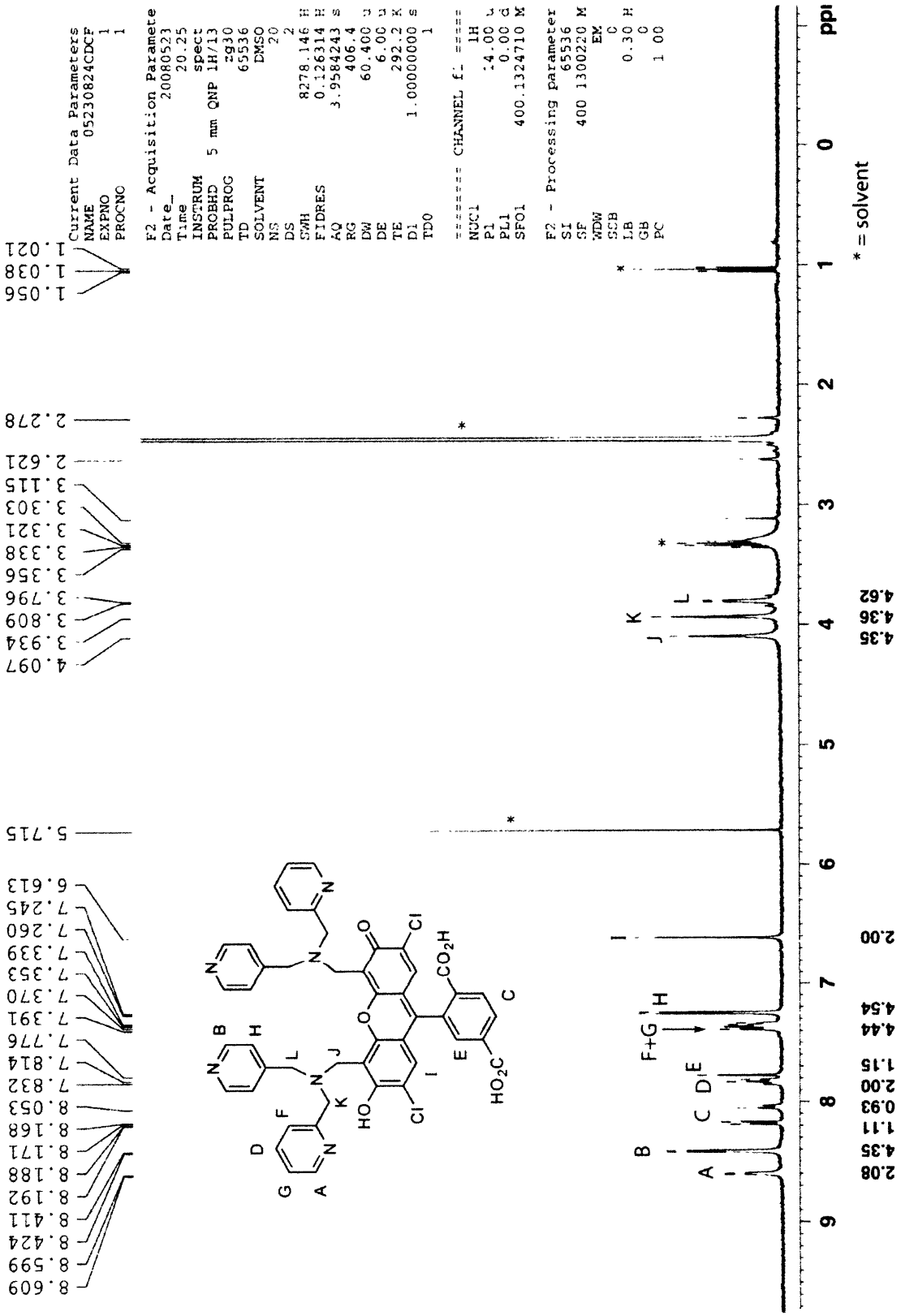

Figure A2.2. ^{1}H NMR Spectrum of ZP1B(6-CO_2H)

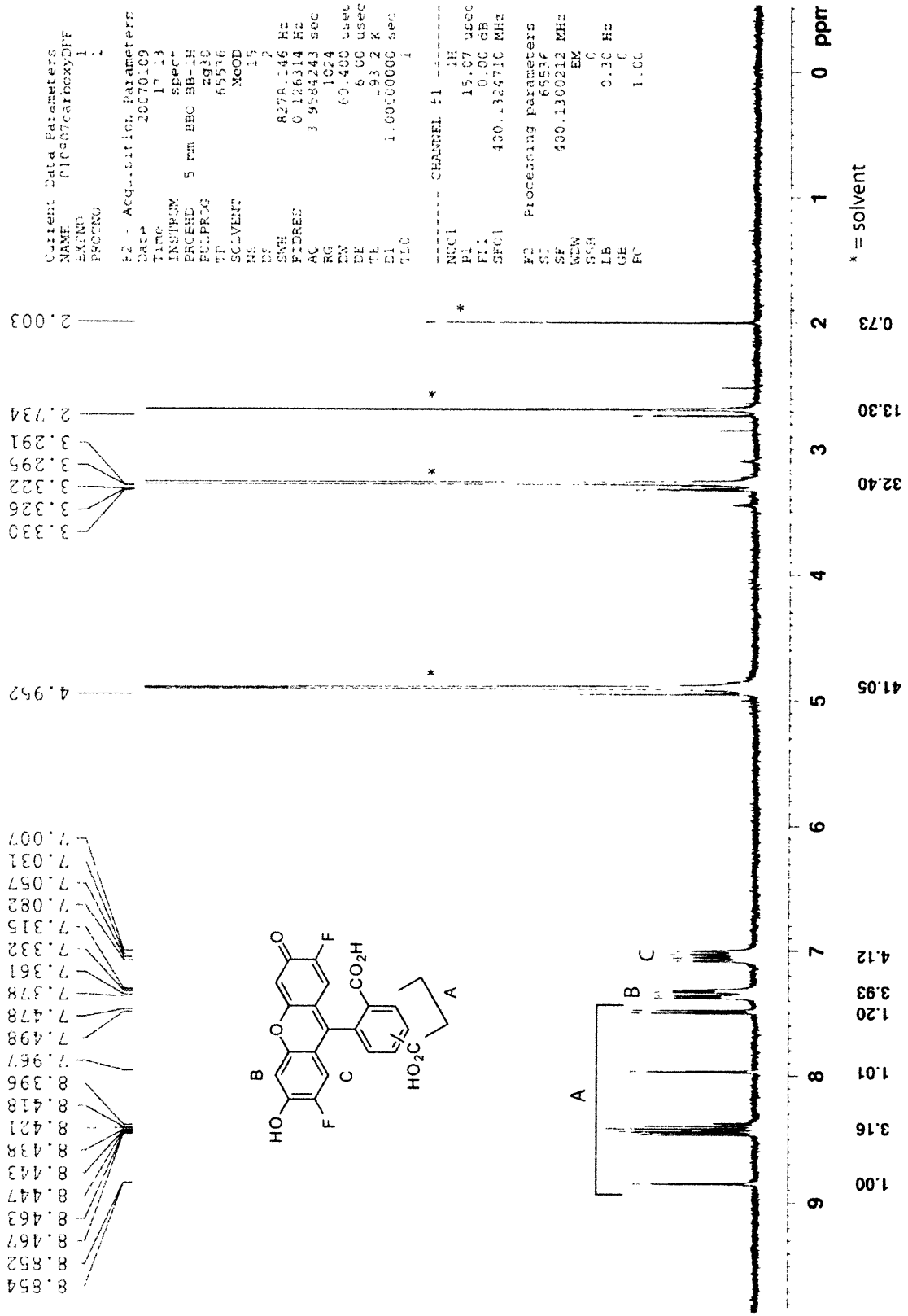

Figure A2.3. ^{1}H NMR Spectrum of DFF(5/6-CO_2H)

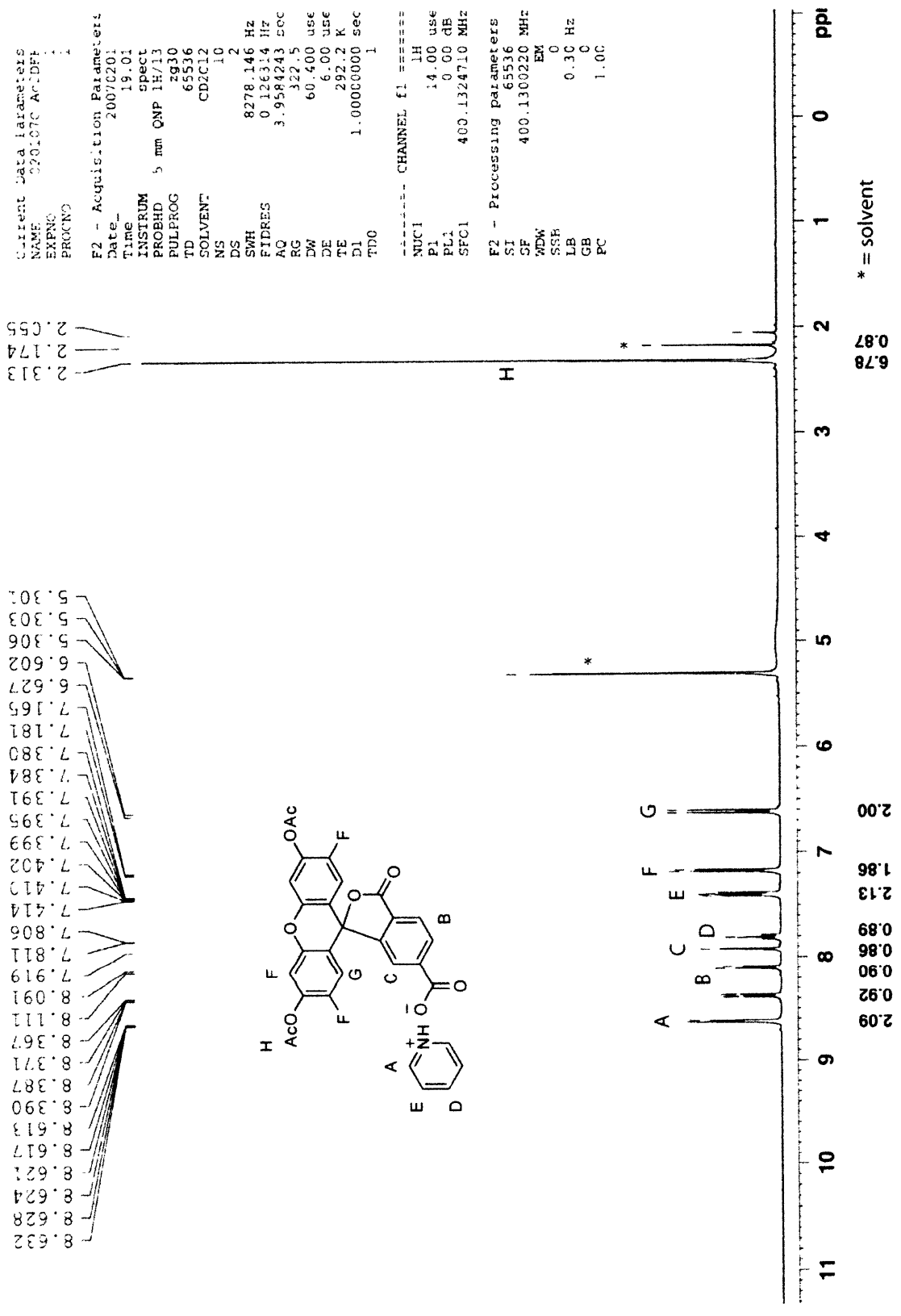

Figure A2.4. ^{1}H NMR Spectrum of $Ac_2DFF(6\text{-}CO_2^-)$ pyridinium salt

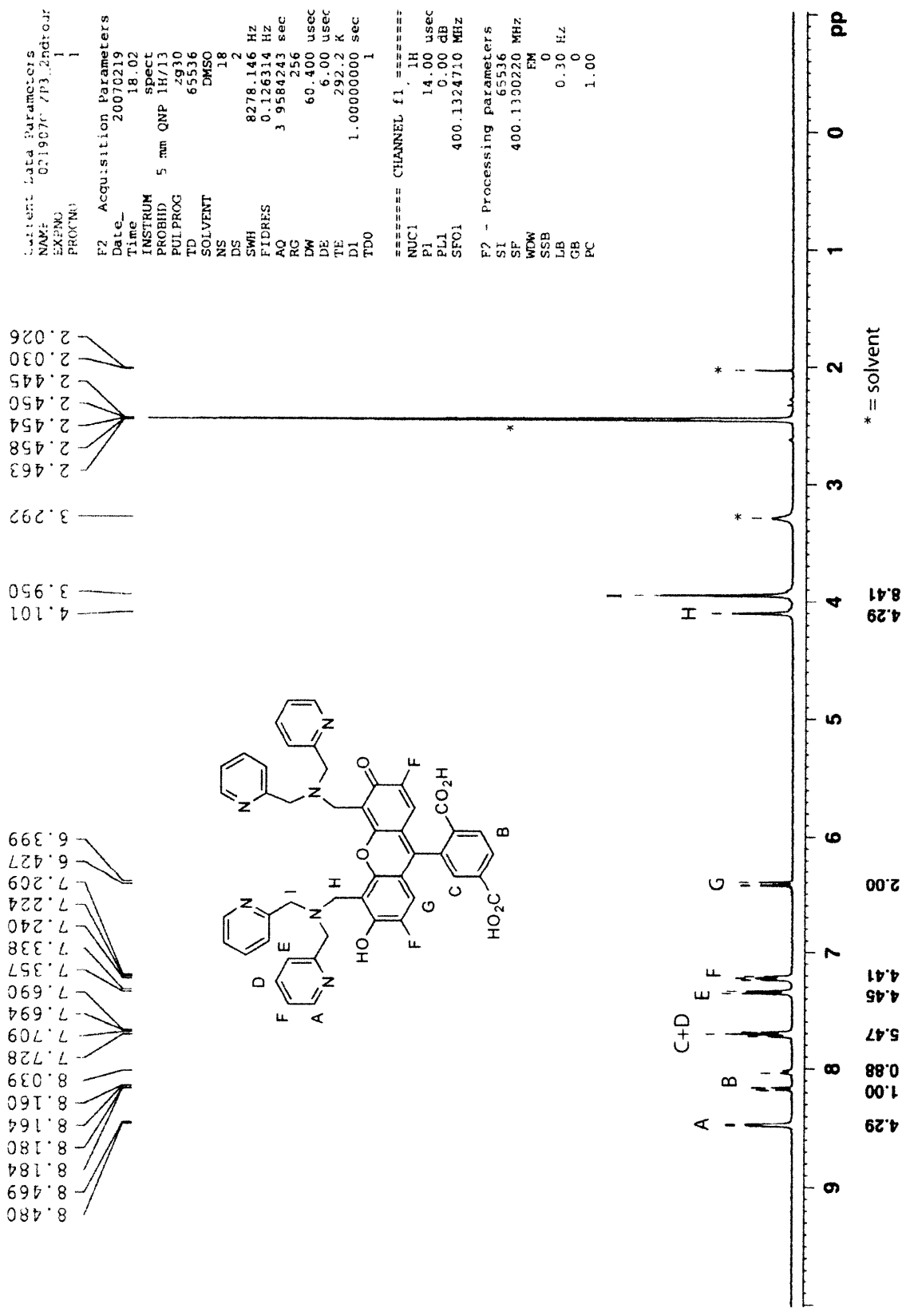

Figure A2.5. ^{1}H NMR Spectrum of ZP3(6-CO_2H)

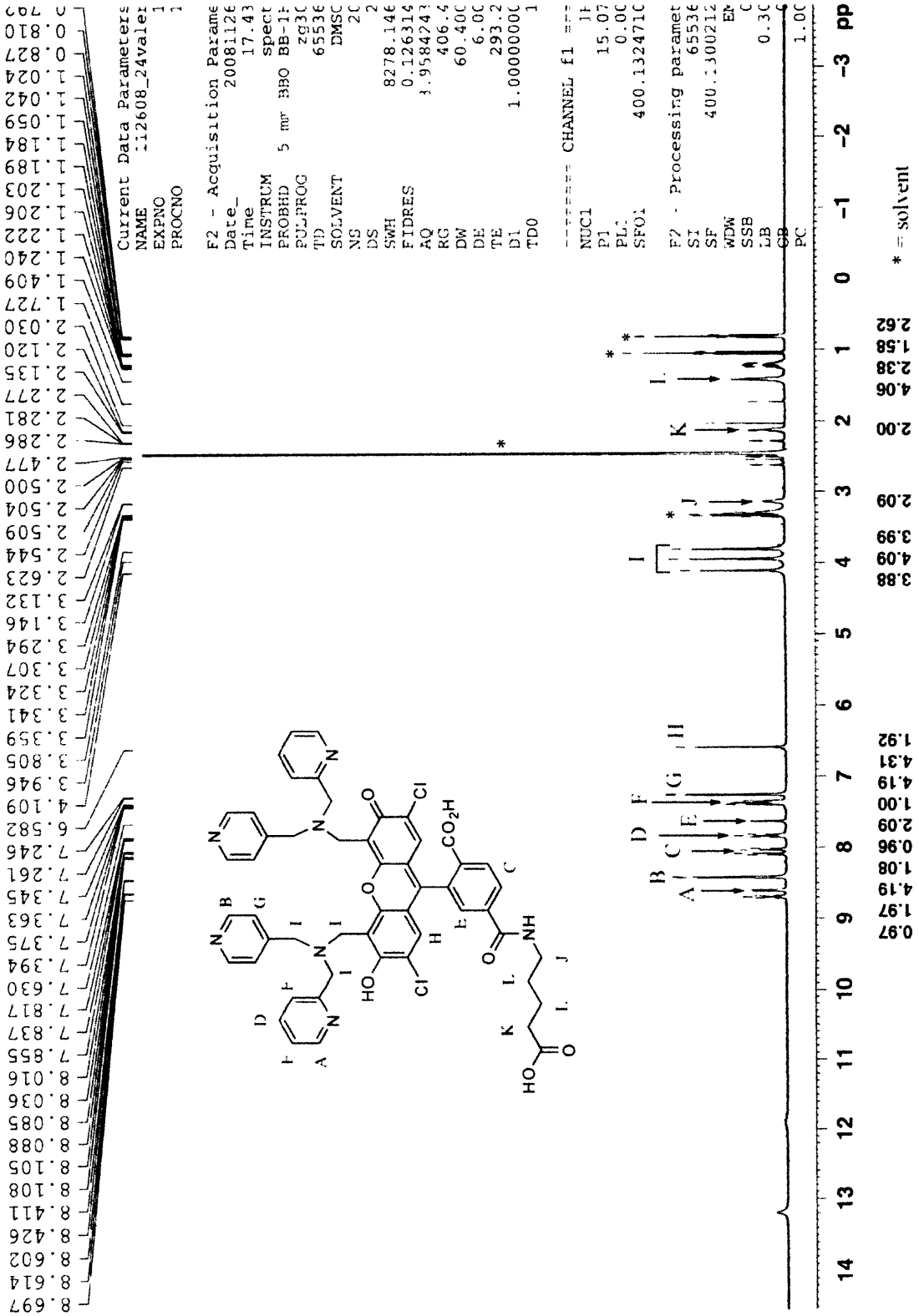

Figure A2.6. ^{1}H NMR Spectrum of ZP1B-valeric acid

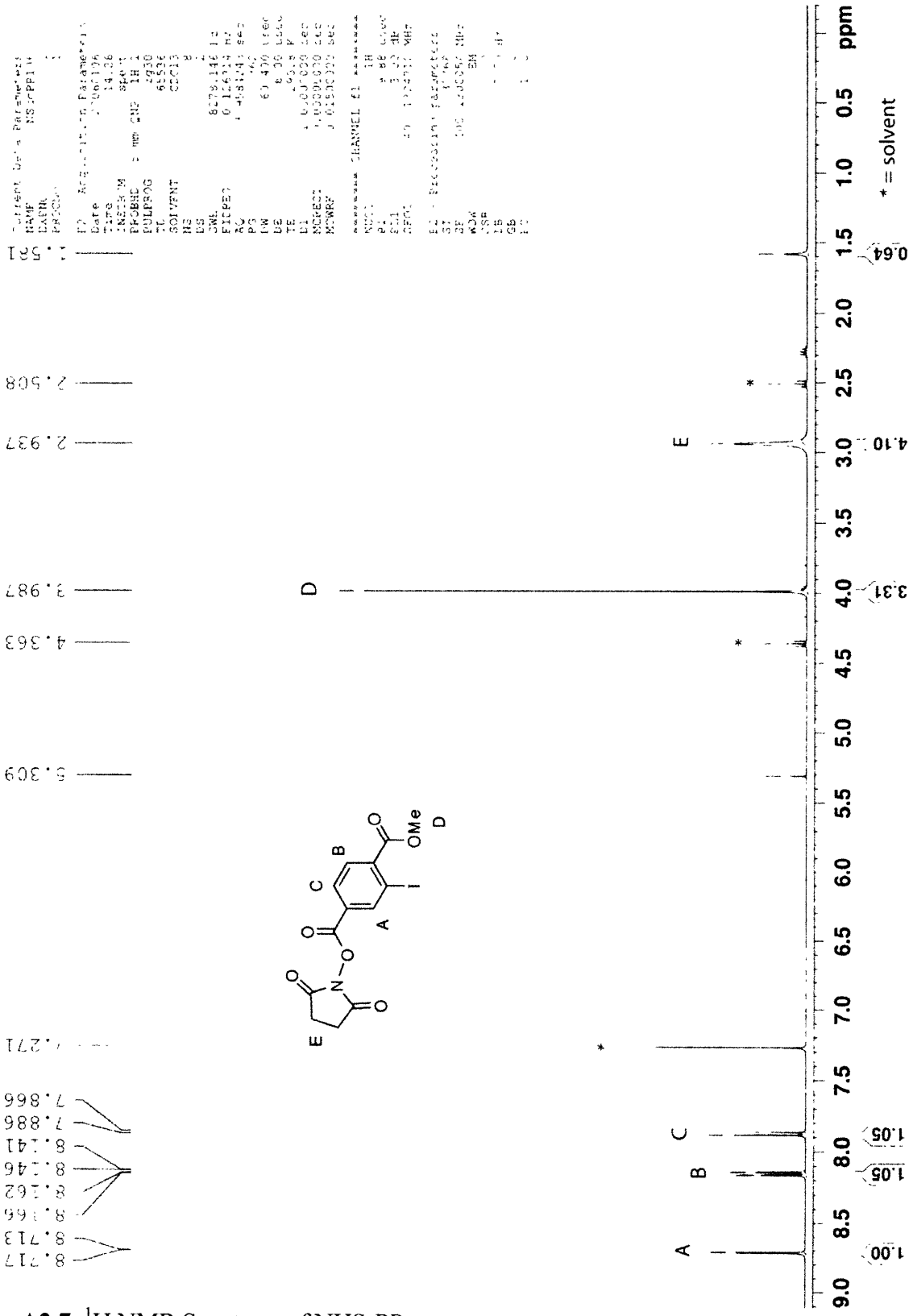

Figure A2.7. ^{1}H NMR Spectrum of NHS-PP

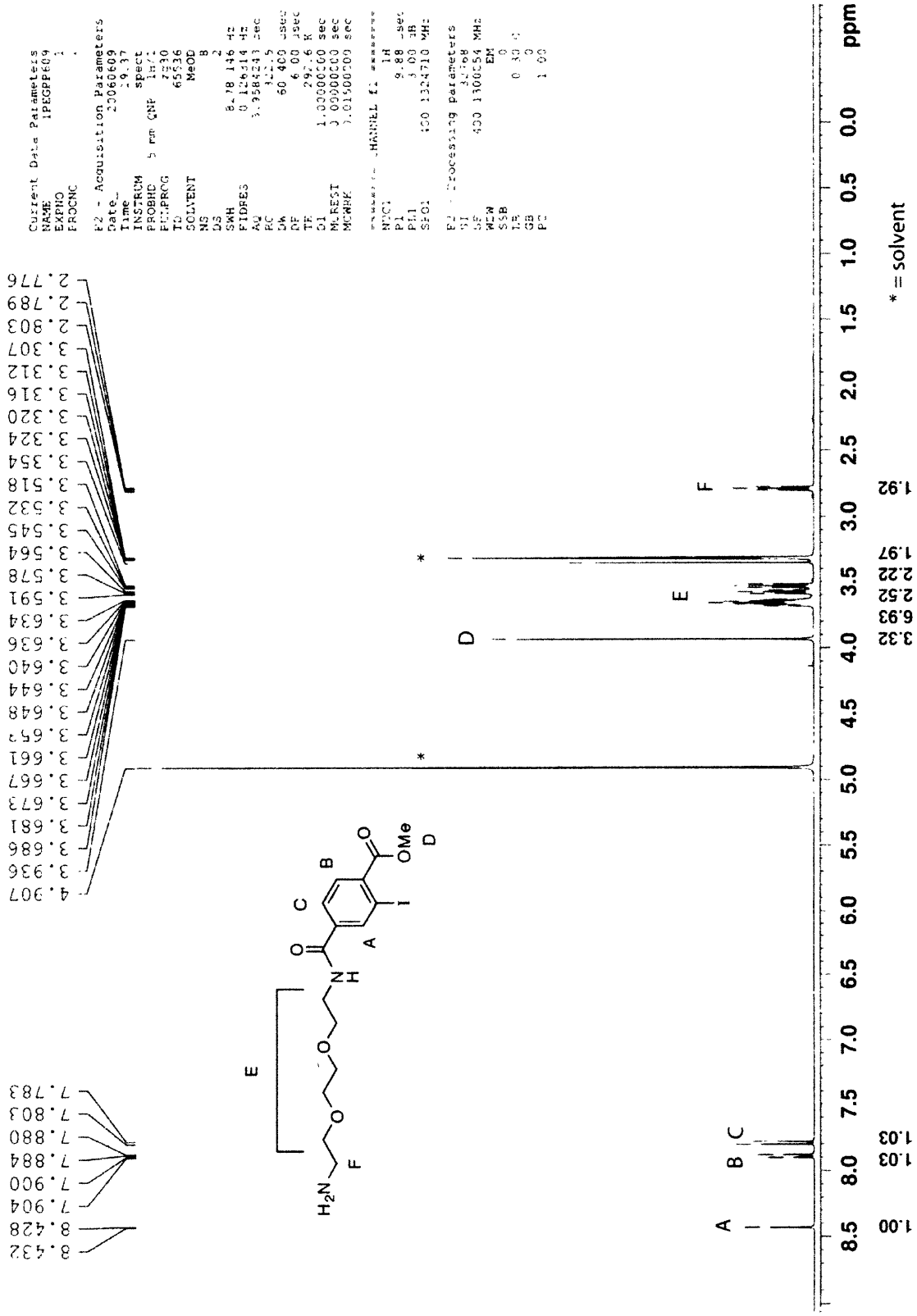

Figure A2.8. ^{1}H NMR Spectrum of PEG-PP

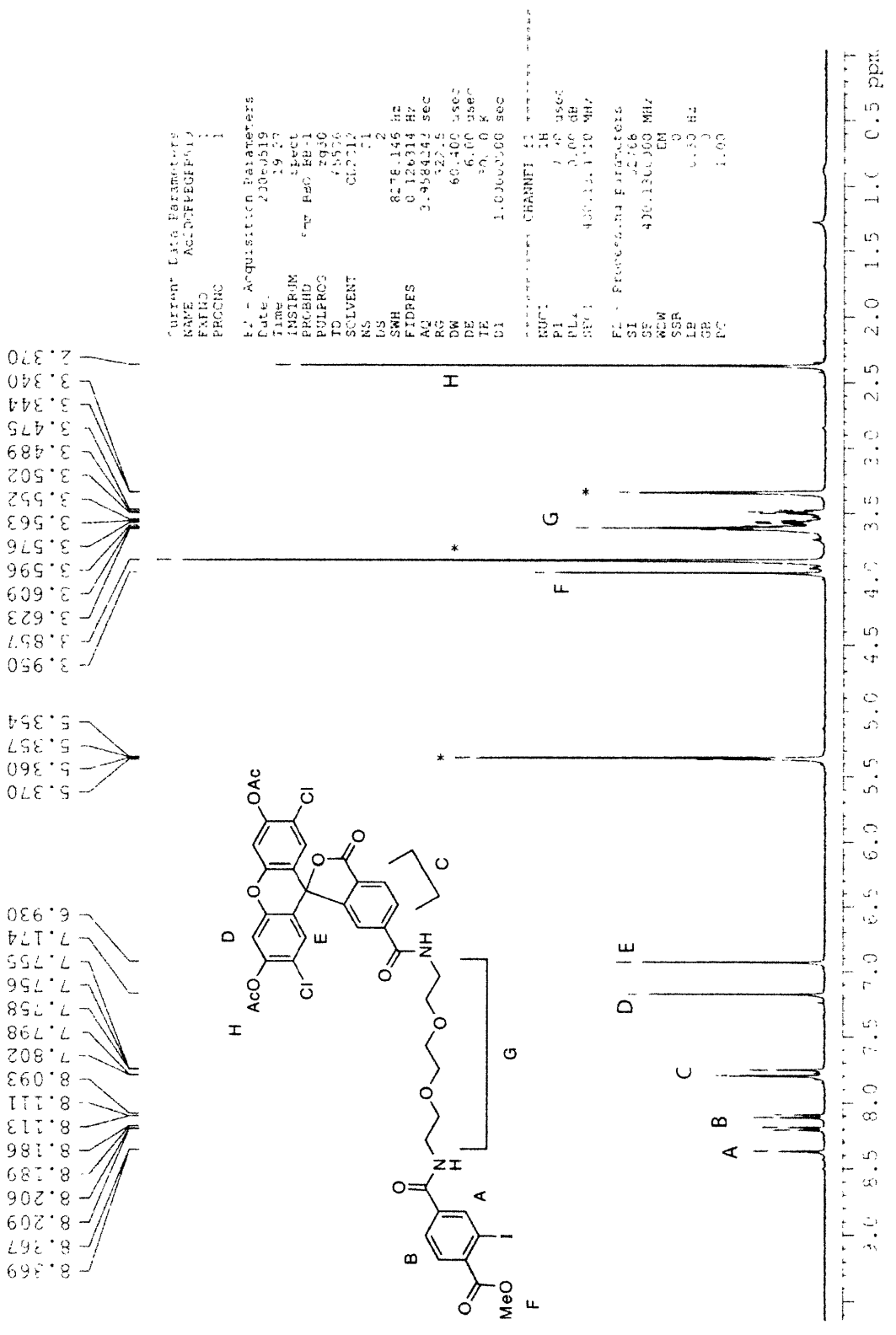

Figure A2.9. ^{1}H NMR Spectrum of Ac_2DCF-PEG-PP

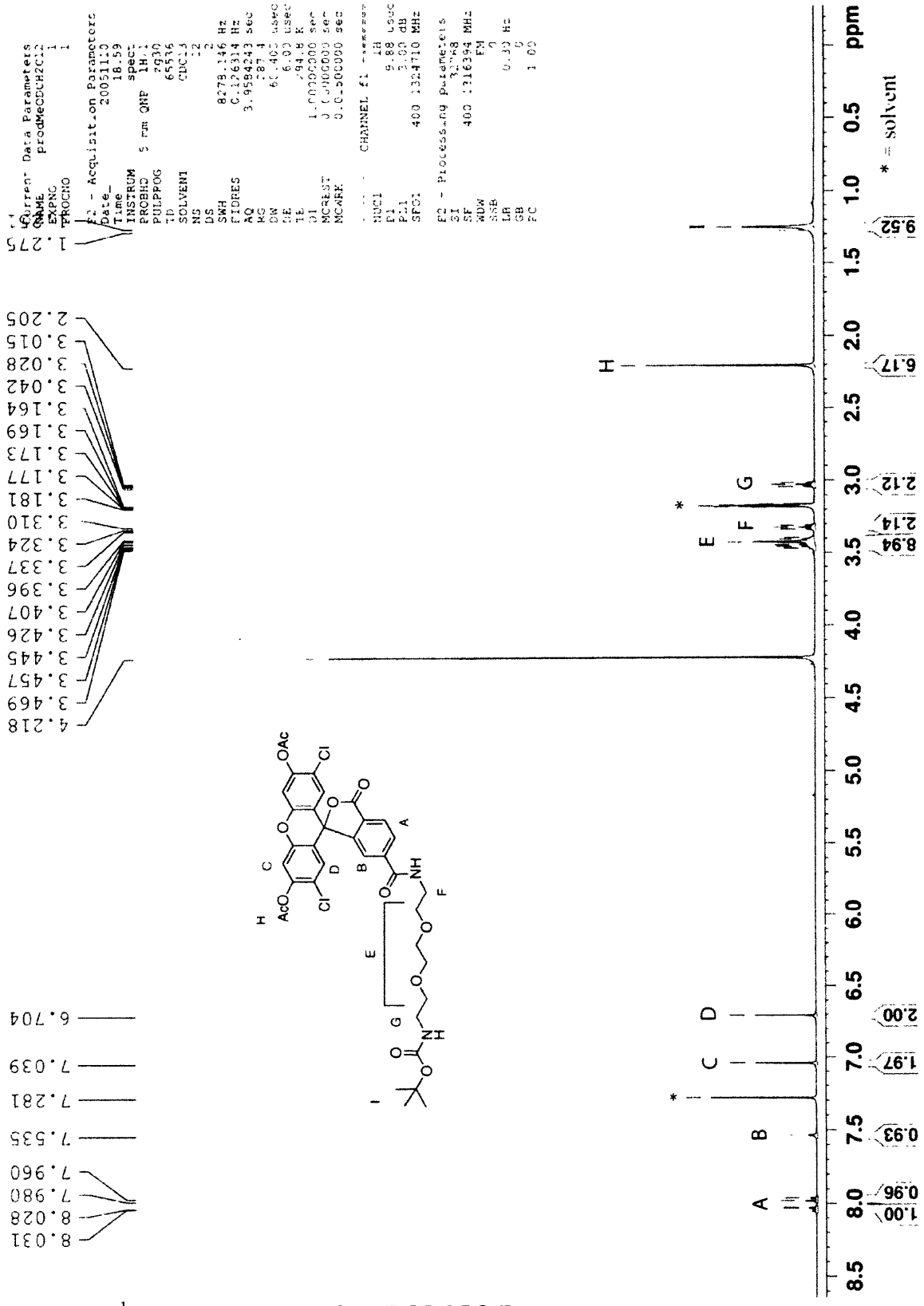

Figure A2.10. ^{1}H NMR Spectrum of Ac_2DCF-PEG-Boc

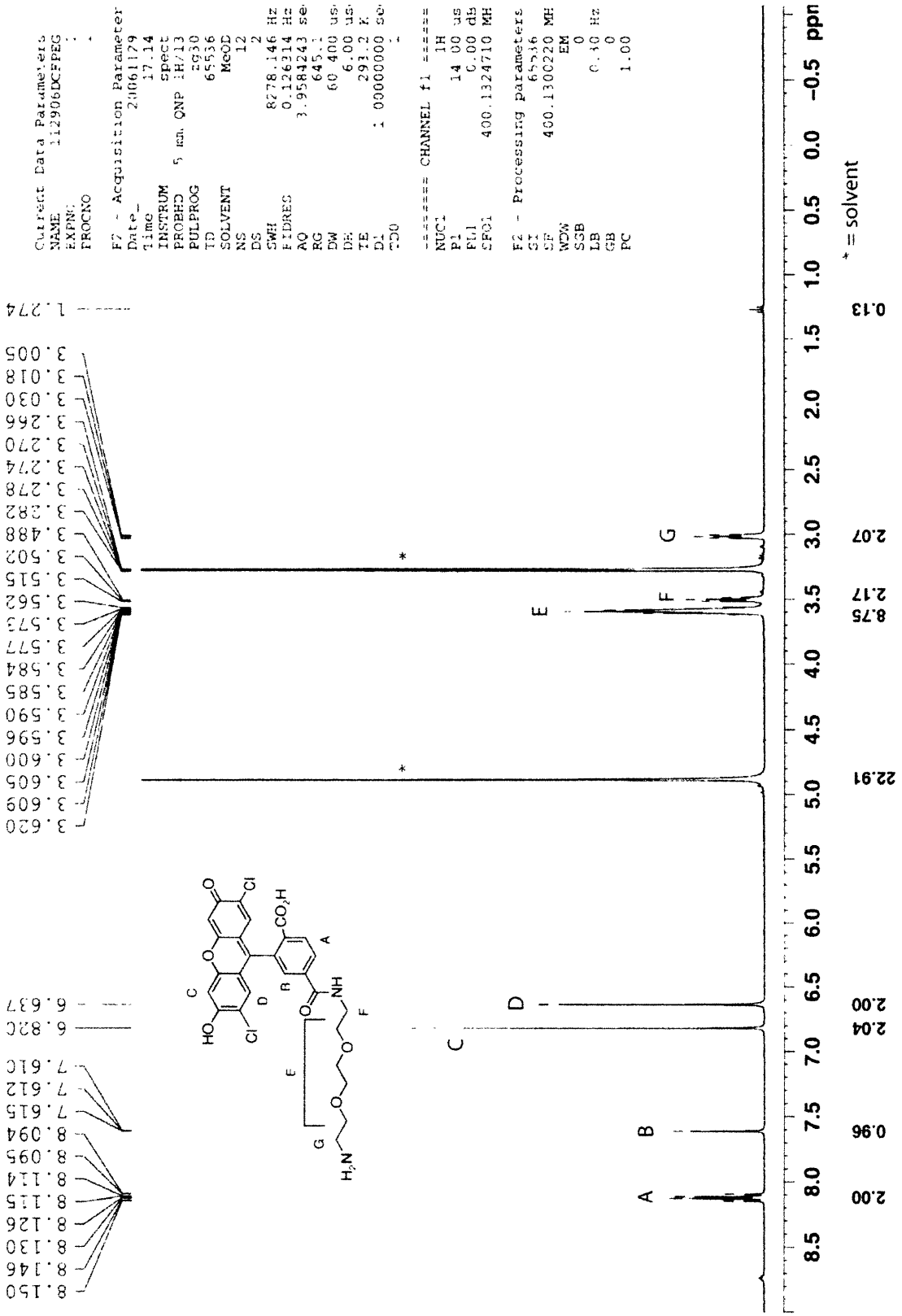

Figure A2.11. ^{1}H NMR Spectrum of DCF-PEG

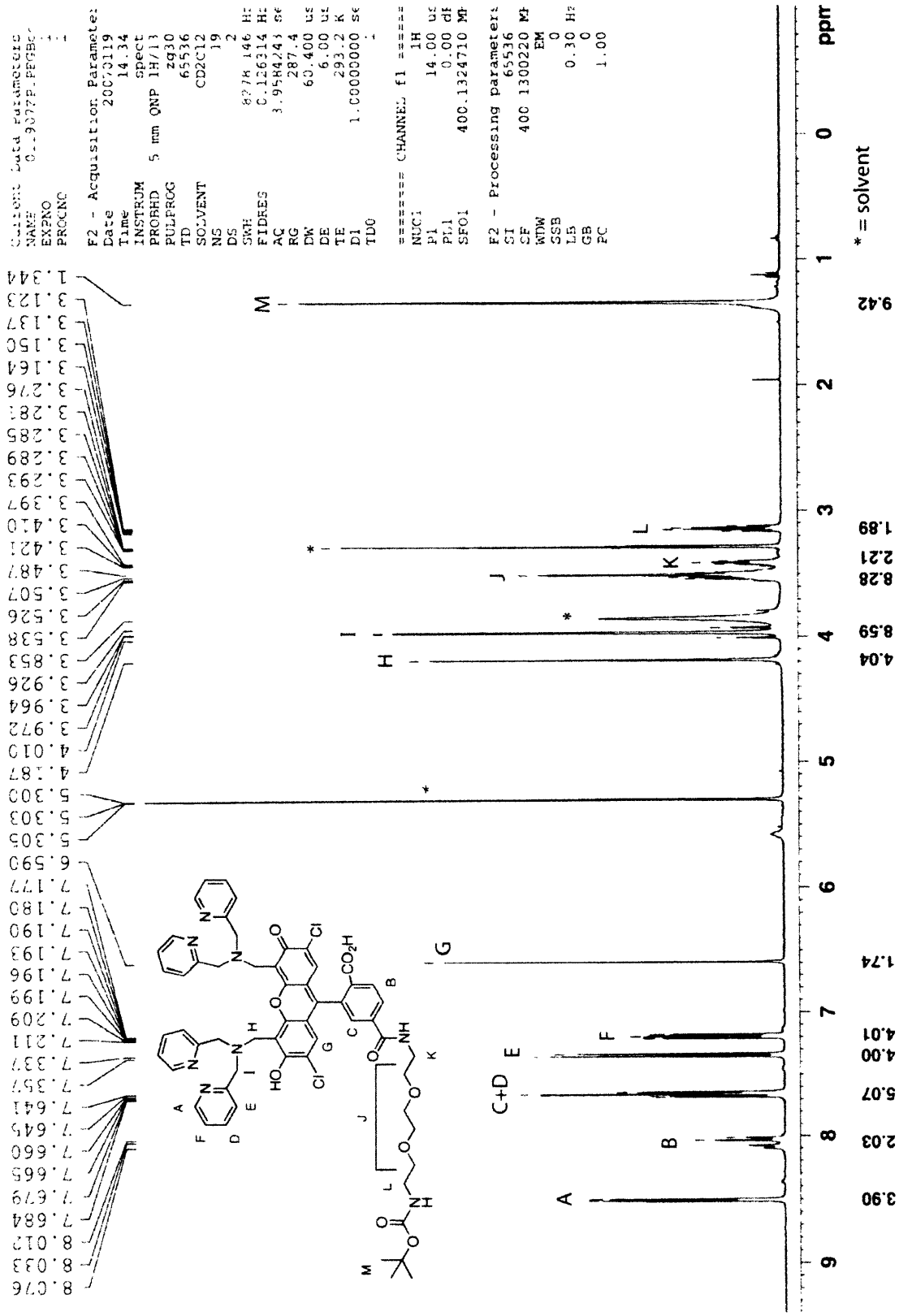

Figure A2.12. ^{1}H NMR Spectrum of ZP1-PEG-Boc

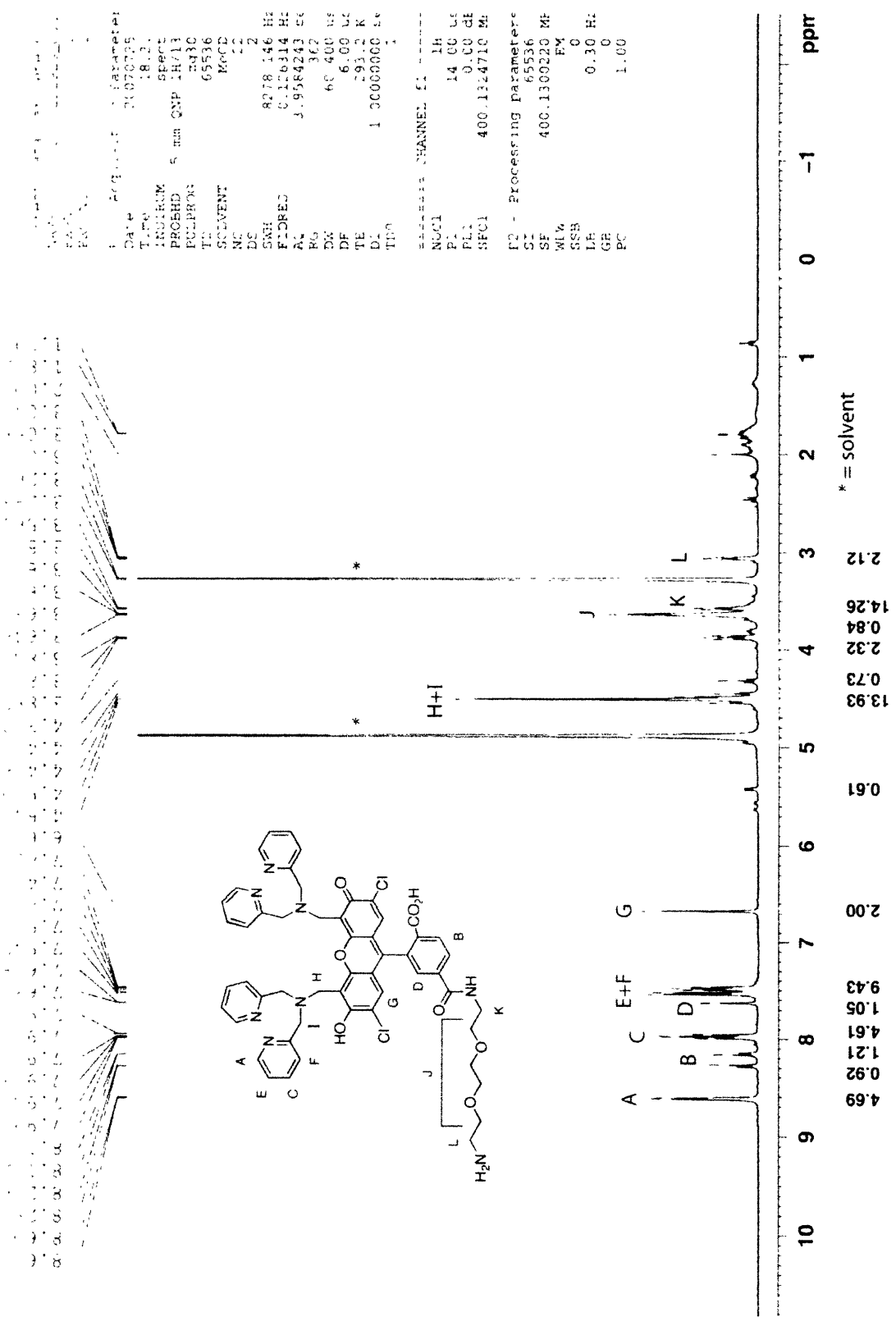

Figure A2.13. ^{1}H NMR Spectrum of ZP1-PEG

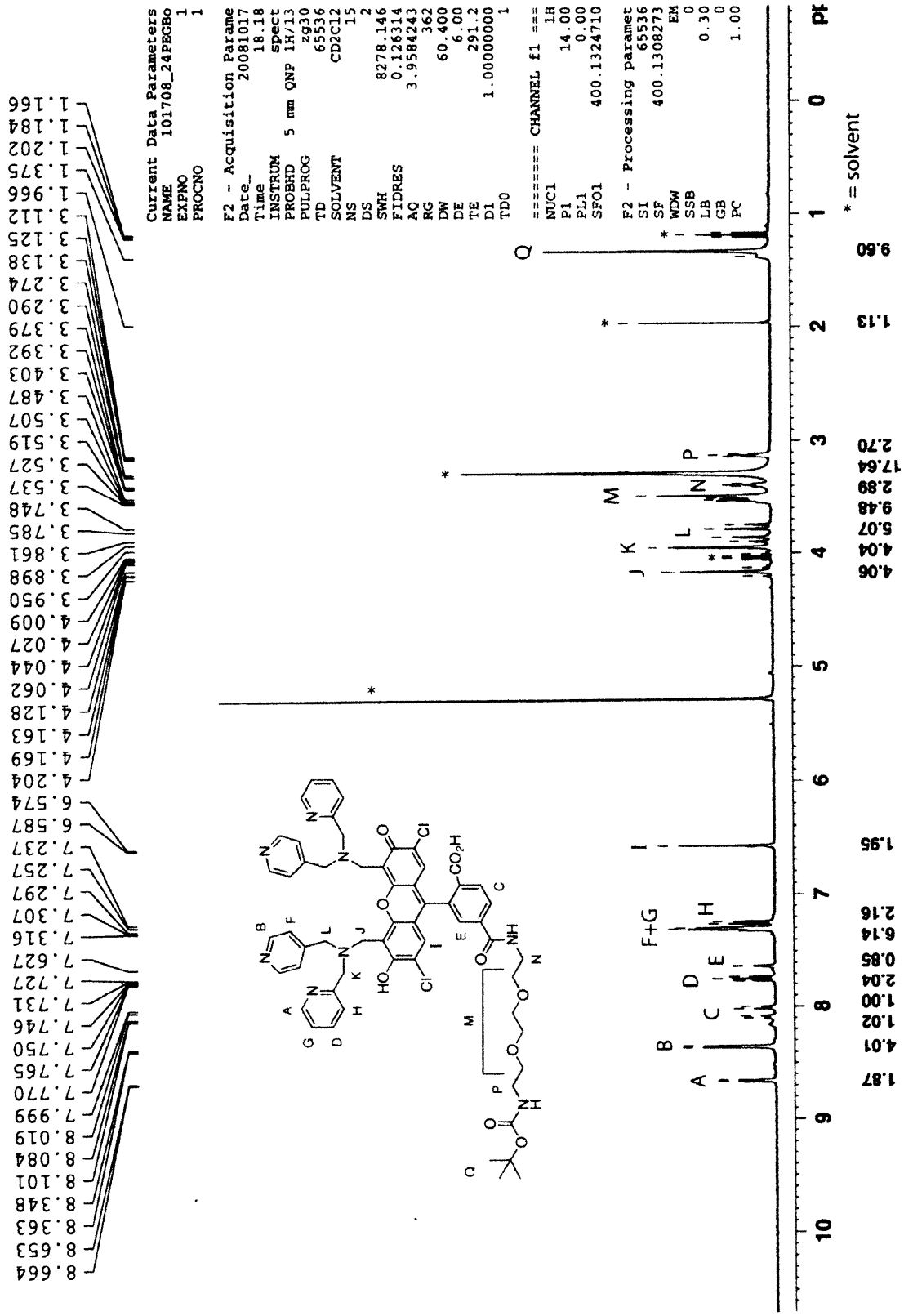

Figure A2.14. ^{1}H NMR Spectrum of ZP1B-PEG-Boc

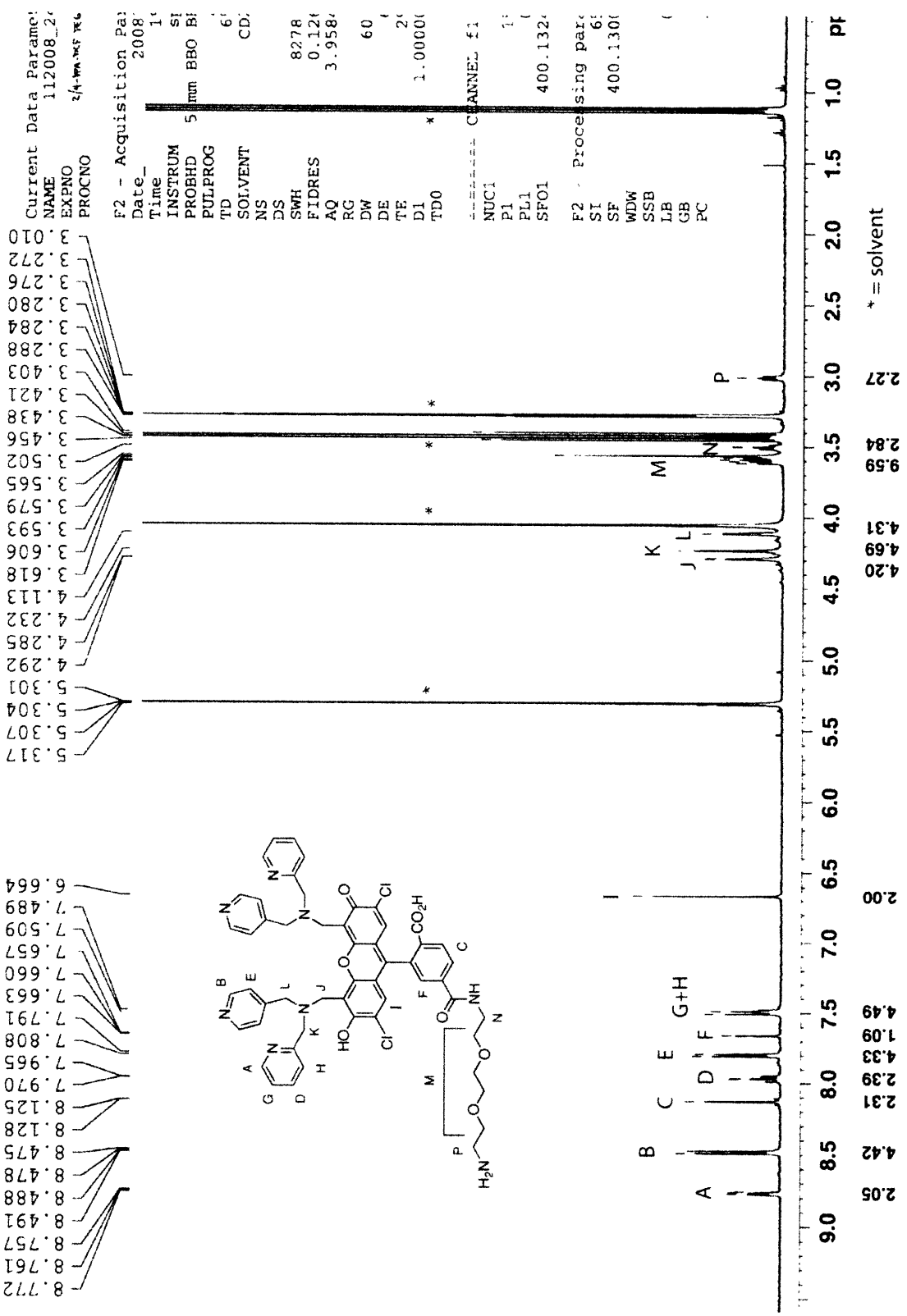

Figure A2.15. ^{1}H NMR Spectrum of ZP1B-PEG

Biographical Note

The author was born in San Francisco, CA in 1972 to Kathleen Anderson and Michael Wong. After living in a number of towns throughout Northern California, his family settled in Santa Rosa, where he attended Montgomery High School. After graduation, he sampled a variety of courses at Santa Rosa Junior College over the span of ten years before recognizing chemistry as his life's calling. He transferred to the University of California, Berkeley, where he worked in the laboratories of Ahamindra Jain and T. Don Tilley. Brian graduated from UCB in 2004, earning a B. S. in chemistry with highest honors, and was awarded the Departmental Citation. Upon graduation from MIT, the author plans to begin a career in teaching chemistry, starting at his alma mater Santa Rosa Junior College.

Brian A. Wong

Education

Massachusetts Institute of Technology
Ph.D. in Inorganic Chemistry, July 2009
Advisor: Stephen J. Lippard

University of California, Berkeley
B.S. in Chemistry, May 2004

Santa Rosa Junior College
A.S. (equivalent), June 2002

Publications

Lim, M. H.; Wong, B. A.; Pitcock, W. H., Jr.; Mokshagundam, D.; Baik, M.-H.; Lippard, S. J., "Direct Nitric Oxide Detection in Aqueous Solution by Copper(II) Fluorescein Complexes," *J. Am. Chem. Soc.* **2006**, *128*, 14364-14373.

Wong, B. A., Friedle, S., Lippard, S. J., "Solution and Fluorescence Properties of Symmetric Dipicolylamine-Containing Dichlorofluorescein-Based Zn^{2+} Sensors," *J. Am. Chem. Soc.* **2009**, *131*, 7142-7152.

Wong, B. A., Friedle, S., Lippard, S. J., "Subtle Modification of 2,2-Dipicolylamine Lowers the Affinity and Improves the Turn-On of Zn(II)-Selective Fluorescent Sensors," *Inorg. Chem.* **2009**, In Press.

Awards

Heath Physics Prize (SRJC, 2002)

Departmental Citation, Chemistry (UCB, 2004)